Differential Dynamic Signal Processing in Frog Vestibular Neurons

Sandra Pfanzelt

München 2008

Differential Dynamic Signal Processing in Frog Vestibular Neurons

Sandra Pfanzelt

Dissertation
an der Fakultät für Biologie
der Ludwig–Maximilians–Universität
München

vorgelegt von
Sandra Pfanzelt
aus München

München, den 27.10.2008

Erstgutachter: Prof. Dr. Hans Straka
Zweitgutachter: Prof. Dr. Benedikt Grothe
Tag der mündlichen Prüfung: 06.02.2009

Summary

Central vestibular neurons process head movement-related signals. Characterization of these neurons and the knowledge about their connectivity is crucial to confer them a particular role in gaze and posture stabilization. Different aspects of the sensory-motor transformation were studied in vestibular neurons recorded from isolated brain preparations of adult frogs. The preparation includes the N.VIII with its individual labyrinthine nerve branches.

Vestibular neurons subdivide into tonic and phasic neurons based on differential intrinsic membrane properties and might be suited to process different dynamic components of vestibular signals. Intracellular injections of oscillatory frequency-modulated currents showed that tonic neurons form neuronal elements with low-pass filter properties. In contrast, phasic neurons exhibited a pronounced subthreshold resonance at $\sim$40 Hz due to the activation of prominent potassium conductances, which conferred to these neurons band-pass filter-like properties. In addition, the different filter behaviors of the two neuronal subtypes correlate with a differential processing of synaptic sensory inputs that renders tonic neurons well-suited for synaptic integration and phasic neurons for signal detection.

The different response dynamics of labyrinthine synaptic inputs in tonic and phasic vestibular neurons is likely the result of a combination of specific intrinsic membrane properties and a differential contribution of synaptic inputs from local circuits. Application of GABAergic and glycinergic antagonists revealed that a semicircular canal-specific disynaptic inhibition is present only in phasic but not in tonic neurons. This inhibitory input on phasic neurons renders the monosynaptic excitatory response more transient, which complies with the high-dynamic, intrinsic properties of this neuronal subtype. Tonic neurons, in contrast, receive inhibitory inputs with considerably longer latencies and are thus not controlled by a short-latency inhibitory side-loop.

The simulation of natural head movement-related activity patterns of labyrinthine afferents by electrically stimulating the afferents with frequency-modulated pulse trains revealed distinct differences in the synaptic response dynamics of tonic and phasic neurons. Tonic neurons transformed the frequency waveform of this stimulus in an almost linear fashion, whereas the synaptic compound responses in phasic neurons exhibited large peak leads thereby generating highly asymmetric response profiles. A modeling approach showed that the asymmetry of the latter neurons was due to membrane properties but was substantially reinforced by GABAergic and glycinergic inhibitory inputs from cerebellar and local vestibular networks.

Thus, the co-adaptation of intrinsic and network properties establishes two distinct neuron types that are well-suited for parallel processing of head movement-related signals with different dynamics.

Contents

1 Introduction

All animals need to know, which way is up and where they are going. In other words, information about the position of the body in the gravitational field and about locomotion are essential for all animals' survival. In vertebrates, vestibular organs are responsible for sensing these signals during stance and gait. The present work focuses on cellular and synaptic mechanisms that are implicated in the processing of information about the position of the body in space at the first synapse of the central nervous system and the generation of appropriate motor responses for gaze and posture control.

1.1 The vestibular system - a special sense

The vestibular organs reside bilaterally in the temporal bone of the skull. They provide a special sense that is unlike any other senses in that we cannot shut it off. There is no tangible sensation provided by this sense; and yet it feeds the brain constantly with messages about our position and motion within the environment. The adequate physical stimulus that the vestibular organs detect is acceleration, how the head rotates and translates in space. Even when we are not moving, they measure the permanent force of gravity on our body posture. This information is used, amongst others, to generate reflexes that stabilize our retinal images of the environment and our posture when we move. Small passive head displacements constantly occur as we walk or run. Since our eyes are locked in the head, we would perceive our environment as constantly moving without compensatory reflexes that stabilize our visual perception of the environment. The vestibulo-ocular reflex (VOR) transforms 3-dimensional vestibular inputs into compensatory eye movements that are directed opposite to the head displacements. Vestibulo-spinal reflexes, in contrast, are important in maintaining a stable posture. Imagine a man

tripping over a stone. His head moves, the vestibular system detects the acceleration and any deviation from the head's normal position, and thus provides a complex pattern of muscle activity to counterbalance the perturbation.

1.1.1 Peripheral endorgans

The vestibular endorgans on both sides have a mirror-symmetrical spatial arrangement. They form a membranous labyrinth that is enclosed by a bony structure of similar shape, the bony labyrinth. The vestibular organs in vertebrates comprise two distinct types of sensory organs, the semicircular canals and the otolith organs.

Semicircular canals

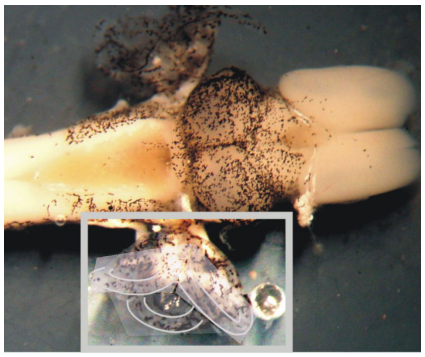

Figure 1.1: Picutre of an *in vitro* preparation; the endorgans are still attached to the labyrinthine nerve branches. Semicircular canals are outlined by clear lines.

The semicircular canals respond to rotational movements (angular acceleration) of the head. The vestibular system contains three semicircular canals on each side for detection of 3-dimensional angular head acceleration (Fig. 1.1). The horizontal, anterior vertical and posterior vertical canal are oriented approximately perpendicular to each other such that they optimally detect acceleration about any axis in the three-dimensional space (Markham and Curthoys, 1972). At one end, the canals widen into a structure termed ampulla. A gelatinous membrane, the cupula, extends across the whole diameter of the ampulla. Hair bundles from the sensory cells project into the basal part of the cupula. The canals are filled with a viscous fluid, the endolymph. As the head rotates it carries the canals with it but the endolymph lags behind because of its inertia. This results in a relative motion of the endolymph within the canal in a direction opposite to that of the head. Since the cupula spans the diameter of the canal in the ampulla the motion of endolymph deflects the flexible cupula and with it the hair bundles of sensory cells. Sensory cells are also denoted hair cells due to their hair bundles that protrude from their apical surface. The bundles consist of

stereocilia, increasing in length towards a single kinocilium. Deflection of the direction-sensitive stereocilia causes a receptor potential. A displacement of the stereocilia towards the kinocilium depolarizes, a displacement away from the kinocilium hyperpolarizes the hair cells (Wersäll, 1972). The semicircular canals are arranged in a coplanar organizational pattern on both sides such that each canal on the left side has a counterpart on the right side. The pairs are located in a common plane and hence function together. Due to their mirror-symmetric organization they work in a push-pull fashion: during rotation in the plane of a functional plane-specific canal pair, the hair cells on one side are depolarized (deflection towards the kinocilium), while the hair cells on the other side are hyperpolarized (deflection away from the kinocilium). All hair bundles in each semicircular canal share a common orientation such that a functional canal pair codes angular acceleration in its respective plane.

Otolith organs

The otolith organs detect linear acceleration including changes of the body (head) relative to gravity. They lie in the central part of the membranous labyrinth. In mammals these vestibular organs consist of an approximately horizontally oriented utricle and a vertically oriented saccule. All other vertebrates are endowed with a third otolith organ, the lagena. From a functional point of view the lagena in anamniotes (fish and amphibians) corresponds to the saccule in amniotes (reptiles, birds and mammals), whereas the saccule in anamniotes, for instance, in frogs largely senses substrate vibration and thus assumes an auditory function (Ashcroft and Hallpike, 1934). However, a clear separation of otolith organs into vestibular or auditory (including detection of substrate-borne vibrations) organs is not possible since all appear to have a dual function depending on the frequency sensitivity of particular hair cells on the macula (see Straka and Dieringer, 2004). The hair cells in the otolith organs are arranged in ovoid patches (maculae). They are covered by a gelatinous sheet, the otolith membrane, which extends over the entire sensory macula. Lying on top, are dense crystals, the otoconia or otoliths. This loading by an inertial mass makes the organs sensitive to linear acceleration and changes of the head position in the gravitational field. The otolith membrane is shifted with respect to the underlying patch of hair cells, thereby deflecting the hair bundles. As in semicircular canals

the deflection either depolarizes or hyperpolarizes the hair cells. In contrast, however, hair cells of otolith organs are arranged in radial arrays that span 360° of polarization directions such that utricle and lagena/saccule encode all linear acceleration vectors in the horizontal (Wersäll and Bagger-Sjöback, 1974) or vertical plane (Caston et al., 1977; Wersäll and Bagger-Sjöback, 1974), respectively. Because of its largely vertical orientation in the space, the lagena/saccule also detects changes of the head position relative to gravity, as for instance during a head tilt. Independent of the spatial orientation of the hair cell bundle or its insertion into a canal cupula or the otolith macula, the shape and length of the cilial bundles determine the frequency spectrum of head acceleration that a particular hair cell can optimally detect (see Goldberg, 2000). Based on the differential morphologies of the cilial bundles that correlate with particular spatial positions within the sensory epithelium, hair cells form distinct subtypes with different dynamic properties. These different subtypes are either suitable to detect and code constant head deviations or high-acceleration profiles during rapid head turns. Accordingly, they form the basis of signal processing in frequency-tuned channels (Goldberg, 2000).

1.1.2 Afferent nerve fibers

Both the hair cells of otolith organs and those of semicircular canals are secondary sensory cells: they do not have a proper axon but are contacted by the terminal structures of ganglion cells whose axons form the afferent fibers of the vestibular nerve. Information between hair cells and the terminals of afferent fibers is transmitted by glutamatergic chemical transmission (Guth et al., 1988; Raymond et al., 1988; Usami et al., 2001). The centrally projecting axons from the vestibular ganglion join with axons from the auditory neurons to form the eighth nerve (N.VIII). Afferent fibers are characterized by a rather high resting discharge of about 90 to 100 Hz in monkey (Goldberg, 1979; Fitzpatrick and Day, 2004) but a considerably lower discharge in frogs (1-10 Hz; Blanks and Precht, 1976). Hair cell receptor potentials are transduced into a modulation of the resting discharge of the afferent fibers. The depolarization of hair cells leads to an increased transmitter release, which, in turn, increases the discharge rate of the postsynaptic afferent fiber. Hyperpolarization decreases the firing rate of the afferent fibers. In contrast to sensory cells, afferent nerve fibers do not form distinct neuronal subtypes but

rather a continuum with regard to several properties. Afferent nerve fibers are characterized by a broad range of axon diameters. Thin to thick-diameter fibers concur with response properties that range from tonic over phasic-tonic to phasic. Thin afferent fibers have a rather regular resting activity, a tonic discharge to step-like acceleration; they exhibit low gains (ratio of discharge rate and acceleration) and large phase shifts following sinusoidal acceleration profiles (Honrubia et al., 1989; Goldberg, 2000). These fibers contact the more peripheral regions of the sensory epithelium (Baird and Schuff, 1994). Thick afferent fibers exhibit a highly irregular resting activity, a phasic discharge to acceleration steps, large gains and small phase shifts. These higher-dynamic fibers tend to target central regions of the sensory epithelium of the semicircular canal cupula or the striolar region of the otolith organs (Goldberg, 2000). Utricular and lagenar macula are subdivided by a striola, a central band, where the polarization of hair cells reverses abruptly. As hair cells in the peripheral/extrastriolar and central/striolar regions are characterized by lower and higher dynamics, respectively they are contacted by afferent fibers with matched dynamic properties, thereby corroborating the notion of information processing in frequency-tuned channels.

1.1.3 Projections

Vestibular nerve fibers relay the information from the vestibular organs to the cerebellum, the reticular formation and the vestibular nuclei (Highstein and Holstein, 2005). In the vestibular nuclei, these first-order vestibular fibers terminate in all four main nuclear areas. The four major nuclei that form the vestibular nuclear complex are the lateral, the medial, the superior and the descending vestibular nucleus, which differ anatomically, with respect to the projection to their target areas, as well as in particular details of cell morphology. In contrast to the sensory topology of e.g. the auditory brainstem nuclei, the vestibular nuclei are organized with respect to the premotor output explaining the absence of an organized spatially-specific projection pattern of vestibular afferents within the different vestibular nuclei (Straka et al., 2003). The vestibular nuclei give rise to second-order vestibular projections to the thalamus, specific areas of the cerebellum, certain cranial nerve motor nuclei and to virtually all levels of the spinal cord. The projections to the cerebellar cortex and the thalamus indicate that the

vestibular system is not only involved in gaze- and posture-stabilizing reflex pathways but also in motor learning, adaptation of motor programs, perception of the position in space and in navigation in space.

1.2 Central vestibular neurons

Central vestibular neurons (neurons located in the vestibular nuclei) are an important relay station in mediating signals from the sensory periphery to various levels of the central nervous system. In addition, they receive convergent proprioceptive and visual input (Fuchs and Kimm, 1975). Why do central vestibular neurons need additional information from other senses? The accurate control of posture and gaze depends on precise spatial and temporal processing of sensory inputs. But there are situations when information provided by the vestibular organs is ambiguous.

Ambiguous information

The vestibular system alone cannot tell apart a situation, in which a person is standing upright, head facing forward, falling sideways (leftwards) from a situation, in which the person is standing upright, head turned 90 ° to the right and falling forward. The two situations necessitate different movement strategies to compensate for the imbalance. In the first situation one has to take a step to the left, whereas in the second situation one takes a step forward to counterbalance the perturbation. In both cases, however, the vestibular system sends a signal that the head is rotating sideways in a vertical plane. This is not surprising. The vestibular system is located in the skull and thus detects signals with respect to the co-ordinate frame of the head. Since the head of most amniote vertebrates can assume almost any position (Fitzpatrick and Day, 2004) relative to the body/trunk our brain resolves this ambiguity by relying on additional senses (proprioceptive and visual). These multiple internal representations of the head and/or body movement are merged into a unique internal frame of reference on the level of central vestibular neurons. Thus, the vestibular nuclei are a multi-sensory relay center that integrates the sensory

inputs from different modalities, all related to self-motion and changes of the body position in space.

Deficient information

Signal convergence is not only essential for postural control but also for stabilizing gaze. The vestibular system is an imperfect sensor of head movement; the semicircular canals are not sensitive to slow head movements and moreover they habituate during prolonged stimulation. To compensate for such deficiencies, the optokinetic system provides central vestibular neurons with visual information that close the open-loop vestibular system and serve as a feed-back for the precise stabilization of the eyes in space. The VOR and the optokinetic reflex supplement each other in time and frequency domain.

Combining information from different sensory modalities at a central level resolves for equivocal vestibular signals and compensates for deficiencies in the vestibular apparatus (Angelaki et al., 2004). Since different sensory inputs are already merged at the level of central vestibular neurons, these neurons play a vital role in the sensori-motor transformation.

This present doctoral work includes three studies that deal with different aspects of signal processing of central vestibular neurons. All three studies employed an *in vitro* preparation of an isolated whole brain of adult frogs as a model. The preparation comprises the brainstem including the vestibular nuclei and the N.VIII with its individual labyrinthine nerve branches (Fig. 1.2A). The first study "Differential Intrinsic Response Dynamics Determine Synaptic Signal Processing in Frog Vestibular Neurons", published as co-first author with Mathieu Beraneck in the Journal of Neuroscience (Beraneck et al., 2007), tested if membrane properties of central vestibular neurons generate cellular filter elements that are specific for particular frequencies. In other words, do these neurons preferably process signals in a particular frequency domain? Neurons were stimulated by intracellular injection of dynamic current waveforms into the cell and were recorded intracellularly by the same electrode (Fig. 1.2A). In a second step, an attempt was made to investigate the interaction between synaptic processing and intrinsic membrane properties. In theory, the synaptic processing depends on the interaction of presynaptic signals with

sets of voltage-gated ion channels of the postsynaptic cell. To study the effect of synaptic processing, frog vestibular neurons were activated synaptically by applying single electrical current pulses to the labyrinthine nerve afferents in the *in vitro* preparation.

Vertebrate vestibular neurons have been shown to receive input from several local networks, which contribute to their response characteristics (Straka and Dieringer, 1996; Minor and Goldberg, 1991). The second study "Differential Inhibitory Control of Semicircular Canal Nerve Afferent-Evoked Inputs in Second-Order Vestibular Neurons by Glycinergic and GABAergic Circuits", published as a co-author in the Journal of Neurophysiology (Biesdorf et al., 2008), investigated the effects of a particular inhibitory network on the signal processing of vestibular neurons. Second-order vestibular neurons were recorded following electrical stimulation of the nerve branches (as above) in the presence and absence of specific transmitter blockers that reduced the component of the inhibitory network (GABA, glycine). Comparison of recordings with and without transmitter blockers allowed describing the differential effect of the network on the response characteristics of the two types of vestibular neurons (Fig. 1.2B).

Finally, in the third study "Differential Dynamic Processing of Afferent Signals in Frog tonic and Phasic Second-order Vestibular Neurons", published as first author in the Journal of Neuroscience (Pfanzelt et al., 2008), the synaptic processing of vestibular neurons was analyzed with a dynamic stimulus paradigm (Fig. 1.2C). The stimulus was constructed such that it mimicked the activity pattern of vestibular afferent fibers during a natural head movement. A sequence of precisely timed pulses was applied to the afferent nerve fibers. *In vivo* recordings of the discharge rate of afferent fibers during sinusoidal rotation of the frog (Blanks and Precht, 1976) formed the basis for this stimulation paradigm. This stimulus evoked a complex response pattern in intracellularly recorded neurons, which was analyzed with respect to its dynamics. Since response characteristics depend on intrinsic membrane as well as on network properties, the influence of inhibitory local and cerebellar networks on the response pattern of vestibular neurons was tested by pharmacological experiments. A modeling approach helped to differentiate between the contribution of intrinsic membrane properties and network components to the observed response patterns.

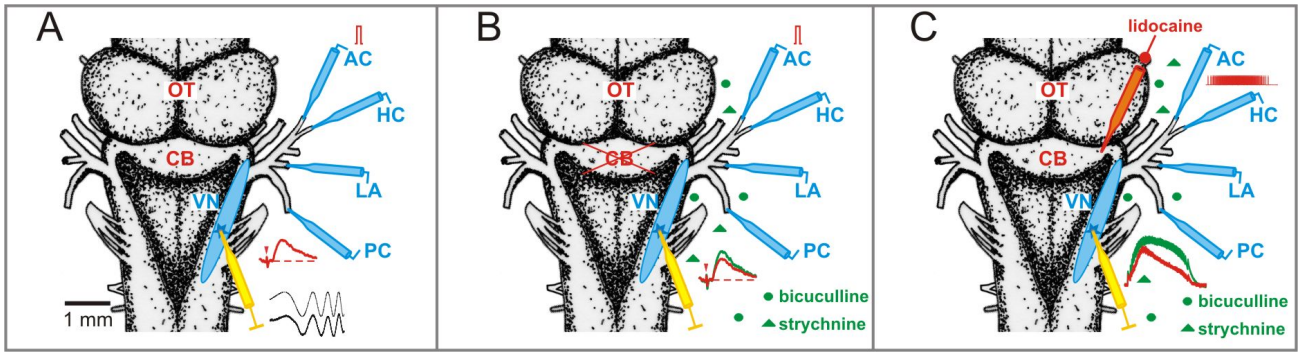

Figure 1.2: Scheme of recording paradigms that are used in the three studies, respectively. The semicircular canal and the lagenar canal nerve branches are electrically stimulated by suction electrodes (blue). Neurons are recorded from the vestibular nuclei (VN) (yellow electrode). **A**, In this paradigm, neurons were stimulated (thin ∼) and recorded (thick ∼) by the same electrode (yellow). Neurons were stimulated by intracellular injection of an oscillatory current. Stimulation of nerve branches served predominantly to identify neurons as vestibular second-order neurons by means of their monosynaptic EPSP (red trace). **B**, The cerebellum (CB) was removed in all experiments. Neurons were synaptically activated by stimulating the labyrinthine nerve branches. Synaptic responses were compared before (red) and after (green) application of GABAergic (bicuculline) and glycinergic (strychnine) canal blockers. **C**, A complex stimulus pattern was applied to the nerve branches. The complex synaptic responses were compared in the absence (red) and presence (green) of bicuculline and strychnine. In addition, the cerebellum (CB) was reversibly blocked by injection of lidocaine. OT, optic tectum.

1.2.1 Intrinsic membrane properties

Vestibular neurons need to be capable of processing a wide variety of signals to cover the whole dynamic range of vestibulo-spinal and vestibulo-ocular motor responses in different situations. The vestibulo-spinal reflex stabilizes the head and body in space. It intervenes during slow postural body adjustments as well as during a rapid turning or during falling. In contrast to these rather large-amplitude compensatory responses, the vestibulo-ocular reflex produces small-amplitude eye movements to keep the image of our environment stable. Vestibular neurons should thus be endowed with membrane properties, which render them suitable for processing low-and high-frequency signals of various amplitudes. Amongst vertebrates the differentiation into at least two main types of neurons according to their intrinsic membrane properties seems to be a general principle of vestibular nuclear organization (Straka et al., 2005). Based on the shape of action potentials, intracellularly recorded neurons in the medial vestibular nucleus (MVN) of rodents have been subdivided into two distinct classes, type A and type B neurons, in rat (Gallagher et al., 1985; Johnston et al., 1994), guinea pig (Serafin et al., 1991a,b; Beraneck et al., 2003) and mice (Dutia et al., 1995). The spike shape correlates with various parameters

such as discharge regularity upon depolarizing current steps. In frog, vestibular neurons also subdivide into two subgroups (Straka et al., 2004), called tonic and phasic neurons. In these neurons, the discharge following a depolarizing current step is most suited to distinguish tonic from phasic neurons. As vestibular neurons are involved in multiple behavioral tasks of varying dynamics, two neuronal subtypes might optimize their performance in signal transformation if they formed the central nervous part of frequency-tuned channels for processing lower and higher dynamic signals, respectively. Based on theoretical considerations (Av-Ron and Vidal, 1999; Quadroni and Knöpfel, 1994) and intracellular recordings (Beraneck et al., 2003), such a task sharing was hypothesized for rodent type A and B MVN neurons. The dynamics of MVN neurons was studied by intracellular injection of sinusoidally modulated currents. As these neurons exhibit a spontaneous resting discharge, their response behavior upon sinusoidal current is mirrored in the modulation of the resting discharge. Type B MVN neurons performed good modulation at low-frequency, sinusoidally modulated currents. At higher frequencies they fired in synchrony with the depolarizing phase of the stimulus, thus promoting high-frequency inputs. Accordingly, these neurons serve as an event detector. In contrast, type A MVN neurons modulate the firing rate over a wider frequency range. This suggests that they have a more linear working range and are well-suited to linearly display a stimulus. The two types of neurons assume thus two distinct roles in the processing of vestibular sensory signals. In frog, stabilizing motor commands also carry response components of various dynamics in situations as different as escaping from predators or during prey catching where long phases of immobility are interrupted by rapid, re-orientating movements. As in rodents, the presence of tonic and phasic neurons (Straka et al., 2004) might correlate with different functional roles in the sensori-motor transformation of vestibular inputs. The different membrane properties of frog vestibular neurons suggest that the two subtypes form different neuronal filters that are likely adapted to the locomotor behavior of these animals.

1.2.2 Inhibitory control of vestibular neurons

The response dynamics of neurons do not only depend on their intrinsic membrane properties but also on the local circuits, in which these neurons are embedded. Optimally, the membrane

characteristics of a given neuron should be reinforced by its local circuits. Such a reinforcement occurs in the well-studied Mauthner cell (M-cell) in fish (Nakayama and Oda, 2004), which plays an important role in initiating fast escape behavior. Particular intrinsic properties (voltage-gated potassium channels) prevent the M-cell from repetitive firing upon a depolarizing current step. In addition, its local circuit (recurrent inhibition) suppresses the initial burst such that a depolarizing current step leads to a single spike at stimulus onset. The recurrent inhibition thus controls the intrinsic properties of the M-cell. In the frog different circuits control output signals and dynamics of vestibular neurons. Two essential inhibitory networks are the cerebellar feed-back loop and an uncrossed vestibular side-loop in the vestibular nuclei that recruit local inhibitory vestibular interneurons (Straka and Dieringer, 2004). Based on the different response properties of tonic and phasic vestibular neurons it is likely that the two vestibular subtypes are differentially embedded in these inhibitory synaptic circuits.

Cerebellar feed-back loop

The cerebellum is generally referred to as the co-ordinator of movements (Ito, 1984). It evaluates disparities between intention and action by modulating motor programs. Cerebellar lesions result in movement co-ordination deficits as well as oculomotor coordination disorders and prevent the adaptation of motor programs to new conditions. The cerebellum thus plays also a key role in adaptation of the VOR (Gittis and du Lac, 2006). Head movements are accompanied by compensatory eye movements that keep the retinal image of our environment stable. Ideally, head and eyes move at the same speed. If eye velocity and head velocity signals diverge, the cerebellum receives an error signal, which leads to persistent changes that account for the new condition. Therefore, the VOR needs to be adjusted throughout live according to age-related deteriorations as well as to pathophysiological deficits (Lisberger, 1998). The output from the cerebellar cortex is mediated via GABAergic Purkinje cells that target cell bodies in the deep cerebellar nuclei and in the vestibular nuclei. The flocculo-nodular lobe is the most primitive portion that first appeared in fish and constitutes only a small part of the cerebellum in mammals. Yet, it plays a vital role in adaptation of motor programs in that it receives the main vestibular input. It receives both, input from first-order vestibular afferents and second-

order vestibular neurons and projects back to the vestibular nuclei. Thus, Purkinje cells inhibit neurons in the vestibular nuclei. In frog, the cerebellum consists of a single lamella across the midline. It is composed of a central plate, the corpus cerebelli, and two lateral parts, the auricular lobes (Larsell, 1967). Although it lacks the complexity of the mammalian cerebellum, the synaptic connectivity is rather conserved. As in mammals, vestibular afferent fibers in frog project directly to the cerebellar auricular lobe (Matesz, 1979) as well as indirectly via central vestibular neurons (Straka et al., 2001). Neurons in the vestibular nuclei are, in turn, targeted monosynaptically by Purkinje cells (Magherini et al., 1975). As the cerebellum is crucial in tuning motor programs like the VOR, learning more about the influence of Purkinje cells onto central vestibular neurons helps to understand the generation of precise motor commands.

Uncrossed vestibular feed-forward side-loop

Second-order vestibular neurons exhibit a monosynaptic EPSP upon stimulation of ipsilateral vestibular nerve branches. In frog, about 90 % of these monosynaptic potentials are superimposed by disynaptic inhibitory inputs (Straka and Dieringer, 1996). A similar organization of disynaptic inhibitory inputs that are superimposed on excitatory inputs were also reported in *in vivo* recordings of vestibular neurons in squirrel monkey (Goldberg et al., 1987): in more than 50 % of vestibular neurons an electrical pulse stimulus applied to the ipsilateral eighth nerve evoked a monosynaptic EPSP and a superimposed disynaptic IPSP. Goldberg and colleagues (1987) assumed the presence of a disynaptic inhibition, which is mediated by the same semicircular canal-related fibers as the monosynaptic potential. In *in vivo* experiments of the squirrel monkeys the origin of such a disynaptic circuit could not be unequivocally determined due to spontaneous activity of the surrounding network. In frog, however, the existence of such a feed-forward inhibition is well established. After application of glycinergic or GABAergic anatgonists monosynaptic EPSPs in most vestibular neurons increased in amplitude (Straka and Dieringer, 1996). Electronic subtraction of the EPSP, recorded in the presence of a canal blocker, from the control EPSP uncovered an inhibitory component. This inhibitory component could be identified as disynaptic due to its onset latency. Lesion studies showed that ipsilateral interneurons in the vestibular nuclei are the origin of this GABAergic and glycinergic inhibition

(Straka and Dieringer, 1996). This feed-forward inhibition can control the amplitude and duration of monosynaptic afferent-evoked inputs by shunting the monosynaptic afferent EPSPs and thus influences critically the afferent-evoked spike discharge. Since it shortens the monosynaptic excitation, it would be well-suited to reinforce the transient response characteristics of phasic neurons (Straka et al., 2004). It is unclear, though, if both tonic and phasic vestibular neurons receive such a disynaptic inhibition. Assuming a co-adaptation of intrinsic membrane properties and emerging network properties, phasic but not tonic vestibular neurons should be embedded in the inhibitory feed-forward side-loop.

1.2.3 Synaptic processing of labyrinthine inputs

In rodents, the two neuronal subtypes in the vestibular nuclei are supposed to process synaptic information differently (Babalian et al., 1997). Type A MVN neurons exhibit a more regular resting discharge than type B MVN neurons. This differential discharge pattern appears to be correlated with differences in synaptic signal processing of these two subtypes. Type B MVN neurons, compared to type A MVN neurons, demonstrate smaller after-hyperpolarizations of the action potentials, which render this subtype more sensitive to small synaptic currents, which, in turn, cause a more irregular resting discharge (see Straka et al., 2005). A differential processing of synaptic inputs in different vestibular subtypes would make these subtypes suitable as cellular correlates for parallel frequency-tuned channels. Such a differential synaptic processing was tested in frog phasic and tonic vestibular neurons by applying electrical pulses to the labyrinthine nerve branches. In the first part of my doctoral thesis (Beraneck et al., 2007), the response of tonic and phasic neurons upon single monosynaptic EPSPs was tested in order to reveal possible interactions between intrinsic membrane properties and the synaptic processing. In the last part of my doctoral thesis, a more complex stimulus was used to uncover differential dynamics of synaptic processing in tonic and phasic vestibular neurons (Pfanzelt et al., 2008). For this purpose, a complex stimulus was designed to mimic a natural head movement. This was done by using the discharge pattern of frog labyrinthine nerve branches during sinusoidal head rotation *in vivo* (Blanks and Precht, 1976) and transforming it into a sequence of pulses, which, in turn, was applied to the labyrinthine nerve branches in the *in vitro* preparation. Each

pulse of the sequence evoked a single spike in the afferent nerve fibers and thus resembled the fiber discharge during sinusoidal movements under *in vivo* conditions. With this stimulation paradigm it was possible to vary different parameters of head movements, such as velocity and/or amplitude. In addition, by increasing the current intensity of the single pulses in the train the postsynaptic processing of inputs from a larger afferent fiber spectrum was investigated. Response dynamics of tonic and phasic neurons are not exclusively determined by the interaction of presynaptic signals with particular intrinsic properties but also by networks, in which these neurons are integrated (Straka and Dieringer, 2004). The influence of the disynaptic feed-forward loop and the cerebellar feed-back loop on the response upon stimulation with the designed stimulation paradigm was therefore tested. Injection of the sodium channel blocker lidocaine into the cerebellum prevented Purkinje cells from firing and allowed recording a given neuron with (before lidocaine injection) and without (after lidocaine injection) cerebellar contribution to the response. The contribution of the feed-forward loop to the response characteristics was determined, as in the study of Biesdorf et al. (2008), by application of glycinergic and GABAergic antagonists. The contribution of intrinsic membrane properties and emerging properties of the network, in which the neurons are embedded were studied by generating computational models of tonic and phasic neurons. To this end, intrinsic cellular models of these neurons have been extended by differential conductance-based synapses (Pfanzelt et al., 2008). As the described stimulation paradigm allows varying several parameters, it provides, in combination with the pharmacological and modeling approach, a useful means to assess differences in synaptic signal processing in frog tonic and phasic neurons.

2 Differential Intrinsic Response Dynamics Determine Synaptic Signal Processing in Frog Vestibular Neurons

The Journal of Neuroscience, April 18, 2007 • 27(16):4283–4296 • 4283

Behavioral/Systems/Cognitive

Differential Intrinsic Response Dynamics Determine Synaptic Signal Processing in Frog Vestibular Neurons

Mathieu Beraneck,[1]* Sandra Pfanzelt,[1]* Isabelle Vassias,[1] Martin Rohregger,[2] Nicolas Vibert,[1] Pierre-Paul Vidal,[1] Lee E. Moore,[1] and Hans Straka[1]

[1]Laboratoire de Neurobiologie des Réseaux Sensorimoteurs, Centre National de la Recherche Scientifique, Unité Mixte de Recherche 7060, Université Paris Descartes, 75270 Paris cedex 06, France, and [2]Department of Physiology, Ludwigs-Maximilians-Universität Munich, 80336 Munich, Germany

Central vestibular neurons process head movement-related sensory signals over a wide dynamic range. In the isolated frog whole brain, second-order vestibular neurons were identified by monosynaptic responses after electrical stimulation of individual semicircular canal nerve branches. Neurons were classified as tonic or phasic vestibular neurons based on their different discharge patterns in response to positive current steps. With increasing frequency of sinusoidally modulated current injections, up to 100 Hz, there was a concomitant decrease in the impedance of tonic vestibular neurons. Subthreshold responses as well as spike discharge showed classical low-pass filter-like characteristics with corner frequencies ranging from 5 to 20 Hz. In contrast, the impedance of phasic vestibular neurons was relatively constant over a wider range of frequencies or showed a resonance at ~40 Hz. Above spike threshold, single spikes of phasic neurons were synchronized with the sinusoidal stimulation between ~20 and 50 Hz, thus showing characteristic bandpass filter-like properties. Both the subthreshold resonance and bandpass filter-like discharge pattern depend on the activation of an I_D potassium conductance. External current or synaptic stimulation that produced impedance increases (i.e., depolarization in tonic or hyperpolarization in phasic neurons) had opposite and complementary effects on the responses of the two types of neurons. Thus, membrane depolarization by current steps or repetitive synaptic excitation amplified synaptic inputs in tonic vestibular neurons and reduced them in phasic neurons. These differential, opposite membrane response properties render the two neuronal types particularly suitable for either integration (tonic neurons) or signal detection (phasic neurons), respectively, and dampens variations of the resting membrane potential in the latter.

Key words: **semicircular canal; resonance; potassium; low-pass filter; bandpass filter; frequency-tuned channels**

Introduction

Parallel channels that mediate sensory signals with different dynamics from the periphery through hierarchical levels of central nervous nuclei seem to be a common feature of sensory pathways as shown by the organization of the visual (Shapley, 1990; Merigan and Maunsell, 1993), auditory (Cant and Benson, 2003), or somatosensory (Johnson and Hsiao, 1992) systems. In the vestibular system, head movement-related signals cover a wide dynamic spectrum that ranges from static head deviation to extremely high acceleration profiles during fast locomotion. As in other sensory systems, signals are likely mediated by multiple frequency-tuned channels (Goldberg, 2000; Straka and Dieringer, 2004). This organization is mirrored by separate pathways for motor commands from second-order vestibular neurons (2°VNs) to extraocular and spinal motor nuclei to meet the different dynamic ranges of individual motoneuronal pools (Büttner-Ennever, 2005; Straka et al., 2005).

The presence of multiple subtypes of vertebrate 2°VNs that differ in intrinsic membrane properties is compatible with parallel vestibulo-motor signal pathways (Straka et al., 2005). In frog, 2°VNs form two distinct, non-overlapping populations of tonic and phasic neurons (Straka et al., 2004). In response to positive current steps, tonic 2°VNs fire continuously, whereas phasic 2°VNs are characterized by rapid spike discharge adaptation and a pronounced rectification. The presence of highly phasic neurons in frog vestibular pathways (Precht et al., 1971; Straka et al., 2005), in contrast to other vertebrates, might be a specific adaptation to its locomotor style. Prey capture in frogs consists of long periods of immobility with static head deviations at the lower end of the dynamic range and brief, rapid head/body movements that can reach up to 1000°/s (Roche King and Comer, 1996). For such a locomotor pattern, a self-motion detection system with particularly phasic neurons as event detectors and tonic neurons that allow stabilization of gaze and posture in the absence of body motion appears most suitable. Accordingly, frog tonic and phasic 2°VNs might function as distinct filter sets, appropriate for coding and transmission of low- and high-dynamic signal components.

Neuronal filter characteristics are primarily determined by

Received Dec. 4, 2006; revised Feb. 9, 2007; accepted March 9, 2007.

This work was supported by the Marie-Curie Training Sites Contracts QLK5-CT-2000-60087 (Germany) and HPMT-CT-2000-00008 (France) and by Deutscher Akademischer Austauschdienst Grant D/05/40377.

*M.B. and S.P. contributed equally to this work.

Correspondence should be addressed to Dr. H. Straka, Laboratoire de Neurobiologie des Réseaux Sensorimoteurs, Centre National de la Recherche Scientifique, Unité Mixte de Recherche 7060, Université Paris Descartes, 45, rue des Saints-Pères, 75270 Paris cedex 06, France. E-mail: hans.straka@univ-paris5.fr.

DOI:10.1523/JNEUROSCI.5232-06.2007

 0270-6474/07/274283-14$15.00/0

intrinsic membrane properties. The ability of a neuron to preferentially respond in a particular frequency range is usually tested by injection of dynamic current waveforms and is expressed by the presence of a response resonance at a non-zero frequency (Moore and Buchanan, 1993; Hutcheon and Yarom, 2000; Izhikevich, 2001). Such a resonance occurs in mammalian 2°VNs and suggests that central vestibular neurons selectively respond to preferred frequencies (du Lac and Lisberger, 1995; Av-Ron and Vidal, 1999; Ris et al., 2001; Beraneck et al., 2003). Because filter properties are the result of specifically adjusted membrane conductances, the integration of synaptic events depend on particular signal features (amplitude/time course) as well as on the interaction with postsynaptic somatic/dendritic voltage-gated channels (Hausser et al., 2000). The present study uses the isolated brain of adult frogs to study the differential dynamics of the intrinsic membrane properties of phasic and tonic 2°VNs and their respective role for the signal processing of monosynaptic labyrinthine inputs.

Materials and Methods

Electrophysiology and pharmacology. In vitro experiments were performed on the isolated brains of 42 grass frogs (*Rana temporaria*) and complied with *Principles of Animal Care* (publication 86-23, revised 1985 by the National Institute of Health). The government of Oberbayern (211-2531-31/95) granted permission for these experiments. As described previously (Straka and Dieringer, 1993), animals were deeply anesthetized with 0.1% 3-aminobenzoic acid ethyl ester (MS-222) and perfused transcardially with iced Ringer's solution (in mM: 75 NaCl, 25 $NaHCO_3$, 2 $CaCl_2$, 2 KCl, 0.5 $MgCl_2$, and 11 glucose, pH 7.4). Thereafter, the skull and the bony labyrinth were opened by a ventral approach. After dissecting the three semicircular canals on each side, the brain was removed with all labyrinthine end organs attached to the VIIIth nerve. Subsequently, the brain was submerged in iced Ringer's solution, and the dura, labyrinthine end organs, and choroid plexus covering the IVth ventricle were removed. In all experiments, the cerebellum remained attached to the brainstem, whereas the forebrain was removed. Brains were used up to 4 d after their isolation and were stored overnight at 6°C in continuously oxygenated Ringer's solution (carbogen, 95% O_2/5% CO_2) with a pH of 7.5 ± 0.1. For the experiments, the brainstem was glued with cyano acrylate to a plastic mesh that was fixed with insect pins to the sylgard floor of a chamber (2.4 ml volume) and continuously perfused with oxygenated Ringer's solution at a rate of 1.3–2.1 ml/min. The temperature of the Ringer's solution in the chamber was electronically controlled and maintained at 14 ± 0.1°C. In some of the experiments, responses of neurons were recorded both at 14°C and after increasing the temperature within 10–15 min to 16–17°C.

The recorded neurons were identified as second-order vestibular neurons by their monosynaptic responses to electrical stimulation of vestibular nerve afferent fibers. For this purpose, all three semicircular canal nerves were stimulated separately with single constant-current pulses (0.2 ms; 1–15 μA) applied across suction electrodes (120–150 μm diameter). Pulses were produced by a stimulus isolation unit (A 360; World Precision Instruments, Sarasota, FL) at a rate of 0.5 Hz. Glass microelectrodes for extracellular and intracellular recordings were made with a horizontal puller (P-87 Brown/Flaming). Electrodes for extracellular field potential recordings were beveled (30°, 20 μm tip diameter) and filled with 2 M sodium chloride (~1 MΩ). Electrodes for intracellular recordings were filled with 3 M potassium chloride, which gave a final resistance of ~70–90 MΩ. Neuronal recordings were made in bridge or in discontinuous current-clamp mode (SEC-05L; NPI Electronic, Tamm, Germany).

At the beginning of each experiment, presynaptic (N_0) and postsynaptic (N_1) field potentials evoked by separate stimulation of the three semicircular canal nerve branches were recorded at a reference recording site in the vestibular nuclei (Straka et al., 1997). The amplitude of the N_1 component served to optimize the positions of the stimulus electrodes and to determine the stimulus threshold for each stimulus site. Vestibular neurons were recorded in all vestibular subnuclei, except the most medial parts of the medial vestibular nucleus. As reported in previous studies, most of the vestibular neurons recorded in the isolated frog brain had no spontaneous discharge at their resting membrane potential, which was usually more than −58 mV (Straka et al., 2004).

The identified 2°VNs were classified as either phasic or tonic neurons based on their responses to the injection of long, positive current steps (Straka et al., 2004). The response properties in the frequency domain and the discharge dynamics of both types of 2°VNs were determined using two protocols of sinusoidally modulated current injections. The first stimulus profile consisted of a 30 or 44 s (t_{total}) sinusoidally modulated current with a frequency that logarithmically increased from 0 to 100 Hz ["ZAP function": $I(t) = A \sin(\omega \times t^b)$, with frequency $F = \omega/2\pi$ and $b = 3$ (Hutcheon et al., 1994)]. Dynamic membrane properties were determined from averaged responses of two to four single sweeps with a peak-to-peak amplitude of 5–25 mV. With larger injected currents, action potentials were triggered on the depolarizing half cycle, and the frequency range of the discharge was determined. For both phasic and tonic 2°VNs, the firing bandwidth was defined as the minimum (F_{min}) and maximum (F_{max}) frequency in which spikes were triggered at a particular current intensity. In addition, the maximal frequency at which neurons still discharged more than one spike per cycle, i.e., the modulation peak frequency (F_{mod}) was determined for tonic 2°VNs. For phasic 2°VNs, the peak frequency was calculated as $F_{peak} = 100 \times (((t_{Fmin} + t_{Fmax})/2)/t_{total})^2$. ZAP stimuli were supplemented in some neurons by a second protocol that consisted of 5-s-long sinusoidally modulated current injections at 19 discrete frequencies between 0.4 and 100 Hz (du Lac and Lisberger, 1995; Ris et al., 2001). The current amplitude was adjusted at 0.4 Hz such that the peak-to-peak response amplitude was ~15 mV. For the analysis of the data, the term impedance was defined as the ratio of the fast Fourier transforms of the voltage and current values. Because the evoked responses were in part nonlinear, the measured first-order ratio may not be identical to a linear impedance. Nevertheless, this is an effective way to distinguish neuronal types.

Because the responses at low frequencies gave somewhat variable results, the impedance function was not used below 1 Hz for ZAP stimuli and 0.4 Hz for single sinusoidal stimulations frequencies. The resonant behavior of the impedance was quantified and expressed as the ratio (Q) between the maximal impedance and the impedance at the lowest frequency.

Bath application of the potassium channel blocker 4-aminopyridine (4-AP) (5 μM to 1 mM) was used to investigate the putative contribution of voltage-dependent potassium conductances to the nonlinear response properties of phasic 2°VNs. Single sweeps of current stimuli and voltage responses were digitized at 4.1 kHz (CED 1401; Cambridge Electronic Design, Cambridge, UK) and analyzed off-line (SIGNAL; Cambridge Electronic Design). Synaptic potentials were digitized at 20 kHz and analyzed from averages of 20–30 single sweeps after electronic subtraction of the extracellular field potential recorded in the vicinity.

Statistical differences in parameters were estimated using the Mann–Whitney U test (unpaired parameters) and the Wilcoxon's signed rank nonparametric test (paired parameters) (Prism; GraphPad Software, San Diego, CA). All averaged results were expressed as means ± SEM unless stated otherwise. Graphical presentations were made with the aid of commercially available computer software [Origin (Microcal Software, Northampton, MA) or Corel Draw (Corel, Ottawa, Ontario, Canada)].

Immunocytochemistry. Immunohistochemical detection of the Kv1.1 potassium channel protein was performed on frog whole brains subsequent to the recording of vestibular neurons for 4 d ($n = 4$) or on brains obtained from frogs freshly perfused with fixative ($n = 3$). In the latter case, frogs were anesthetized with MS-222 and transcardially perfused with 30 ml of an ice-cold 0.9% NaCl solution, followed by 100 ml of 4% paraformaldehyde in 0.1 M phosphate buffer. Brains from freshly perfused frogs and those from *in vitro* experiments were kept overnight in the fixative. After cryoprotection in 15 and 30% sucrose, coronal sections were cut at 30 μm on a cryostat and kept in 0.01 M PBS, pH 7.4. Immunohistochemical detection of Kv1.1 was performed as described by Popratiloff et al. (2003). Briefly, after rinse in 0.1% Triton in 0.01 M PBS (PBS-T), free-floating sections were treated with 50% alcohol and preincubated in 10% normal goat serum in PBS-T for 30 min. After incubation

overnight at room temperature in a 1:500 dilution of the primary rabbit anti-Kv1.1 polyclonal antibody (Alomone Labs via Euromedex, Strasbourg, France) in PBS-T, antibody binding was detected with a cyanine 3-conjugated goat anti-rabbit antibody (Jackson ImmunoResearch via Interchim, Montluçon, France). Subsequently, sections were washed, air dried, and coverslipped with Vectashield (Vector Laboratories via Biovalley, Conches, France). Sections were analyzed by laser scanning confocal microscopy (LSM 510; Zeiss, Oberkochen, Germany) at a wavelength of 543 nm. Stacks of 10–20 confocal images were generated with a 20×/0.5 objective and a plan Apochromat 40×/1.3 oil immersion objective. Images for the figures were produced by horizontal projection of the entire stack. The diameters of the Kv1.1 immunopositive neurons in the dorsal hindbrain between the cerebellum and the obex were determined using Metaview software (Roper Scientific, Paris, France).

Results

Classification of second-order vestibular neurons

Intracellular recordings were obtained from a total of 220 neurons in the vestibular nuclei of the isolated frog whole brain. Based on the differences of their responses to long positive current steps with amplitudes that depolarized neurons above spike threshold, all VNs were characterized as either phasic or tonic (Straka et al., 2004). The response of the larger population of neurons ($n = 167$; 76%) consisted of a high-frequency burst of one to three spikes within the first 100 ms and the absence of a subsequent continuous discharge (Fig. 1*A*; *C*, black bar). In contrast, the smaller population of neurons ($n = 53$; 24%) fired continuously throughout the positive current step (Fig. 1*B*; *C*, gray bar). In the latter, the discharge frequency increased with the amplitude of the current step until the firing rate saturated at ~70–80 spikes/s. The presence of, as opposed to the lack of, a persistent discharge during positive current steps unequivocally separated tonic from phasic neurons (Fig. 1*C*, gray and black bars) and suggests that the two distinct populations of neurons differ considerably in their intrinsic membrane properties. The ~4:1 ratio of phasic to tonic neurons agrees with the previously reported predominance of phasic VNs in frog (Straka et al., 2004).

All phasic and tonic VNs were identified as second-order (2°) neurons by the activation of a monosynaptic EPSP after separate electrical stimulation of the three ipsilateral semicircular canal nerves (Fig. 1*C*, insets). The majority of phasic and tonic 2°VNs (~85%) received their monosynaptic afferent input from only one of the three semicircular canals. This input originated in approximately equal proportions from the horizontal, the anterior vertical, and the posterior vertical canal. In the remaining neurons (~15%), a monosynaptic response was evoked by stimulation of two or all three ipsilateral canal nerves. No differences were encountered between phasic and tonic 2°VNs concerning the origin or amount of convergence of the inputs from a particular semicircular canal. This suggests that the two subtypes are not exclusive parts of distinct vestibular pathways that would differ in their spatial selectivity for different angular head acceleration signals. In fact, as shown previously, both types contribute to vestibulo-ocular and vestibulo-spinal reflexes and mediate semicircular canal and macular organ signals (Straka et al., 2004).

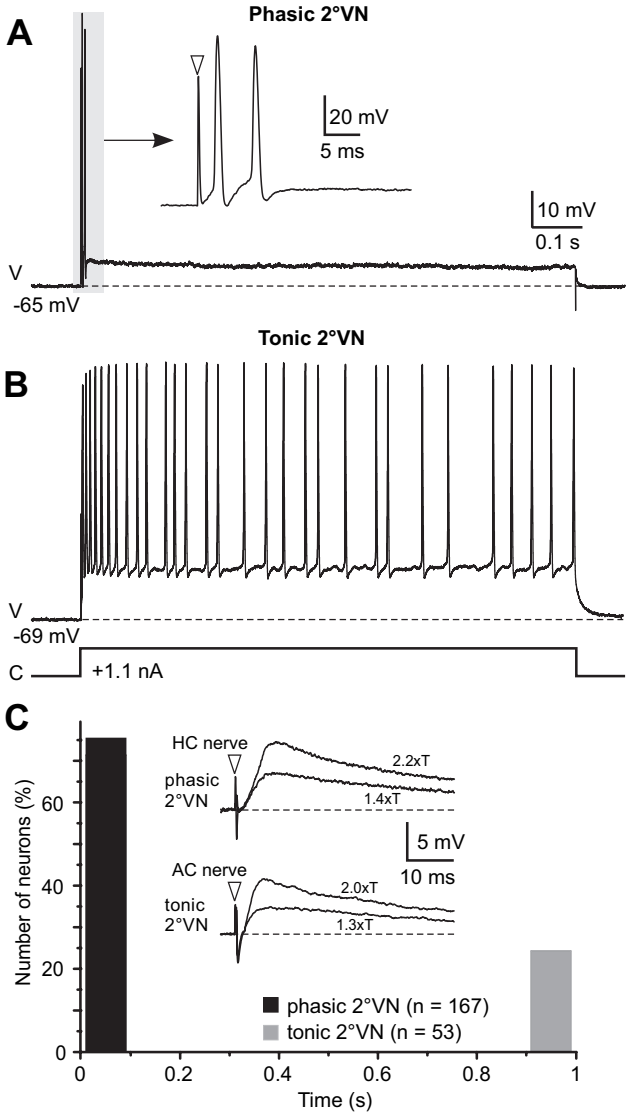

Figure 1. Discharge pattern of phasic and tonic 2°VNs. ***A***, ***B***, A short burst of two spikes (***A***) and a continuous discharge (***B***) evoked by injection of positive current steps of 1.1 nA (trace below tonic cell) differentiate between phasic and tonic 2°VNs; the inset in ***A*** shows the short initial burst (gray area) of the phasic 2°VNs at an extended timescale. ***C***, The evoked burst discharge in all phasic 2°VNs (76%) was confined to the first 100 ms (black bar); the continuous discharge of all tonic 2°VNs (24%) began immediately after stimulus onset and lasted throughout the entire length of current step (gray bar). Insets in ***C*** show monosynaptic EPSPs evoked by stimulation of the horizontal (HC) and the anterior (AC) vertical canal nerve at two stimulus intensities, given as multiples of the N_1 field potential component (xT) in the phasic and tonic 2°VNs illustrated in ***A*** and ***B***. Horizontal dashed lines in ***A*** and ***B*** and insets in ***C*** indicate resting membrane potentials at −65 and −69 mV, respectively. Arrowheads in the insets in ***A*** and ***C*** indicate stimulus onset. Records in ***A*** and ***B*** are single sweeps and in ***C*** averages of 24 responses. The calibration in ***A*** applies also to ***B***. V, Voltage; C, current.

Subthreshold response dynamics of tonic and phasic second-order vestibular neurons

Tonic second-order vestibular neurons

Injection into tonic 2°VNs ($n = 12$) of sinusoidally modulated currents of relatively small amplitude (±0.1–0.3 nA) with a frequency that increased logarithmically up to 100 Hz (ZAP stimuli) resulted in a maximal peak-to-peak voltage modulation of ~13 mV (Fig. 2*A*). Because of the rather negative resting membrane potential of these neurons (mean, −71.6 ± 3.2 mV), the small voltage modulation did not trigger a spike discharge.

The sinusoidally modulated responses in all tonic 2°VNs were maximal at the lowest frequency used for the analysis of the responses to ZAP stimuli (1 Hz) and decreased gradually with stimulus frequency (Fig. 2*A*). Accordingly, the calculated impedance was maximal at 1 Hz (mean, 26.9 ± 5.5 MΩ) and declined in a manner consistent with the nearly passive electronic structure for

4286 • J. Neurosci., April 18, 2007 • 27(16):4283–4296

individual neurons (Fig. 2C_2) to reach ~50% of the initial value at 100 Hz (mean, 14.0 ± 3.0 MΩ). The sinusoidal responses were essentially in-phase with the stimulus at low frequencies (mean, −4.6 ± 1.9° at 1 Hz) but were considerable phase lagged at 100 Hz (mean, −50.6 ± 14.2°) (Fig. 2C_2). This phase shift was variable between individual tonic 2°VNs and reached up to −90° at 100 Hz in some neurons. Given the gradual reduction in impedance and the increasing phase lag of the responses at higher stimulus frequencies, tonic 2°VNs behaved like a low-pass filter. Because in all tonic 2°VNs the impedance was maximal at the lowest modulation frequency, the *Q* value (see Material and Methods) was 1, thus indicating the absence of a resonance of the impedance in these 2°VNs.

To exclude the possibility that the reduction in the impedance with increasing frequency was related to the absence of a steady-state frequency in the ZAP stimuli, sequences of sinusoidally modulated currents with discrete frequencies (between 0.4 and 100 Hz) were applied (Fig. 2*B*). As for the ZAP stimuli, the impedance of the tested neurons ($n = 5$) was maximal at the lowest frequency used for stimulation and gradually decreased with increasing frequency in parallel with an increase in phase lag (Fig. 2C_1) as for the ZAP stimuli (Fig. 2C_2). Independent of the stimulus paradigm, the impedance profile exhibited characteristic low-pass filter-like properties with a range of the corner frequency in most neurons between 5 and 20 Hz (Fig. 2C_1,C_2).

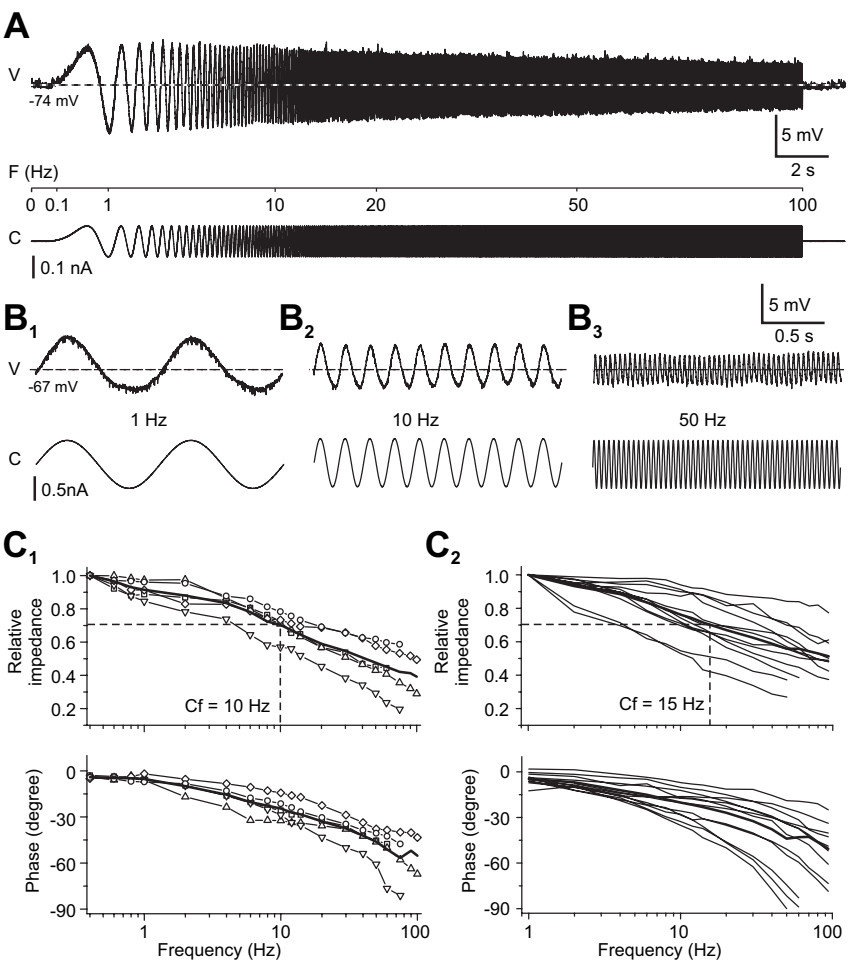

Figure 2. Response dynamics of tonic 2°VNs. ***A***, Response evoked by injection of a small-amplitude, sinusoidally modulated current that increased logarithmically in frequency up to 100 Hz (ZAP). ***B***, Responses of a tonic 2°VN to injection of multiple cycles of sinusoidally modulated currents at discrete frequencies of 1 Hz (***B*$_1$**), 10 Hz (***B*$_2$**), and 50 Hz (***B*$_3$**). Horizontal dashed lines indicate the resting membrane potential at −74 mV (***A***) and −67 mV (***B*$_1$**–***B*$_3$**). Calibration in ***B*$_3$** applies to ***B*$_1$** and ***B*$_2$**. ***C***, Bode plots of impedance and phase of the responses of tonic 2°VNs tested with discrete frequencies ($n = 5$; ***C*$_1$**) and Bode plots obtained from tonic 2°VNs tested with ZAP stimuli ($n = 12$; ***C*$_2$**). The impedance of each neuron was normalized to the value obtained at a stimulation frequency of 0.4 Hz in ***C*$_1$** and of 1 Hz in ***C*$_2$**; thick lines in ***C*$_1$** and ***C*$_2$** are the average of the respective population of neurons, and the dashed lines are the corner frequency (Cf). V, Voltage; F, frequency; C, current.

Phasic second-order vestibular neurons

The dynamics of the intrinsic membrane properties was tested in 47 phasic 2°VNs using injection of sinusoidal currents up to 100 Hz in the ZAP mode or with sequences of discrete frequencies. At resting membrane potential (mean, −64.8 ± 1.2 mV; $n = 47$), sinusoidally modulated currents of ± 0.6 nA evoked a mean peak-to-peak voltage modulation at low stimulus frequencies of ~16 mV that was subthreshold for spike discharge (see Figs. 3A_1–A_3, 4*A*,*C*). The mean impedance of phasic 2°VNs at 1 Hz was on the average 17.0 ± 1.6 MΩ, and responses were in-phase with the stimulus (mean, −0.4 ± 0.6°) (Fig. 3*B*). At a stimulus frequency of 100 Hz, the impedance decreased to ~60% of the initial value (mean, 10.8 ± 1.6 MΩ), with an average phase lag of −52.5 ± 7.7° (Fig. 3*B*). Compared with tonic 2°VNs, the impedance of phasic 2°VNs was significantly lower ($p \leq 0.05$), compatible with the larger current required for approximately the same peak-to-peak responses in the latter neurons (Straka et al., 2004).

Most importantly, in contrast to tonic 2°VNs, the sinusoidally modulated responses of most phasic 2°VNs (36 of 47 neurons; 77%) increased in amplitude with stimulus frequency to exhibit a maximum at frequencies ranging from 2 to 60 Hz in different neurons (Fig. 3*A*). Because the impedance resonance at resting membrane potential varied in magnitude and frequency between different phasic 2°VNs, the impedance profile was quantified by determining the ratio between the impedance at the resonance frequency and at the lowest stimulus frequency used for the analysis (1 Hz; *Q* value; see Materials and Methods). Three different types of responses of phasic 2°VNs were distinguished (Fig. 3A_1–A_3; *B*, gray squares, circles, and triangles). The most common profile ($n = 31$) had a *Q* value >1, with a resonance centered at ~4 Hz (simple-resonant response) (Fig. 3A_2, *; *B*, gray circles). A second group of phasic 2°VNs ($n = 11$) had a *Q* value of 1, with an impedance profile comparable with those of tonic 2°VNs (non-resonant response) (Fig. 3A_1; *B*, gray squares). Finally, five phasic 2°VNs were recorded that had *Q* values of ~1 but exhibited a trough-like depression (Figs. 3A_3, 4*A*, black diamonds) before the resonance peak (Figs. 3A_3, 4*A*, **) (trough-resonant response). The trough usually occurred above 10 Hz, whereas the resonance peak was usually at ~45 Hz (Figs. 3*B*, gray triangles, 4*B*). Thus, up to ~20–30 Hz, the impedance of most phasic 2°VNs (simple- and trough-resonant neurons) decreased only

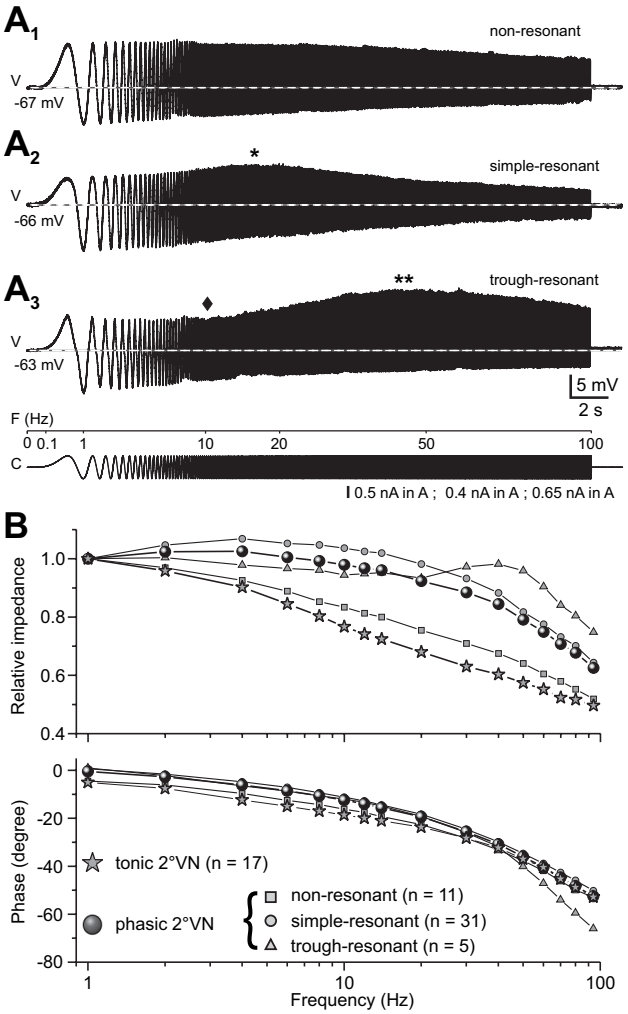

Figure 3. Response dynamics of phasic 2°VNs. ***A*$_1$–*A*$_3$**, Typical examples of impedance profiles of three different phasic 2°VNs calculated from responses to injection of small-amplitude ZAP currents. Based on their shape, responses were classified as nonresonant (***A*$_1$**), simple resonant (***A*$_2$**), or trough resonant (***A*$_3$**). Simple-resonant responses exhibit a single resonance peak (*), and trough-resonant responses exhibit a trough-like depression (black diamond) before the resonance peak (**). Horizontal dashed lines indicate resting membrane potential (−67 mV in ***A*$_1$**; −66 mV in ***A*$_2$**; −63 mV in ***A*$_3$**). Calibration in ***A*$_3$** applies to ***A*$_1$** and ***A*$_2$**. ***B***, Bode plots comparing impedance and phase profiles of all phasic (filled circles) and tonic (filled stars) 2°VNs; phasic neurons were further separated as nonresonant (gray circles), simple resonant (gray circles), and trough resonant (gray triangles). V, Voltage; F, frequency; C, current.

slightly with stimulus frequencies, whereas the impedance of tonic 2°VNs declined gradually and continuously from the lowest frequencies (Fig. 3*B*).

The different response profiles of phasic 2°VNs, however, do not imply the presence of distinctly different subtypes of phasic 2°VNs but suggest that the response dynamics of the phasic cells are variable and depend on particular membrane parameters. Trough-resonant responses were observed in neurons with a more depolarized resting membrane potential (−59.0 ± 3.0 mV; $n = 5$; $p \leq 0.05$) compared with simple-resonant (−66.4 ± 2.4 mV; $n = 31$) or nonresonant (−66.7 ± 1.6 mV; $n = 11$) responses. In a given neuron, the resonance changed in magnitude and frequency with polarization of the membrane potential. After membrane hyperpolarization, trough-resonant responses changed into simple-resonant responses, as illustrated by the responses of the phasic 2°VNs in Figure 4 (*A*, gray and black traces, *B*, black and white circles). The observed shift in the profile and the occurrence of trough-resonant responses at a more depolarized membrane potential was always accompanied by a decrease in impedance (Fig. 4*B*), compatible with the general observation that neurons with trough-resonant responses had a significantly lower impedance than neurons exhibiting other impedance profiles ($p \leq 0.01$). Assuming thus a continuous range of impedance resonance profiles that depend on the actual membrane potential, phasic 2°VNs seem to vary between different, interchangeable response modes.

Different conductances in tonic and phasic second-order vestibular neurons

Responses evoked by sinusoidally modulated current injections of both tonic and phasic 2°VNs exhibited a marked asymmetry (Fig. 5*A*). This asymmetry resulted from different relative contributions of the depolarizing and the hyperpolarizing half cycles to the peak-to-peak responses and was oppositely oriented in tonic and phasic 2°VNs and particularly obvious for responses with peak-to-peak amplitudes >20–25 mV (Fig. 5A_1,A_2). The asymmetry was quantified by calculating the ratio of the amplitudes (>20 mV) of the depolarizing and hyperpolarizing half cycles of sinusoidally modulated responses at low stimulus frequencies (Fig. 5A_1,A_2, arrows). This ratio indicated that the depolarizing half waves of all tonic 2°VNs were larger than the hyperpolarizing half waves (ratio >1) (Fig. 5A_1,A_3). In contrast, in phasic 2°VNs, the sinusoidal responses were dominated by the considerably larger amplitude of the hyperpolarizing half cycle (ratio <1) (Fig. 5A_2,A_3). In some phasic 2°VNs with a resting membrane potential close to −60 mV, the asymmetry between the hyperpolarizing and depolarizing component was pronounced and resulted from a particularly small depolarizing half wave (Fig. 5*B*, red trace). In addition, with larger current stimulus amplitude, a distortion appeared in the falling phase of the depolarizing half wave response of these neurons (Fig. 5*B*, pink and black traces). This was attributable to the fact that the membrane potential started to hyperpolarize (white arrowhead and vertical dashed line) before the maximal depolarizing current is reached (vertical dotted line). This distortion likely reflects the activation of a voltage-dependent conductance with a threshold close to the resting membrane potential of this neuron. The increase in amplitude and advance of the peak depolarization with current intensity (Fig. 5*B*, red, pink, and black traces) is compatible with previous results on the slope threshold of phasic neurons during ramp-like current injection (Straka et al., 2004).

The differential sinusoidal responses of the two types of 2°VNs suggest that the impedance in tonic 2°VNs increases with depolarization, whereas the impedance in phasic 2°VNs increases with hyperpolarization. Such an antagonistic behavior was in fact observed in neurons in which the membrane potential was changed by constant-current injections (Fig. 5*C*,*D*). The impedance of tonic 2°VNs increased by 50–100% with membrane depolarizations of ~10 mV at low stimulus frequencies of up to 10 Hz (Fig. 5C_1,C_2). This increase was particularly obvious during the depolarizing half cycles (Fig. 5C_1, compare red and black traces) and complies with the dominance of this half cycle in the responses of tonic 2°VNs (Fig. 5A_1,*C*). This suggests an activation of non-inactivating calcium or sodium inward currents that would allow boosting excitatory responses in these neurons. In contrast, the impedance of phasic 2°VNs decreased by ~50% during a depolarization of similar magnitude for stimulus frequencies of up to 40 Hz (Fig. 5D_1,D_2). The decreased impedance, however, reduced

4288 • J. Neurosci., April 18, 2007 • 27(16):4283–4296

the hyperpolarizing half cycle to a larger extent than the depolarizing half cycle (Fig. 5D_1, compare red and black traces). Given the pronounced decrease in impedance during depolarization, the intrinsic membrane properties of phasic 2°VNs appear to be dominated by voltage-gated potassium conductances that are activated during depolarization of the neuron. Moreover, the kinetics of the latter conductance might be essential for the particularly fast termination of the discharge during injection of step-like currents.

Discharge dynamics of phasic and tonic second-order vestibular neurons

Using large-amplitude sinusoidal currents, spike discharge was evoked in both tonic and phasic 2°VNs. Because none of the recorded 2°VNs were spontaneously active at resting membrane potential (see discussion by Straka et al., 2004), there was no modulation of a tonic activity but rather a correlation of the discharge with the depolarizing half cycles of the sinusoidal responses. In accordance with the differences in subthreshold responses, the discharge dynamics of the two types of neurons differed as well.

Tonic second-order vestibular neurons

Injection of large sinusoidally modulated currents in tonic 2°VNs at resting membrane potential ($n = 10$) evoked voltage modulations with peak-to-peak amplitudes of ~35 mV and superimposed action potentials on the depolarizing half cycle (Fig. 6A,B). At low stimulus frequencies, the discharge consisted of multiple spikes per depolarizing half cycle (Fig. 6B_1) that decreased in number with increasingly shorter cycle length up to 6 Hz (F_{mod}; mean, 5.7 ± 0.6 Hz; $n = 10$). Thus, the spike discharge between the lowest stimulus frequency (F_{min} of 1 Hz) and F_{mod} was modulated in firing rate in relation to the underlying membrane potential. Above F_{mod}, only single spikes were triggered that were synchronized with the depolarizing half cycle (Fig. 6B_2,C_1). The regular and reliable firing with each depolarizing half cycle stopped at ~20 Hz (F_{max}; mean, 22.3 ± 3.5 Hz) (Fig. 6B_3). Above F_{max}, few single spikes were elicited on some depolarizing half cycles, but increasingly more cycles were skipped (Fig. 6C_2).

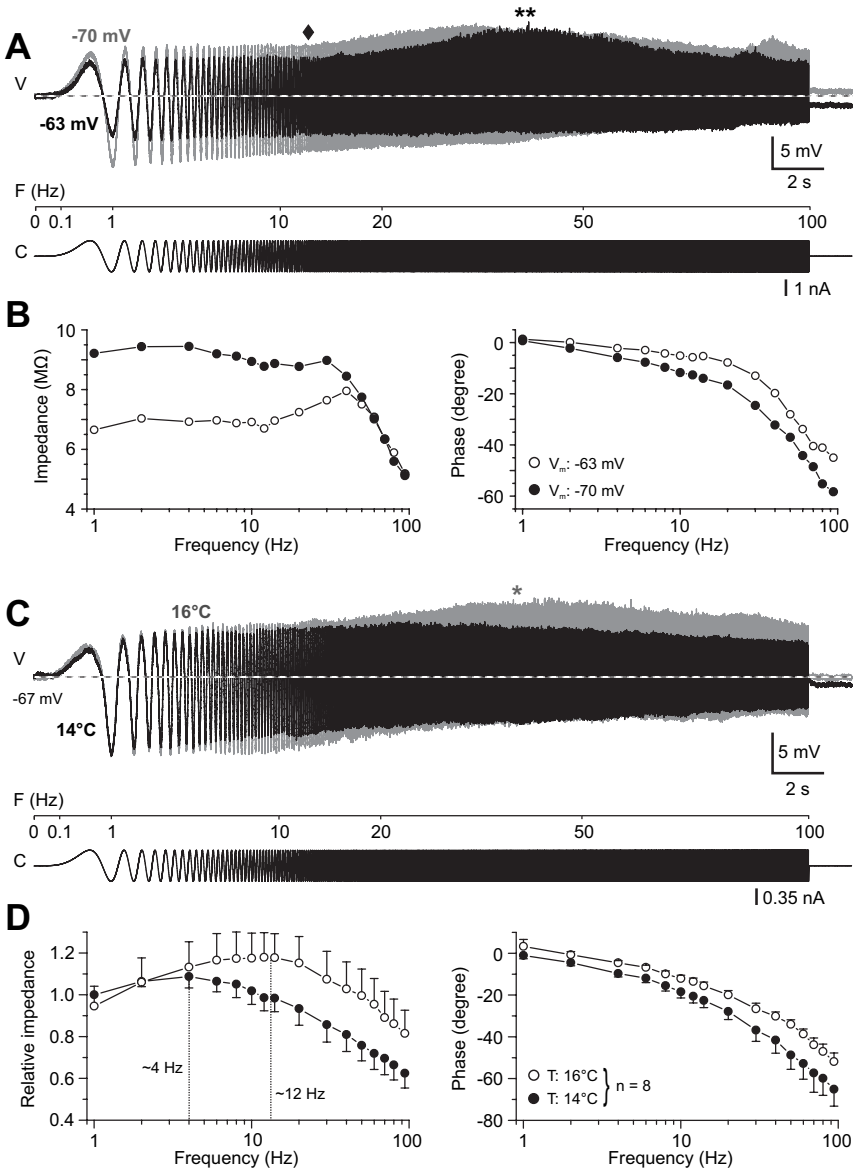

Figure 4. Membrane potential and temperature dependence of the impedance profile of phasic 2°VNs. ***A***, Responses of a phasic 2°VN evoked by injection of small-amplitude ZAP currents at two membrane potentials at −63 mV (black trace) and −70 mV (gray trace). At the more depolarized membrane potential, the response exhibited a trough-like depression (black diamond) before the resonance peak (**) that is facilitated and shifted to higher frequencies compared with the resonance peak at the more hyperpolarized membrane potential. ***B***, Bode plots of impedance and phase of the responses at the two membrane potentials (white and black circles) shown in ***A***. ***C***, Responses of a phasic 2°VN evoked by injection of small-amplitude, ZAP currents at two recording temperatures (14°C, black trace; 16°C, gray trace). Note the increased impedance of the response at higher stimulus frequencies and the pronounced resonance peak (*) at 16°C. ***D***, Bode plots summarizing the impedance and phase of the responses of phasic neurons ($n = 8$) recorded at both 14°C (black circles) and 16°C (white circles). Vertical dashed lines indicate resonance peak frequencies. V, Voltage; F, frequency; C, current.

The discharge pattern was qualitatively similar in all tonic 2°VNs, suggesting a homogeneous population of neurons. However, F_{mod} and F_{max} differed between individual neurons and were sigmoidally distributed across the population (Fig. 6D). According to this distribution, <50% of the neurons discharged multiple spikes above 6 Hz (Fig. 6D, dashed vertical line, F_{mod}) and fired a single spike at each depolarizing half cycle above ~20 Hz (Fig. 6D, dotted vertical line, F_{max}). Inspection indicated, however, that the two limits (F_{mod}, F_{max}) not only depended on the amplitude of the current stimulus but also on the actual resting membrane potential. Therefore, in neurons with a more negative resting membrane potential (e.g., −82 mV in the neuron shown in Fig. 6B), both limits were lower compared with neurons with a less negative resting membrane potential (e.g., −72 mV in the neuron shown in Fig. 6A,C). The restriction of discharge modulation and synchronization to lower stimulus frequencies is compatible with the observed low-pass filter-like

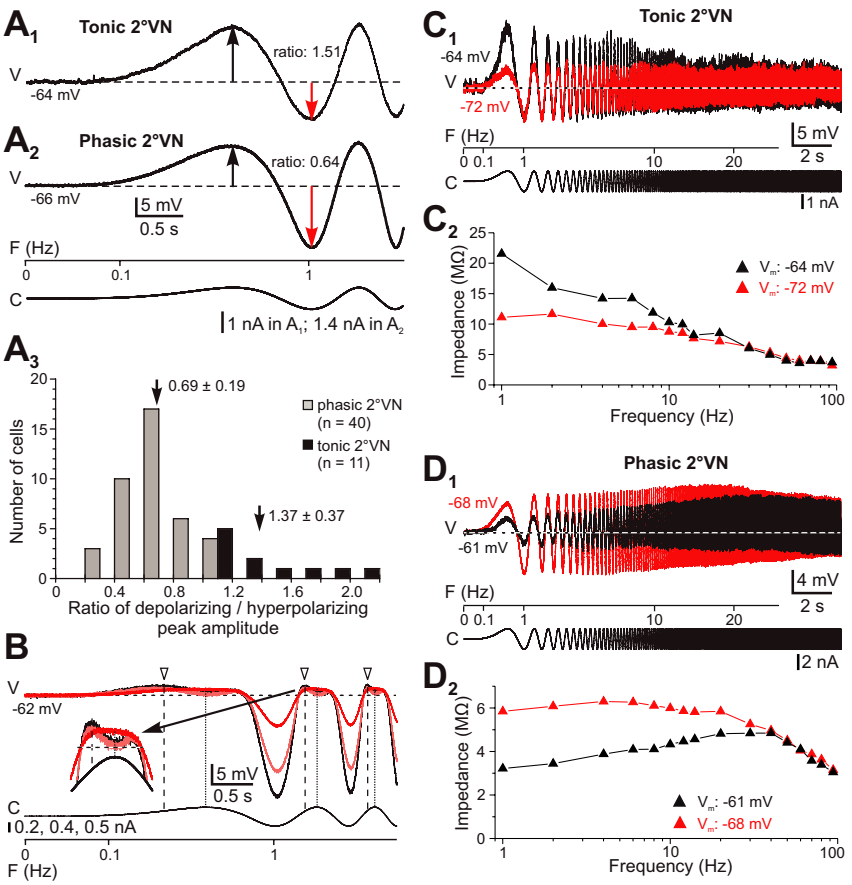

Figure 5. Response asymmetry in tonic and phasic 2°VNs. ***A***, The ratio of the depolarizing (black arrows in A_1, A_2)/hyperpolarizing half wave (red arrow in A_1, A_2) of the responses evoked by sinusoidally modulated currents is >1 for tonic and <1 for phasic 2°VNs (A_3). Horizontal dashed lines in A_1 and A_2 indicate resting membrane potential at −64 mV (A_1) and −66 mV (A_2); arrows and numbers in A_3 indicate mean ± SD of the ratios for tonic and phasic 2°VNs. Calibration in A_2 applies to A_1. ***B***, Response of a phasic 2°VN evoked by ZAP currents. The response shows a marked asymmetry and a particular distortion in the falling phase of the depolarizing half wave at higher stimulus intensities (pink and black traces; see inset for extended timescale); the response peak (white arrowhead and vertical dashed line) occurs before the maximal depolarizing current is reached (vertical dotted line), and the membrane potential starts to hyperpolarize. ***C***, ***D***, Overlay of responses evoked by injection of ZAP currents at resting membrane potential (red traces) and during constant depolarization (black traces) of a tonic (***C***) and a phasic 2°VN (***D***). The impedance during depolarization of the membrane potential (V_m) increases in tonic but decreases in phasic 2°VNs at low- and mid-range frequencies (black triangles in C_2, D_2). Dashed lines in C_1 and D_1 indicate membrane potential before the onset of the stimulus. V, Voltage; F, frequency; C, current.

properties of the subthreshold responses. However, the upper limit of the evoked discharge is not fixed but depends on the membrane potential. In fact, it can be shifted to considerably higher values with increasing membrane depolarization. At membrane potentials close to spike threshold, tonic 2°VNs reliably fire action potentials that are synchronized with each depolarizing half cycle at stimulus frequencies up to ~70 Hz (data not shown) as long as the amplitude of the underlying depolarization reaches spike threshold.

This differential behavior indicates that the filter properties of tonic 2°VNs can be modified by alterations of the membrane potential. Thus, tonic 2°VNs behave like low-pass filters with low cutoff frequencies at particularly negative membrane potentials. With increasing depolarization, e.g., as a result of augmented excitatory inputs or higher temperatures (see below), the cutoff frequency is shifted to higher values, thereby extending the frequency bandwidth for signal transmission. This suggests that, at the more depolarized membrane potentials, the response properties of tonic 2°VNs would be adjusted to the dynamics of the synaptic inputs from labyrinthine nerve afferents that code static head deviation *in vivo* (see Discussion).

Phasic second-order vestibular neurons

Injection at resting membrane potential of large sinusoidally modulated currents in 29 phasic 2°VNs triggered action potentials at stimulus frequencies above ~10 Hz (Fig. 7A_1,A_2,B_2,C,D). At stimulus frequencies below ~10 Hz, no spike discharge was evoked (Fig. 7B_1,D), even with stimulus intensities that exceeded approximately twice the spike threshold at higher frequencies. Analysis indicated that, for peak-to-peak voltage amplitudes of ~30 mV, the minimum frequency required to trigger action potentials was on the average 19.3 ± 1.6 Hz (n = 29). Above this lower limit, the discharge consisted of single action potentials that were synchronized with the peaks of each depolarizing half cycle (Fig. 7B_2,C). This particular firing mode continued with increasing frequency until a sudden cutoff was reached at 40–60 Hz (mean, 47.9 ± 2.7 Hz; n = 29). This upper limit depended on the amount of injected current, was shifted to higher frequencies with larger current intensity (Fig. 7, compare A_1, A_2), and was variable between individual phasic 2°VNs. In some neurons, the discharge was maintained up to 70 Hz. As for tonic 2°VNs, the upper firing limit seemed to be correlated with the decrease in impedance at higher stimulus frequencies as indicated by the reduction in the peak-to-peak response amplitude (Fig. 7B_3).

In contrast to the upper firing limit, the lower limit of phasic 2°VNs was generally more homogeneous. The absence of a spike discharge below ~10 Hz is likely to be related to the fact that the generation of action potentials in phasic 2°VNs not only depends on a particular membrane potential threshold but also on the rate of change of the membrane potential to reach this threshold (~1.4 mV/ms) (Straka et al., 2004). This particular rate threshold is usually not reached with sinusoidally modulated currents <10 Hz and peak-to-peak sine-wave response amplitudes of ~30 mV, thus corroborating the absence of spike discharge at low frequencies in these neurons.

Comparison of the discharge parameters with the subthreshold sinusoidal response parameters indicated that the variability of the lower and upper limits of the evoked discharge in phasic 2°VNs was related to nonresonant, simple-resonant, and trough-resonant impedance profiles of these neurons. Phasic 2°VNs with nonresonant or simple-resonant impedance profiles started to fire action potentials at significantly lower frequencies (17.5 ± 1.4 Hz; n = 42) compared with phasic 2°VNs with a trough-resonant impedance profile (29.9 ± 4.8 Hz; n = 5; $p \leq 0.05$). In the latter neurons, the midpoint of the firing bandwidth (mean,

43.7 ± 3.5 Hz; $n = 5$) and the extended upper limit of the firing range (mean, 60.4 ± 3.4) coincides very well with the resonance peak frequency of the subthreshold responses (~45 Hz) and the impedance profile at high frequencies (Figs. 3*B*, 4*B*). The similarities in the discharge parameters of nonresonant and simple-resonant phasic 2°VNs furthermore support the idea of a continuum of neurons with overlapping and adaptable membrane and discharge properties.

The particular firing behavior and subthreshold responses of phasic 2°VNs can be described as bandpass filters, with peaks centered at 20–40 Hz (Fig. 7*D*, black triangles) and a bandwidth for firing that ranges from 15 to 100 Hz. This contrasts with the low-pass filter properties of tonic 2°VNs in which spike discharge modulation (Fig. 7*D*, white squares) and synchronized activity (Fig. 7*D*, white circles) is restricted to the lower and middle range frequency domains.

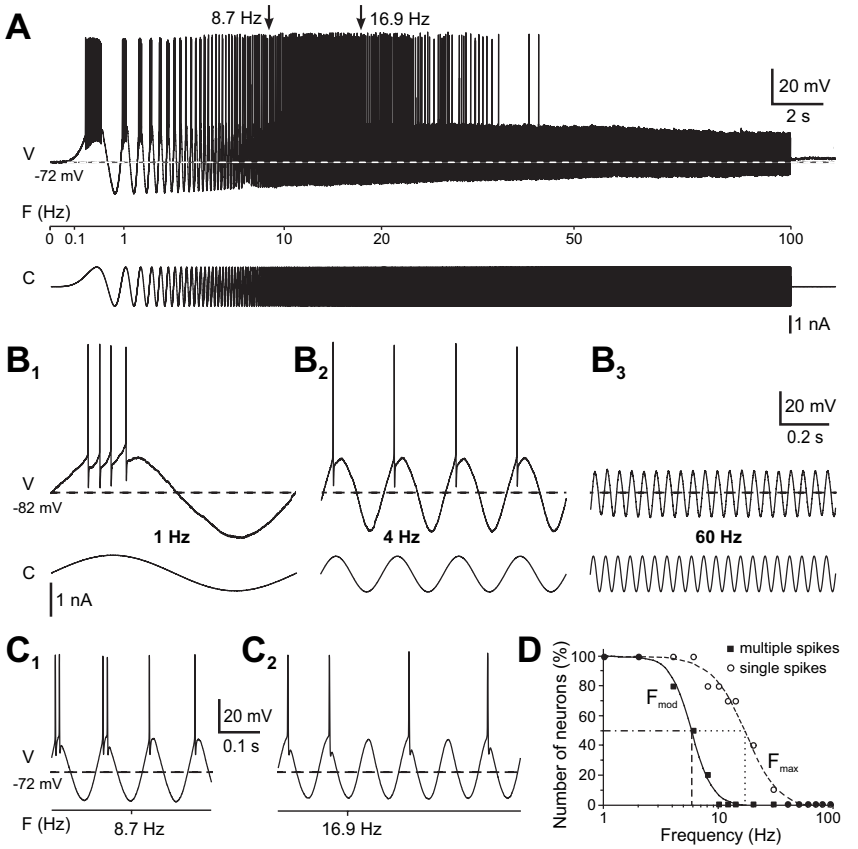

Figure 6. Discharge dynamics of tonic 2°VNs. ***A***, Example of the discharge evoked by injection of large-amplitude ZAP currents. ***B***, Responses of a tonic 2°VN to injection of sinusoidally modulated currents at discrete frequencies of 1 Hz (***B*** $_1$), 4 Hz (***B*** $_2$), and 60 Hz (***B*** $_3$). ***C***, Transition from multiple to single spike discharge (8.7 Hz in ***C*** $_1$) and upper limit of single spike synchronization (16.9 Hz in ***C*** $_2$) of the neuron shown in ***A*** (see arrows in ***A***). Responses in ***A–C*** are single sweeps, and horizontal dashed lines indicate resting membrane potential at −72 mV (***A***, ***C***) and −82 mV (***B***). Calibration in ***B*** $_3$ applies to ***B*** $_1$ and ***B*** $_2$. ***D***, Distribution of the upper limits of multiple spike modulation (black squares and solid line; F_{mod}) and of single spike synchronization (white circles and dashed line; F_{max}) among the tested tonic 2°VNs ($n = 10$). Note that <50% of the tonic 2°VNs fire multiple spikes above ~6 Hz (dashed vertical line) and single spikes above ~20 Hz (dotted vertical line) on each depolarizing half cycle. V, Voltage; F, frequency; C, current.

Temperature dependence of subthreshold responses and discharge range

A direct comparison of the resulting functional aspects of the *in vitro* experiments with data obtained *in viv*o in intact animals is usually aggravated by the temperature difference between both experimental conditions. To facilitate a functional interpretation of the dynamics of frog 2°VNs, the frequency range of responses was determined at different recording temperatures. After a temperature increase of the Ringer's solution in the recording chamber from 14 to 16°C, the impedance of a given phasic 2°VN increased at higher stimulus frequencies (Fig. 4*C*) and the resonance peak shifted by ~8 Hz from 4.0 ± 2.3 to 12.2 ± 2.5 Hz ($p \leq 0.01$; $n = 8$) (Fig. 4*D*). Because the membrane potential did not change during the 2°C increase, this shift in the resonance profile must be attributable to the elevated temperature. An even larger temperature increase consistently caused a depolarization of the membrane potential and thus any change of the impedance resonance profile at higher recording temperatures is attributable to a combined effect of both depolarization (Fig. 4*A*,*B*) and increased temperature (Fig. 4*C*,*D*). The observed impedance increase and the shift of the subthreshold response profiles of phasic 2°VNs at 16°C was paralleled at larger injected sine-wave currents by an extension of the discharge range by 15–20 Hz ($n = 5$; data not shown) toward higher frequencies. In tonic 2°VNs ($n = 2$), a qualitatively similar change, although much less pronounced than in phasic 2°VNs, was observed during a temperature increase from 14 to 16°C. At larger sinusoidal currents that triggered spike discharge, the upper firing limit in the tonic 2°VNs increased by ~10 Hz during the 2°C temperature increase. Taking both the effect of membrane depolarization and higher temperatures on membrane properties into account, a considerably higher impedance peak resonance and upper firing limit of frog vestibular neurons can be assumed in *in vivo* experiments, usually performed at a room temperature of ~22°C (Precht et al., 1974; Rossi and Martini, 1986).

Effect of 4-aminopyridine on the responses of phasic second-order vestibular neurons

The bandpass filter-like properties of phasic 2°VNs require specific conductances that differ from those of tonic 2°VNs. The particularly phasic response to current steps, the marked impedance resonance and its voltage dependence, and the distorted depolarizing half cycle of some phasic 2°VNs (Fig. 5*B*) are likely related to the activation of a voltage-dependent potassium conductance. Bath application of 4-AP at a concentration of 5 μM to 1 mM ($n = 18$) was used to test the presence of inactivating potassium conductances. At high concentrations of 4-AP (>100 μM), which also blocks I_A potassium channels, all recorded 2°VNs became spontaneously active with broad spikes. At low concentrations of 4-AP (5–10 μM; $n = 10$), known to specifically block the I_D potassium channel (Storm, 1988; McCormick, 1991; Wu et al., 2001), neurons remained silent but the amplitude of the responses evoked by injection of sinusoidally modulated currents increased (Fig. 8*A* $_1$,*A* $_2$). In particular, the amplitude of the depolarizing half cycle was enhanced by 4-AP, whereas the hyper-

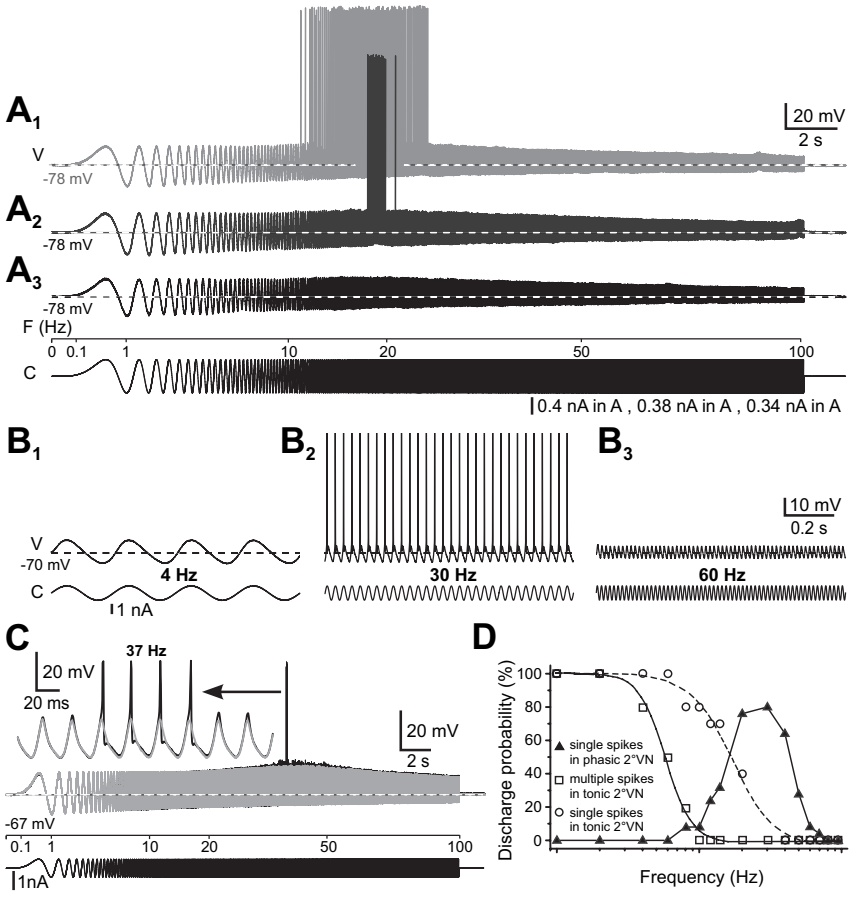

Figure 7. Discharge dynamics of phasic 2°VNs. ***A***, Discharge evoked by injection of ZAP currents. With increasing current intensity (***A*** $_1$–***A*** $_3$), responses increased in amplitude and triggered spikes (***A*** $_1$,***A*** $_2$) at a stimulus frequency of ~20 Hz. ***B***, Responses of a phasic 2°VN to injection of multiple cycles of sinusoidally modulated currents at constant frequencies of 4 Hz (***B*** $_1$), 30 Hz (***B*** $_2$), and 60 Hz (***B*** $_3$). ***C***, Responses of a phasic 2°VN evoked by injection of sinusoidally modulated currents below (gray) and above (black) spike threshold; spikes occurred at the resonance peak of the subthreshold response (gray trace). The inset in ***C*** shows superimposed subthreshold responses (gray) and the four spikes (black, amplitude truncated) riding on top of the depolarizing half cycles at the resonance peak (37 Hz) at an extended timescale. Responses in ***A–C*** are single sweeps, and horizontal dashed lines indicate resting membrane potential at −78 mV (***A***), −70 mV (***B***), and −67 mV (***C***). Calibration in ***A*** $_1$ and ***B*** $_3$ applies to ***A*** $_2$, ***A*** $_3$ and ***B*** $_1$, ***B*** $_2$, respectively. ***D***, Frequency dependence of single (white circles) and multiple (white squares) spike modulation in tonic ($n = 10$) and phasic (filled triangles; $n = 29$) 2°VNs. The frequency dependence of the discharge probability for multiple spike discharge (white squares) in tonic 2°VNs was calculated by determining the proportion of neurons that fired two or more spikes per sine wave, respectively, at each one of the 16 tested frequencies between 1 and 100 Hz. Accordingly, the discharge probability for single spike synchronization in tonic (white circles) and phasic (filled triangles) 2°VNs was calculated as the proportion of neurons at each particular frequency point that fired one spike per sine wave. V, Voltage; F, frequency; C, current.

polarizing component remained unchanged. Because of this selective increase of the depolarizing half cycle, the asymmetric responses of phasic 2°VNs (ratio, 0.60 ± 0.29) (Fig. 5*A*) became more symmetrical after application of 4-AP (ratio, 0.88 ± 0.19; $n = 7$; $p \leq 0.01$). Comparison of the profiles indicated that the increase in impedance by ~50–60% after application of 4-AP (Fig. 8A_2,A_3) mostly occurred for frequencies below 40 Hz. Because of the impedance increase, the typical resonance disappeared almost completely and the impedance profile became more similar to the low-pass filter-like impedance profile of tonic 2°VNs (Fig. 8A_3). The distortion of the sine-wave response observed in some phasic 2°VNs with a resting membrane potential close to −60 mV (Fig. 8*B*, black trace) was also eliminated by the application of 10 μM 4-AP to reveal an undistorted depolarizing half cycle (Fig. 8*B*, red trace). This effect of 4-AP corroborates the notion that the initial distortion of the response observed at particular low membrane potentials in phasic 2°VNs is in fact attributable to the activation of a voltage-dependent I_D conductance before the peak of the depolarizing half cycle is reached.

At higher intensities of the sinusoidally modulated current, a limited number of action potentials were evoked on the depolarizing half cycle at a frequency centered around the subthreshold resonance (Fig. 8*C*, black *). Bath application of 10 μM 4-AP not only increased the subthreshold sinusoidal responses (Fig. 8*C*, red trace) but also extended the firing range for action potentials, mainly toward lower frequencies (Fig. 8*C*, red *). However, spikes were never encountered within the first 15–20 cycles after application of 10 μM 4-AP.

The activation of the I_D conductance in phasic 2°VNs, in conjunction with one or more other potassium conductances, explains the absence of pacemaker activity in these neurons (Straka et al., 2005). This is primarily attributable to the fact that the potassium conductances shunt any slow inward current that could generate the depolarization necessary to reach spike threshold and cause a repetitive discharge in the absence of synaptic inputs. This also suggests that the low spontaneous activity of frog 2°VNs *in vivo* (Dieringer and Precht, 1979) is caused by the presynaptic activity of labyrinthine nerve afferent fibers. Consequently, the absence of afferent activity in the isolated frog whole brain attributable to the disconnection from the end organs would explain the absence of a resting discharge in 2°VNs *in vitro*.

The structural correlate of the I_D conductance is the Kv1 potassium channel (Harvey, 1997). In particular, the Kv1.1 potassium channel has been shown to be present in the embryonic chicken tangential vestibular neurons that also have an I_D conductance and a pronounced firing accommodation (Gamkrelidze et al., 1998; Popratiloff et al., 2003). Kv1.1 immunohistochemistry on isolated frog whole brains and on perfused and freshly fixed brains was used to study the presence of this potassium channel protein in neurons of the dorsal hindbrain (Fig. 8*D*). Kv1.1 immunolabeled neurons were encountered along the whole rostrocaudal extent of the vestibular nuclei with predominance in the lateral and descending vestibular nuclei (Fig. 8D_1). Fewer neurons were encountered in the superior vestibular nucleus and the dorsal (acoustic) nucleus, whereas in the medial vestibular nucleus, Kv1.1 immunolabeled neurons were sparse (Fig. 8D_1). The large number of Kv1.1 immunopositive neurons in vestibular nuclei known to give rise to descending spinal projections corroborates previous findings that relatively more phasic 2°VNs were antidromically activated from the spinal cord than from the oculomotor nuclei (Straka et al., 2004).

At the cellular level, the Kv1.1 immunolabeling varied in in-

4292 • J. Neurosci., April 18, 2007 • 27(16):4283–4296

tensity between different neurons and consisted of a more or less complete staining of the cell body that only spared the cell nucleus (Fig. 8D_2,D_3). The majority of the labeled neurons were oval shaped, medium to large sized, with an average diameter of 21.7 ± 4.0 μm (long axis, 26.8 ± 6.5 μm; short axis, 16.6 ± 3.3 μm; n = 45). Comparison with unlabeled neurons in the same area (average diameter, 17.9 ± 6.2 μm; n = 56) indicated that Kv1.1 immunolabeled neurons were significantly larger ($p \leq 0.001$), compatible with the lower input resistance of phasic 2°VNs (Straka et al., 2004). The apparent size difference between Kv1.1-positive and -negative neurons might in part explain the larger numbers of recorded phasic versus tonic 2°VNs. The possible relationship between the Kv1.1 labeling intensity of the neuron and the strength of its discharge adaptation during positive currents steps will be explored in future studies.

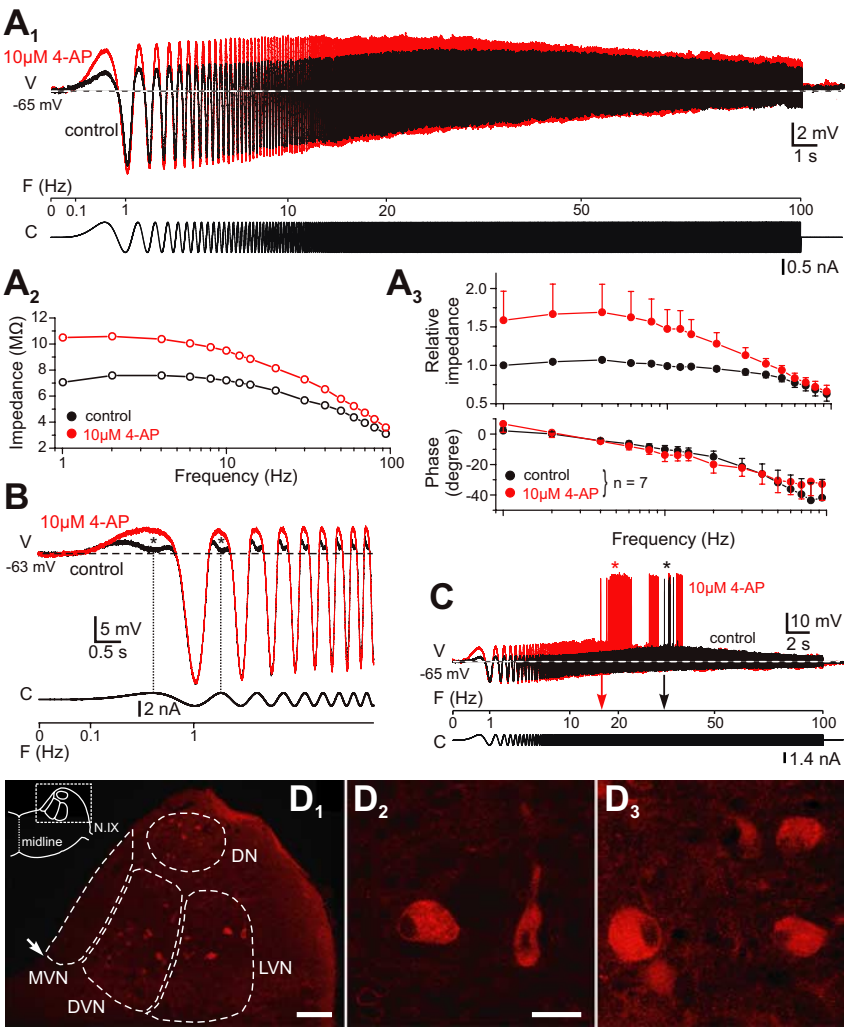

Figure 8. Effect of 4-AP on impedance and resonance of phasic 2°VNs. ***A***, Overlay of responses evoked by injection of ZAP currents (***A*** $_1$) before (control, black) and after (red) application of 10 μM 4-AP. Bode plots illustrate the impedance increase of the phasic 2°VN shown in ***A*** $_1$ (***A*** $_2$) and of the population of all tested phasic 2°VNs (***A*** $_3$); in ***A*** $_3$, the relative impedance is the average of the values normalized to the impedance at 1 Hz of each neuron before drug application. ***B***, Sinusoidally modulated responses of a phasic 2°VN before (control, black) and after (red) application of 10 μM 4-AP; the distortion in the falling phase of the depolarizing half wave (*) was abolished by 4-AP. ***C***, Spike discharge of the 2°VN shown in ***A*** evoked by sinusoidally modulated current injection before (control, black *) and after (red *) application of 10 μM 4-AP; the control range of spike discharge (black arrow) is mainly extended toward lower frequencies (red arrow) by 4-AP. Horizontal dashed lines indicate resting membrane potentials at −65 mV (***A*** $_1$, ***C***) and −63 mV (***B***). ***D***, Transverse section through the vestibular nuclei at the level indicated in the top left corner of ***D*** $_1$ treated with an antibody for the Kv1.1 potassium channel. Immunopositive neurons are located in the dorsal (auditory) nucleus (DN), the descending (DVN) and lateral (LVN) vestibular nuclei, but not the medial vestibular nucleus (MVN); higher magnification of labeled neurons in the lateral vestibular nucleus of this section (***D*** $_2$) and in the descending vestibular nucleus of the adjacent rostral section (***D*** $_3$). Outlines of vestibular nuclei are based on Kuruvilla et al. (1985). Scale bars: ***D*** $_1$, 100 μm; ***D*** $_2$, ***D*** $_3$, 20 μm. Arrow in ***D*** $_1$ indicates the sulcus limitans. V, Voltage; F, frequency; C, current.

Differential synaptic processing of vestibular nerve afferent inputs in phasic and tonic 2°VNs

Experiments on the isolated frog whole brain allows for synaptic activation of 2°VN by selective electrical stimulation of individual vestibular nerve branches. It is therefore possible to investigate the consequences of the different membrane properties of tonic and phasic 2°VN on synaptic signal processing of labyrinthine inputs. Activation of synaptic inputs at different membrane potentials indicated that the voltage-dependent opposite impedance changes of tonic and phasic 2°VNs not only affect external current responses but also determine the processing of afferent synaptic inputs. In fact, monosynaptic EPSP amplitude subthreshold to spike discharge change with depolarization and hyperpolarization by 6–10 mV of tonic and phasic 2°VNs at membrane potentials between spike threshold and approximately −68 mV (Fig. 9). In tonic 2°VNs, monosynaptic EPSPs were larger in amplitude during depolarizing and smaller during hyperpolarizing current steps when compared with EPSPs at resting membrane potential (Fig. 9A_1,A_2, 1–3). The increase in EPSP amplitude, however, was not only obtained by changing the membrane potential by injection of positive current steps (Fig. 9A_1) but also during membrane depolarization attributable to preceding EPSPs (Fig. 9A_3, dashed lines). Thus, monosynaptic EPSPs evoked by a train of single electrical pulses to an individual semicircular canal nerve increased in amplitude with each stimulus (Fig. 9A_3,A_4, 1–3) until spike threshold was reached (data not shown). Thus, independent of how membrane depolarization was achieved, EPSPs in tonic 2°VNs were more and more enlarged with increasing membrane depolarization (Fig. 9C_1, white circles, C_2, white squares). This is compatible with the fact that, during current steps, the input resistance of tonic 2°VNs increased with depolarization and decreased with hyperpolarization (Fig. 9C_3, white triangles).

In contrast, phasic 2°VNs exhibited an opposite behavior. The amplitudes of monosynaptic EPSPs became smaller during depolarizing and larger during hyperpolarizing current steps when compared with EPSPs at resting membrane potential (Fig. 9B_1,B_2, 1–3). The decrease of EPSP amplitudes with membrane depolarization was not only observed during positive current steps (Fig. 9B_1) but also during membrane depolarization attrib-

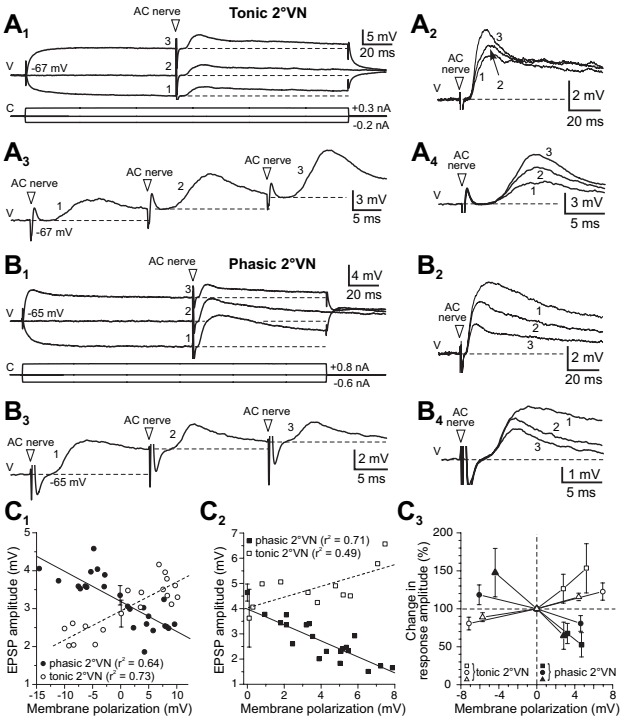

Figure 9. Differential synaptic processing of semicircular canal nerve afferent inputs in phasic and tonic 2°VNs. ***A***, ***B***, Monosynaptic EPSPs in a tonic (***A***) and a phasic (***B***) 2°VN evoked by electrical pulse stimulation of the anterior vertical canal (AC) nerve (white arrowheads). Different membrane potentials were obtained by current injection (***A*** $_1$, ***A*** $_2$, ***B*** $_1$, ***B*** $_2$), or by preceding EPSPs in a stimulus train (***A*** $_3$, ***A*** $_4$, ***B*** $_3$, ***B*** $_4$). ***A*** $_1$, ***B*** $_1$, EPSPs in a tonic (***A*** $_1$) and a phasic (***B*** $_1$) 2°VN during depolarizing (3) and hyperpolarizing (1) current steps (current traces plotted below) and in the absence of membrane polarization (2). ***A*** $_3$, ***B*** $_3$, Sequence of three EPSPs (1–3) in the same tonic (***A*** $_3$) and phasic (***B*** $_3$) 2°VNs evoked by a pulse train to the anterior vertical canal nerve at 50 Hz; EPSPs (1–3) start from successively more depolarized membrane potentials (dashed lines). Higher-magnification overlays (***A*** $_2$, ***A*** $_4$, ***B*** $_2$, ***B*** $_4$) illustrate the increase of EPSP amplitudes in tonic (***A*** $_2$, ***A*** $_4$) and the decrease of EPSP amplitudes in phasic 2°VNs (***B*** $_2$, ***B*** $_4$) with depolarization. Horizontal dashed lines indicate membrane potentials at rest (−67 mV in ***A***; −65 mV in ***B***) and during polarization. ***C***, Correlation between EPSP amplitude and membrane potential altered by depolarizing and hyperpolarizing current steps (***C*** $_1$), respectively, or by preceding EPSPs (***C*** $_2$) in tonic (white circles and squares with dashed lines) and phasic (black circles and squares with solid lines) 2°VNs; the slope of the linear regressions in ***C*** $_1$ and ***C*** $_2$ is significantly different from zero in all cases ($p \leq 0.001$, except for white squares in ***C*** $_2$, for which $p \leq 0.05$). In ***C*** $_3$, the inverse correlation between EPSP amplitude and membrane polarization (white and black circles from ***C*** $_1$; white and black squares from ***C*** $_2$) in tonic and phasic 2°VNs is corroborated by respective changes in input resistance during depolarization and hyperpolarizing current steps (white and black triangles). Values in ***C*** $_3$ were obtained by normalization using control values at resting membrane potential (dashed lines). V, Voltage; C, current.

utable to preceding EPSPs (Fig. 9B_3, dashed lines). Accordingly, the monosynaptic EPSPs evoked by a train of single electrical pulses to an individual semicircular canal nerve decreased in amplitude with each stimulus (Fig. 9B_3,B_4, 1–3). This change in EPSP amplitude (Fig. 9C_1, black circles, C_2, black squares) fits well with the fact that, during current steps, the input resistance of phasic 2°VNs decreased with depolarization and increased with hyperpolarization (Fig. 9C_3, black triangles). Based on this differential change of amplitudes, the EPSPs in phasic and tonic 2°VNs exhibit opposite behaviors during membrane polarization regardless of how the membrane potential was altered (Fig. 9C_1,C_2). Boosting EPSP amplitudes by depolarization in tonic 2°VNs comprises an efficient mechanism for amplification and integration of synaptic inputs. In contrast, the decrease of EPSP amplitudes in phasic 2°VNs likely attributable to the activation of a gK_D restores the membrane potential and thus enables efficient event detection.

Discussion

The intrinsic membrane properties of frog tonic and phasic 2°VNs show low-pass and bandpass filter-like characteristics, respectively. In addition, the low-frequency impedance increases during depolarization in the former and decreases in the latter, which enhances the ability of tonic neurons to integrate synaptic inputs, whereas the resonance properties of phasic neurons are well suited for synchronization and event detection. The bandpass filter-like properties of the latter neurons depend on the activation of an I_D conductance, which is consistent with the presence of the Kv1.1 channel protein in vestibular neurons. The existence of two discrete sets of vestibular neurons for processing different frequency ranges of sensory inputs suggests that vestibulo-motor pathways are organized into frequency-tuned channels.

Membrane conductances underlying the different dynamic working range of frog 2°VNs

The response dynamics of tonic and phasic 2°VNs results from the activation of different sets of conductances. The characteristic increase in impedance during depolarization of tonic 2°VNs suggests the activation of a steady-state negative conductance, which would cause larger responses at more depolarized membrane potentials. Functionally, this would allow tonic 2°VNs to boost synaptic inputs in the membrane potential range of ~10 mV below spike threshold, consistent with non-inactivating calcium or sodium inward currents (Crill, 1996). The activation of a steady-state negative conductance could promote synaptic integration (Major and Tank, 2004), as well as amplification of inhibitory and excitatory inputs (Vervaeke et al., 2006). This latter effect is compatible with the response properties of tonic 2°VNs (Straka et al., 2004) and would render these neurons especially suitable for the processing of tonic presynaptic inputs having slow dynamics.

The sensitivity of both the subthreshold resonance as well as the corresponding discharge of phasic 2°VNs to very low concentrations of 4-AP suggests the activation of a voltage-dependent I_D-type potassium conductance (Wu et al., 2001), with properties similar to those of principal tangential vestibular neurons in chicken embryos (Gamkrelidze et al., 1998, 2000). The absence of spikes in phasic 2°VNs at stimulus frequencies below 10 Hz, even in the presence of 4-AP, suggests that other potassium conductances are likely involved in determining the particular bandpass filter properties of the phasic 2°VNs. An I_A, or more likely a delayed rectifier, could be activated in addition to the I_D conductance to account for the pronounced spike discharge adaptation and the impedance decrease during depolarization of these neurons. The dominance of potassium conductances for shaping the filter properties of frog phasic 2°VNs is compatible with the widespread occurrence of these conductances as a mechanism for specific frequency tuning of neuronal discharge (Peusner et al., 1998; Hutcheon and Yarom, 2000).

Intrinsic membrane properties as basis for filter properties of phasic and tonic neurons

Neuronal types with complementary frequency bandwidths as frog tonic and phasic 2°VNs (Fig. 10A) seem to be a widespread phenomenon in the nervous system [e.g., entorhinal cortex (Haas and White, 2002; Erchova et al., 2004), auditory cortex (Schwarz et al., 1998), and retinal ganglion cells (Tabata and Kano, 2002)]. Any difference in resonance and frequency re-

4294 • J. Neurosci., April 18, 2007 • 27(16):4283–4296

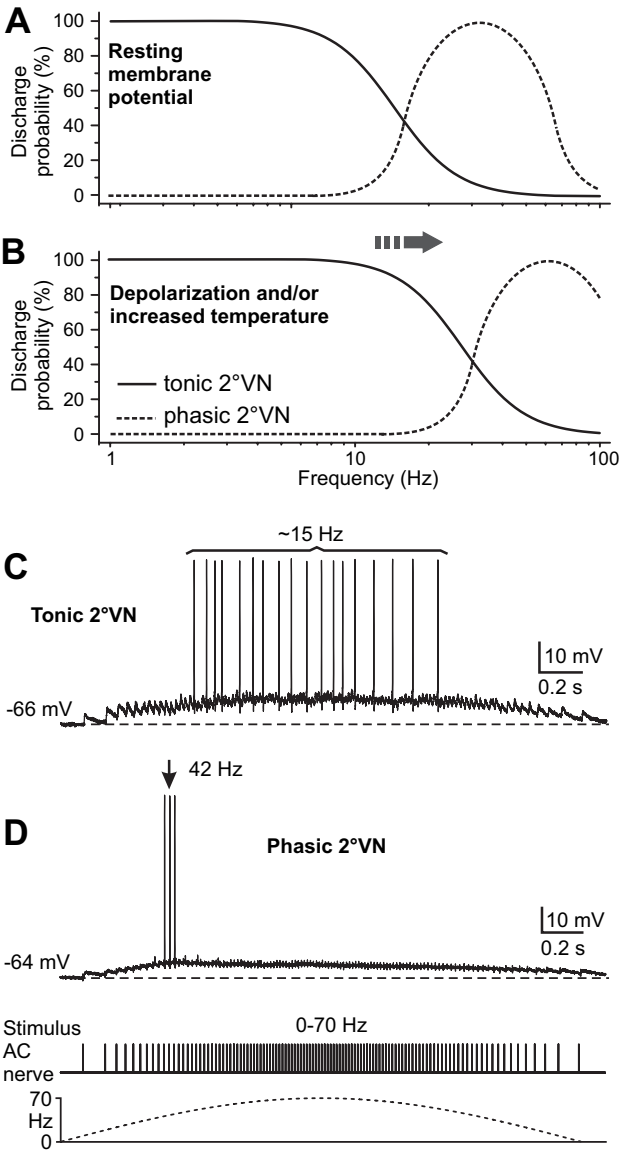

Figure 10. Filter properties of tonic and phasic 2°VNs affect their synaptic response dynamics. ***A***, ***B***, Schematic filter characteristics of tonic and phasic 2°VN discharge at resting membrane potential (***A***) shift to higher frequencies (arrow) during depolarization and/or increased temperature (***B***). ***C***, ***D***, Typical responses of a tonic (***C***) and a phasic (***D***) 2°VN to stimulation of the anterior vertical canal (AC) nerve with a train of electrical pulses that were sinusoidally modulated in frequency between 0 and 70 Hz (bottom trace). The discharge in the tonic 2°VN essentially mirrors the subthreshold compound response and has a relatively low rate (~15 Hz); the discharge in the phasic 2°VN consists of three spikes at the response peak at a rate (~40 Hz) that matches the resonance bandwidth of these neurons.

sponse behavior of phasic and tonic neurons is likely related to the processing of presynaptic signals with different dynamics. It is thus not specific to any particular aspects of vestibular information processing but can be generalized to all vertebrate neurons with similar membrane properties and firing patterns as observed in phasic and tonic 2°VNs.

Neurons with a subthreshold resonance form filters with characteristic frequency bandwidths that preferentially allow presynaptic inputs to trigger a discharge when they are close to the resonant frequency (Hutcheon and Yarom, 2000; Izhikevich et al., 2003). This suggests that the different filter properties of the two types of frog 2°VNs might be adjusted to the activity spectrum of the different types of labyrinthine nerve afferent fibers (Goldberg, 2000). Accordingly, the filter characteristics of phasic 2°VNs should be adjusted to the discharge pattern of phasic, thick-diameter afferent fibers during head movements to detect high-dynamic response components (Goldberg, 2000). In contrast, the filter properties of tonic 2°VNs should be adapted to the regular discharge of the tonic, thin-diameter fibers that transmit sensory signal components related to static head deviation (Goldberg, 2000).

Assuming that the filter properties of tonic and phasic 2°VNs are in fact adapted to the input from labyrinthine nerves, how is this implemented on a single-cell level? Stimulation of semicircular canal nerves with sinusoidally modulated pulse trains showed that the time course of the synaptically evoked response and the discharge pattern of action potentials differ between tonic and phasic 2°VNs (Fig. 10*C*,*D*). The evoked discharge in tonic 2°VNs is primarily linear, mirrors the waveform of the underlying depolarization of the membrane potential, and follows stimulus frequencies of up to 15 Hz (Fig. 10*C*). This result clearly demonstrates that the dynamics of the synaptically evoked response coincides with the filter properties of these neurons revealed by intracellular current injection (Fig. 10*A*). Moreover, the synaptic response of phasic 2°VNs is nonlinear, with only few spikes around the advanced subthreshold response peak in which individual stimuli have a frequency of 40–50 Hz (Fig. 10*D*), again consistent with their resonance bandwidth. The differential responses of the two types of 2°VNs indicate that the intrinsic filter properties determine a specific frequency range at which synaptic inputs preferentially evoke spikes.

The preferred frequency ranges of tonic and phasic 2°VNs in our study, however, is lower than the frequency bandwidth of signals in semicircular canal afferent fibers recorded *in vivo* at room temperature (Precht et al., 1971; Blanks and Precht, 1976; Rossi and Martini, 1986; Honrubia et al., 1989). This difference can be explained by a more depolarized resting membrane potential of frog 2°VNs and a higher temperature *in vivo* (Precht et al., 1974; Dieringer and Precht, 1979; Rossi and Martini, 1986; Rossi et al., 1989). Both parameters affect membrane conductances and shift resonance peaks to higher frequencies (Fig. 10*A*,*B*) in 2°VNs as in other CNS neurons (Lampl and Yarom, 1997; Tennigkeit et al., 1999; Hu et al., 2002; Erchova et al., 2004).

Compensating for experimental conditions, an average resonance frequency of >100 Hz in phasic 2°VNs and a cutoff frequency of ~90 Hz for spike discharge in tonic 2°VNs under *in vivo* conditions can be assumed. These frequencies would fit well with the dynamic ranges of responses that characterize adapting and nonadapting vestibular afferent fibers, respectively (Precht et al., 1971; Blanks and Precht, 1976; Rossi and Martini, 1986; Honrubia et al., 1989; Rossi et al., 1989). This coadaptation of discharge properties of afferent fibers and response frequency bandwidths of 2°VNs suggests the presence of parallel pathways that separately process different dynamic aspects of head movement-related signals (Goldberg, 2000; Straka and Dieringer, 2004).

Compared with the dichotomy of frog tonic and phasic 2°VNs, rodent type A and type B vestibular neurons identified *in vitro* are more homogeneous in their response dynamics (du Lac et al., 1995) but are most likely the functional mammalian counterparts (Straka et al., 2005). Both type A and type B vestibular neurons exhibit pacemaker activity as well as a resonance below 10 Hz. However, type B vestibular neurons have a higher gain of spike discharge modulation (Ris et al., 2001; Beraneck et al., 2003). The complex repertoire of nonlinear, voltage-dependent

channels in type B but not type A neurons (Serafin et al., 1990, 1991) is ideally suited for a function of the former ones as signal detectors (Straka et al., 2005). According to real data and neuronal modeling (Av-Ron and Vidal, 1999; Ris et al., 2001; Moore et al., 2004), type A and type B neurons also form separate channels for encoding low- and high-frequency signals, but with more continuous filter tuning than frog tonic and phasic 2°VNs. The different dynamic tuning of frog versus rodent vestibular neurons might mirror the differences in head movement-related signal dynamics attributable to the particular locomotor patterns of the different species.

Frequency-tuned channels for sensorimotor signal processing

Parallel pathways with different dynamics for the processing of head movement-related signals seem to be a common organizational principle of the vertebrate vestibulo-ocular system. On the sensory side at the level of labyrinthine hair cells, vestibular nerve afferent fibers, and central vestibular neurons, multiple cell types with complementary response dynamics for detection and coding of different components of the frequency spectrum of naturally occurring head movements are present (Baird, 1994a,b; Eatock et al., 1998; Goldberg, 2000; Straka and Dieringer, 2004; Straka et al., 2005). A similar organization occurs on the motor side, in which extraocular motoneurons and their target muscles form separate functional subunits that are responsible for different dynamic aspects of eye movements (Evinger and Baker, 1991; Straka and Dieringer, 2004; Büttner-Ennever, 2005; Spencer and Porter, 2005). The differences in response dynamics and preferred frequency bandwidths of corresponding neuronal populations at each synaptic stage are mainly attributable to a specific tuning of intrinsic properties at the cellular level. Accordingly, the activation of distinct membrane properties generates sets of neurons with particular filter properties along the vestibulo-ocular pathway that form flexible, frequency-tuned channels for optimal mediation of all dynamic aspects necessary for gaze stabilization.

References

Av-Ron E, Vidal PP (1999) Intrinsic membrane properties and dynamics of medial vestibular neurons: a simulation. Biol Cybern 80:383–392.

Baird RA (1994a) Comparative transduction mechanisms of hair cells in the bullfrog utriculus. I. Responses to intracellular current. J Neurophysiol 71:666–684.

Baird RA (1994b) Comparative transduction mechanisms of hair cells in the bullfrog utriculus. II. Sensitivity and response dynamics to hair bundle displacement. J Neurophysiol 71:685–705.

Beraneck M, Hachemaoui M, Idoux E, Ris L, Uno A, Godaux E, Vidal PP, Moore LE, Vibert N (2003) Long-term plasticity of ipsilesional medial vestibular nucleus neurons after unilateral labyrinthectomy. J Neurophysiol 90:184–203.

Blanks RH, Precht W (1976) Functional characterization of primary vestibular afferents in the frog. Exp Brain Res 25:369–390.

Büttner-Ennever JA (2005) The extraocular motor nuclei: organization and functional neuroanatomy. Prog Brain Res 151:95–125.

Cant NB, Benson CG (2003) Parallel auditory pathways: projection patterns of the different neuronal populations in the dorsal and ventral cochlear nuclei. Brain Res Bull 60:457–474.

Crill WE (1996) Persistent sodium current in mammalian central neurons. Annu Rev Physiol 58:349–362.

Dieringer N, Precht W (1979) Mechanisms of compensation for vestibular deficits in the frog. I. Modification of the excitatory commissural system. Exp Brain Res 36:311–328.

Dieringer N, Precht W (1986) Functional organization of eye velocity and eye position signals in abducens motoneurons of the frog. J Comp Physiol 158:179–194.

du Lac S, Lisberger SG (1995) Cellular processing of temporal information in medial vestibular nucleus neurons. J Neurosci 15:8000–8010.

Eatock RA, Rusch A, Lysakowski A, Saeki M (1998) Hair cells in mammalian utricles. Otolaryngol Head Neck Surg 119:172–181.

Erchova I, Kreck G, Heinemann U, Herz AV (2004) Dynamics of rat entorhinal cortex layer II and III cells: characteristics of membrane potential resonance at rest predict oscillation properties near threshold. J Physiol (Lond) 560:89–110.

Evinger C, Baker R (1991) Are there subdivisions of extraocular motoneuronal pools that can be controlled separately. In: Motor control: concepts and issues (Humphrey D, Freund H-J, eds), pp 22–31. Chichester, UK: Wiley.

Gamkrelidze G, Giaume C, Peusner KD (1998) The differential expression of low-threshold sustained potassium current contributes to the distinct firing patterns in embryonic central vestibular neurons. J Neurosci 18:1449–1464.

Gamkrelidze G, Giaume C, Peusner KD (2000) Firing properties and dendrotoxin-sensitive sustained potassium current in vestibular nuclei neurons of the hatchling chick. Exp Brain Res 134:398–401.

Goldberg JM (2000) Afferent diversity and the organization of central vestibular pathways. Exp Brain Res 130:277–297.

Haas JS, White JA (2002) Frequency selectivity of layer II stellate cells in the medial entorhinal cortex. J Neurophysiol 88:2422–2429.

Harvey AL (1997) Recent studies on dendrotoxins and potassium ion channels. Gen Pharmacol 28:7–12.

Hausser M, Spruston N, Stuart GJ (2000) Diversity and dynamics of dendritic signaling. Science 290:739–744.

Honrubia V, Hoffman LF, Sitko S, Schwartz IR (1989) Anatomic and physiological correlates in bullfrog vestibular nerve. J Neurophysiol 61:688–701.

Hu H, Vervaeke K, Storm JF (2002) Two forms of electrical resonance at theta frequencies, generated by M-current, h-current and persistent Na^+ current in rat hippocampal pyramidal cells. J Physiol (Lond) 545:783–805.

Hutcheon B, Yarom Y (2000) Resonance, oscillation and the intrinsic frequency preferences of neurons. Trends Neurosci 23:216–222.

Hutcheon B, Miura RM, Yarom Y, Puil E (1994) Low-threshold calcium current and resonance in thalamic neurons: a model of frequency preference. J Neurophysiol 71:583–594.

Izhikevich EM (2001) Resonate-and-fire neurons. Neural Netw 14:883–894.

Izhikevich EM, Desai NS, Walcott EC, Hoppensteadt FC (2003) Bursts as a unit of neural information: selective communication via resonance. Trends Neurosci 26:161–167.

Johnson KO, Hsiao SS (1992) Neural mechanisms of tactual form and texture perception. Annu Rev Neurosci 15:227–250.

Kuruvilla A, Sitko S, Schwartz IR, Honrubia V (1985) Central projections of primary vestibular fibers in the bullfrog. I. The vestibular nuclei. Laryngoscope 95:692–707.

Lampl I, Yarom Y (1997) Subthreshold oscillations and resonant behavior: two manifestations of the same mechanism. Neuroscience 78:325–341.

Major G, Tank D (2004) Persistent neural activity: prevalence and mechanisms. Curr Opin Neurobiol 14:675–684.

McCormick DA (1991) Functional properties of a slowly inactivating potassium current in guinea pig dorsal lateral geniculate relay neurons. J Neurophysiol 66:1176–1189.

Merigan WH, Maunsell JH (1993) How parallel are the primate visual pathways? Annu Rev Neurosci 16:369–402.

Moore LE, Buchanan JT (1993) The effects of neurotransmitters on the integrative properties of spinal neurons in the lamprey. J Exp Biol 175:89–114.

Moore LE, Hachemaoui M, Idoux E, Vibert N, Vidal PP (2004) The linear and non-linear relationships between action potential discharge rates and membrane potential in model vestibular neurons. Nonlinear Studies 11:423–447.

Peusner KD, Gamkrelidze G, Giaume C (1998) Potassium currents and excitability in second-order auditory and vestibular neurons. J Neurosci Res 53:511–520.

Popratiloff A, Giaume C, Peusner KD (2003) Developmental change in expression and subcellular localization of two shaker-related potassium channel proteins (Kv1.1 and Kv1.2) in the chick tangential vestibular nucleus. J Comp Neurol 461:466–482.

Precht W, Llinas R, Clarke M (1971) Physiological responses of frog vestibular fibers to horizontal angular rotation. Exp Brain Res 13:378–407.

Precht W, Richter A, Ozawa S, Shimazu H (1974) Intracellular study of frog's vestibular neurons in relation to the labyrinth and spinal cord. Exp Brain Res 19:377–393.

Ris L, Hachemaoui M, Vibert N, Godaux E, Vidal PP, Moore LE (2001) Resonance of spike discharge modulation in neurons of the guinea pig medial vestibular nucleus. J Neurophysiol 86:703–716.

Roche King J, Comer C (1996) Visually elicited turning behavior in rana pipiens: comparative organization and neural control of escape and prey capture. J Comp Physiol 178:293–305.

Rossi ML, Martini M (1986) Afferent activity recorded during rotation from single fibres of the posterior nerve in the isolated frog labyrinth. Exp Brain Res 62:312–320.

Rossi ML, Bonifazzi C, Martini M, Fesce R (1989) Static and dynamic properties of synaptic transmission at the cyto-neural junction of frog labyrinth posterior canal. J Gen Physiol 94:303–327.

Schwarz DW, Tennigkeit F, Adam T, Finlayson P, Puil E (1998) Membrane properties that shape the auditory code in three nuclei of the central nervous system. J Otolaryngol 27:311–317.

Serafin M, Khateb A, de Waele C, Vidal PP, Muhlethaler M (1990) Low threshold calcium spikes in medial vestibular nuclei neurones in vitro: a role in the generation of the vestibular nystagmus quick phase in vivo? Exp Brain Res 82:187–190.

Serafin, M, de Waele C, Khateb A, Vidal PP, Muhlethaler M (1991) Medial vestibular nucleus in the guinea-pig. I. Intrinsic membrane properties in brainstem slices. Exp Brain Res 84:417–425.

Shapley R (1990) Visual sensitivity and parallel retinocortical channels. Annu Rev Psychol 41:635–658.

Spencer RF, Porter JD (2005) Biological organization of the extraocular muscles. Prog Brain Res 151:43–80.

Storm JF (1988) Temporal integration by a slowly inactivating K+ current in hippocampal neurons. Nature 336:379–381.

Straka H, Dieringer N (1993) Electrophysiological and pharmacological characterization of vestibular inputs to identified frog abducens motoneurons and internuclear neurons in vitro. Eur J Neurosci 5:251–260.

Straka H, Dieringer N (2004) Basic organization principles of the VOR: lessons from frogs. Prog Neurobiol 73:259–309.

Straka H, Biesdorf S, Dieringer N (1997) Canal-specific excitation and inhibition of frog second-order vestibular neurons. J Neurophysiol 78:1363–1372.

Straka H, Beraneck M, Rohregger M, Moore LE, Vidal PP, Vibert N (2004) Second-order vestibular neurons form separate pathways with different membrane and discharge properties. J Neurophysiol 92:845–861.

Straka H, Vibert N, Vidal PP, Moore LE, Dutia MB (2005) Intrinsic membrane properties of vertebrate vestibular neurons: function, development and plasticity. Prog Neurobiol 76:349–392.

Tabata T, Kano M (2002) Heterogeneous intrinsic firing properties of vertebrate retinal ganglion cells. J Neurophysiol 87:30–41.

Tennigkeit F, Schwarz DW, Puil E (1999) Modulation of frequency selectivity by Na^+- and K^+-conductances in neurons of auditory thalamus. Hear Res 127:77–85.

Vervaeke K, Hu H, Graham LJ, Storm JF (2006) Contrasting effects of the persistent Na^+ current on neuronal excitability and spike timing. Neuron 49:257–270.

Wu N, Hsiao CF, Chandler SH (2001) Membrane resonance and subthreshold membrane oscillations in mesencephalic V neurons: participants in burst generation. J Neurosci 21:3729–3739.

3 Differential Inhibitory Control of Semicircular Canal Nerve Afferent-Evoked Inputs in Second-Order Vestibular Neurons by Glycinergic and GABAergic Circuits

J Neurophysiol 99: 1758–1769, 2008.
First published February 6, 2008; doi:10.1152/jn.01207.2007.

Differential Inhibitory Control of Semicircular Canal Nerve Afferent-Evoked Inputs in Second-Order Vestibular Neurons by Glycinergic and GABAergic Circuits

Stefan Biesdorf,[2] David Malinvaud,[1] Ingrid Reichenberger,[2] Sandra Pfanzelt,[1,3] and Hans Straka[1]

[1] *Laboratoire de Neurobiologie des Réseaux Sensorimoteurs, Centre National de la Recherche Scientifique Unité Mixte de Recherche 7060, Université Paris Descartes, Paris, France; and* [2]*Departments of Physiology and* [3]*Neurology, Ludwig-Maximilians-Universität Munich, Munich, Germany*

Submitted 30 October 2007; accepted in final form 2 February 2008

Biesdorf S, Malinvaud D, Reichenberger I, Pfanzelt S, Straka H. Differential inhibitory control of semicircular canal nerve afferent-evoked inputs in second-order vestibular neurons by glycinergic and GABAergic circuits. *J Neurophysiol* 99: 1758–1769, 2008. First published February 6, 2008; doi:10.1152/jn.01207.2007. Labyrinthine nerve-evoked monosynaptic excitatory postsynaptic potentials (EPSPs) in second-order vestibular neurons (2°VN) sum with disynaptic inhibitory postsynaptic potentials (IPSPs) that originate from the thickest afferent fibers of the same nerve branch and are mediated by neurons in the ipsilateral vestibular nucleus. Pharmacological properties of the inhibition and the interaction with the afferent excitation were studied by recording monosynaptic responses of phasic and tonic 2°VN in an isolated frog brain after electrical stimulation of individual semicircular canal nerves. Specific transmitter antagonists revealed glycine and $GABA_A$ receptor-mediated IPSPs with a disynaptic onset only in phasic but not in tonic 2°VN. Compared with GABAergic IPSPs, glycinergic responses in phasic 2°VN have larger amplitudes and a longer duration and reduce early and late components of the afferent nerve-evoked subthreshold activation and spike discharge. The difference in profile of the disynaptic glycinergic and GABAergic inhibition is compatible with the larger number of glycinergic as opposed to GABAergic terminal-like structures on 2°VN. The increase in monosynaptic excitation after a block of the disynaptic inhibition in phasic 2°VN is in part mediated by a *N*-methyl-D-aspartate receptor-activated component. Although inhibitory inputs were superimposed on monosynaptic EPSPs in tonic 2°VN as well, the much longer latency of these IPSPs excludes a control by short-latency inhibitory feed-forward side-loops as observed in phasic 2°VN. The differential synaptic organization of the inhibitory control of labyrinthine afferent signals in phasic and tonic 2°VN is consistent with the different intrinsic signal processing modes of the two neuronal types and suggests a co-adaptation of intrinsic membrane properties and emerging network properties.

INTRODUCTION

Central vestibular neurons play a key role in the sensory-motor transformation of body motion-related multi-sensory signals. Head motion is decomposed by semicircular canal and macula organs into different spatial vector and dynamic components and mediated as neuronal discharge by a large number of vestibular nerve afferent fibers to second-order vestibular neurons (2°VN) (see Straka and Dieringer 2004). The presence of physiologically different types of hair cells, vestibular nerve afferents and 2°VN suggests that labyrinthine signals are processed in frequency-tuned channels (for review, see Goldberg 2000; Straka et al. 2005). The relative proportions of 2°VN with high and low response dynamics vary between different species and are likely related to locomotor styles and/or dynamics (Straka et al. 2005). Although vertebrate 2°VN form separate subpopulations, the vast majority of these neurons receive monosynaptic inputs, although in different proportions, from physiologically diverse vestibular nerve afferents, i.e., thick, irregular-, and thin, regular-firing afferents (Goldberg et al. 1987; Straka and Dieringer 2000; Straka et al. 2004; see Goldberg 2000).

Vestibular nerve afferent-evoked monosynaptic excitatory postsynaptic potentials (EPSPs) in most 2°VN are superimposed by inhibitory inputs as shown in monkey and frog (Goldberg et al. 1987; Straka and Dieringer 1996, 2000; Straka et al. 1997). In frog, these superimposed inhibitory postsynaptic potentials (IPSPs) have disynaptic onset latencies and are mediated by glycinergic and GABAergic neurons in the ipsilateral vestibular nuclei (Straka and Dieringer 1996). Moreover, these inhibitory neurons are activated by the thickest vestibular nerve afferent fibers (Straka and Dieringer 2000) and allow a control of the magnitude of the monosynaptic afferent excitatory inputs. This morpho-physiological organization is identical to the suggested neuronal circuit of the side-loop model of Minor and Goldberg (1991).

This model was developed to explain in monkeys the absence of changes in the performance of the vestibuloocular reflex during a block of irregularly firing thick vestibular nerve afferent fibers (Angelaki and Perachio 1993; Chen-Huang et al. 1997; Minor and Goldberg 1991). However, the direct experimental verification in frogs suggests that the functional circuitry, on which the model is based, is a general feature of the vertebrate vestibulomotor network. Because most 2°VN receive monosynaptic inputs from irregularly firing vestibular nerve afferent fibers (Boyle et al. 1992; Goldberg et al. 1987; Highstein et al. 1987; Straka et al. 2004), the inhibitory feed-forward circuitry could control the dynamics of the responses in 2°VN evoked from the same fiber types and in particular the timing and extent of the afferent-evoked spike discharge. Consequently, the activation of disynaptic IPSPs would render the monosynaptic excitation more transient. However, it is unknown if the inhibitory side-loop exerts its

Address for reprint requests and other correspondence: H. Straka, L.N.R.S., CNRS UMR 7060, Université Descartes, 45 Rue des Saints-Pères, 75270 Paris Cedex 06, France (E-mail: hans.straka@univ-paris5.fr).

The costs of publication of this article were defrayed in part by the payment of page charges. The article must therefore be hereby marked "*advertisement*" in accordance with 18 U.S.C. Section 1734 solely to indicate this fact.

effect on all functional subtypes of 2°VN, independent of their intrinsic response properties (Straka et al. 2005).

The present study is based on earlier results showing that electrical stimulation of vestibular nerve afferent fibers evoke disynaptic GABAergic as well as glycinergic IPSPs that sum on monosynaptic EPSPs in most but not all central vestibular neurons (Straka and Dieringer 1996, 2000). Because only few vestibular neurons co-localize these two transmitters (Reichenberger et al. 1997), the presence of a GABAergic as well as a glycinergic IPSP in most 2°VN suggests that these inhibitory inputs are mediated by separate neuronal subpopulations. However, it is unknown if the two pharmacological types of IPSPs have the same kinetics and how this inhibition affects the synaptically activated discharge. Furthermore, in earlier studies, all recorded frog 2°VN were treated as a single homogeneous population (Straka and Dieringer 1996, 2000). Frog 2°VN have been recently differentiated into two distinct functional subtypes based on differences in intrinsic membrane and discharge properties (Beraneck et al. 2007; Straka et al. 2004). This latter distinction opens the possibility that a disynaptic inhibition might only be present in phasic 2°VN which form the majority of vestibular neurons (Straka et al. 2004). In these neurons, the disynaptic inhibitory input would then reinforce the highly dynamic membrane properties (Beraneck et al. 2007). Alternatively, both types are targets for ipsilateral vestibular inhibitory interneurons because tonic and phasic 2°VN receive inputs from the thickest vestibular nerve afferents (Straka et al. 2004) that also activate the disynaptic inhibition.

The present study uses an isolated brain of adult frogs to investigate the properties of the ipsilateral semicircular canal nerve afferent-evoked GABAergic and glycinergic inhibition and their respective roles in the control of the monosynaptic EPSPs and spike discharge in phasic and tonic 2°VN. Preliminary results have been published in abstract form (Biesdorf and Straka 2004).

METHODS

Immunocytochemistry

Glutamate, glycine, and GABA immunocytochemistry of terminal-like structures in the vestibular nuclei was studied in five adult grass frogs (*Rana temporaria*). The characterization of the antibodies and the immunostaining with positive and negative controls have been performed and described along with methodological details in earlier studies (Reichenberger and Dieringer 1994; Reichenberger et al. 1997). The presence of glutamate, glycine, and GABA in terminal-like structures surrounding central vestibular neurons was quantitatively analyzed on three consecutive 0.5-μm-thick transverse sections at particular rostrocaudal levels of the frog hindbrain. This was repeated on a total of 28 levels that were separated by 80 μm and spanned the whole rostrocaudal extent of the vestibular nuclear complex, including the medial (MVN), superior (SVN), lateral (LVN), and descending vestibular nuclei (DVN).

Electrophysiology and pharmacology

In vitro experiments were performed on the isolated brains of 15 adult grass frogs (*R. temporaria*) and complied with the "Principles of Animal Care, " Publication No. 86-23, revised 1985 by the National Institutes of Health. As described earlier (Straka and Dieringer 1993), animals were deeply anesthetized with 0.1% 3-aminobenzoic acid ethyl ester (MS-222) and perfused transcardially with iced Ringer solution [(in mM) 75 NaCl, 25 $NaHCO_3$, 2 $CaCl_2$, 2 KCl, 0.5 $MgCl_2$, and 11 glucose; pH 7.4]. Thereafter, the skull and the bony labyrinth were opened by a ventral approach. After dissecting the three semicircular canals on each side, the brain was removed from the skull with all labyrinthine end organs attached to the VIIIth nerve. Subsequently, the brain was submerged in iced Ringer and the dura, labyrinthine end organs and choroid plexus covering the IVth ventricle were removed. In all experiments, the cerebellum and forebrain were disconnected. Brains were used $\leq$4 days after their isolation and were stored overnight at 6°C in continuously oxygenated Ringer solution (carbogen: 95% O_2-5% CO_2) with a pH of 7.4 $\pm$ 0.1. For the experiments, the brain stem was glued with cyanoacrylate to a plastic mesh which was fixed with insect pins to the silicone elastomer (Sylgard) floor of a chamber (volume: 2.4 ml) and continuously perfused with oxygenated Ringer solution at a rate of 1.3–2.1 ml/min. The temperature of the Ringer solution in the chamber was electronically controlled and maintained at 14 $\pm$ 0.1°C. Technical aspects of the isolation and the maintenance of the preparation have been published earlier (Luksch et al. 1996; Straka and Dieringer 1993).

Neuronal activity in the vestibular nuclei was evoked by electrical stimulation of individual ipsilateral vestibular nerve branches (Straka et al. 1997). For practical purposes and to constrain the study to one set of vestibular endorgans, only the three semicircular canal nerves were stimulated separately with single constant current pulses (0.2 ms; 1–15 μA) applied across suction electrodes (diameter: 120–150 μm). Pulses were produced by a stimulus isolation unit (WPI A 360) at a rate of 0.5 Hz. Glass microelectrodes for extra- and intracellular recordings were made with a horizontal puller (P-87 Brown/Flaming). Electrodes for extracellular field potential recordings were beveled (30°, 20 μm tip diameter) and filled with 2 M sodium chloride (~1 MΩ). Electrodes for intracellular recordings were filled with a mixture of 2 M potassium acetate and 3 M potassium chloride (10:1) which gave a final resistance of 80–100 MΩ. Neuronal recordings were made in bridge mode (SEC-05L; npi electronic GmbH, Tamm).

At the beginning of each experiment, pre- (N_0) and postsynaptic field potential components (N_1) evoked by separate stimulation of the three semicircular canal nerve branches were recorded at a reference recording site to optimize the position of the stimulus electrodes and to determine the stimulus threshold (T) for each nerve branch (Straka et al. 1997). This reference recording site was located 0.4 mm caudal to the VIIIth nerve root at a depth of 0.4 mm below the top of the brain stem. Neurons were recorded in all vestibular nuclei except the most medial parts of the medial vestibular nucleus. Vestibular neurons were identified as second order by their monosynaptic EPSPs and were classified as either phasic or tonic based on their discharge pattern evoked by the injection of long, positive current steps (Beraneck et al. 2007; Straka et al. 1997, 2004). Only neurons with a resting membrane potential more than $-$58 mV and spike amplitudes $>$60 mV were included in this study. As reported earlier, no differences were encountered in the parameters related to intrinsic membrane properties or synaptically activated responses of neurons recorded on subsequent days after the isolation of the brain stem (Luksch et al. 1996; Straka and Dieringer 2004).

Bath application of the glycine receptor antagonist strychnine hydrochloride (1 μM; Sigma) or of the $GABA_A$ receptor antagonist bicuculline methochloride (1–8 μM; Sigma) was used to unmask inhibitory components superimposed on afferent-evoked responses in 2°VN. Both substances in the used chemical form have been shown to be specific for the block of the respective neurotransmitter-evoked responses, e.g., in chicken tangential vestibular neurons (Shao et al. 2003, 2004). Bath application of 7-chloro kynurenic acid (7-Cl KYNA; Sigma; 10 μM) was used to reveal the *N*-methyl-D-aspartate (NMDA) receptor-mediated component of the afferent nerve-evoked EPSPs. Antagonist-related changes of the evoked responses occurred after ~5 min and reached steady state after 10–15 min. After 30–40 min, the washout of the different antagonists was usually complete.

Synaptic potentials were digitized at 20 kHz and analyzed from averages of 20–30 single sweeps after electronic subtraction of the

extracellular field potential recorded in the vicinity. Statistical differences of the analyzed parameters were obtained using the Mann-Whitney *U* test (unpaired parameters) or the Wilcoxon signed-rank nonparametric test (paired parameters; Prism, Graphpad Software). Averaged results were expressed as means ± SD. Graphical presentations were made with the aid of commercially available computer software (Origin, Microcal Software; Corel Draw, Corel).

RESULTS

Immunohistochemistry of amino acids in terminal-like structures on vestibular neurons

Glutamate, glycine, and GABA immunoreactive puncta were abundant throughout the vestibular nuclei although in differential quantity for the three amino acids (Fig. 1, *A–C*). Immunoreactive puncta of all three amino acids were observed in close contact to cell bodies and stem dendrites and likely reflect synaptic structures that often outlined dendrites and cell bodies (green and red arrows in Fig. 1, *A2–C2*). In general, glutamatergic terminal-like structures were located more on proximal dendrites (green arrows in Fig. 1*A2*), whereas glycinergic and GABAergic terminal-like structures were more densely distributed around the cell bodies (red arrows in Fig. 1, *B2* and *C2*). However, GABAergic structures seemed to be less numerous than glycinergic puncta independent of the location within the vestibular nuclei. The numbers of immunoreactive, terminal-like structures was quantified on 0.5-μm-thick serial sections through all vestibular nuclei for cell bodies with a visible nucleus (e.g., * in Fig. 1, *A2–C2*). Central vestibular neurons ($n = 145$) were more frequently contacted by glutamate ($n = 1{,}632$)- than by glycine ($n = 1{,}375$)- or GABA-immunoreactive terminal-like structures ($n = 866$). The significantly higher number of glycinergic compared with GABAergic terminal-like structures ($P \leq 0.0001$) on individual vestibular neurons suggests that glycinergic inputs are more pronounced than GABAergic inputs, assuming that other pre- and postsynaptic parameters of these inhibitory synapses are otherwise similar.

Unmasking of glycinergic and GABAergic components in semicircular canal nerve-evoked field potentials

Field potentials evoked by separate electrical stimulation of the ipsilateral horizontal (HC), anterior (AC) and posterior vertical canal (PC) nerves at an intensity of 4 × T were recorded either in the caudal part (i.e., DVN/LVN; Fig. 1, *D–F*) or in the rostral part (SVN/MVN; not shown) of the vestibular nuclear complex. Independent of the recording site and the activated nerve branch, the evoked responses consisted of a short, transient pre- (N_0) and a longer postsynaptic (N_1) component that usually lasted up to ~30 ms (e.g., Fig. 1*D1*). The N_0-component reflects the activity of vestibular nerve afferent fibers and the N_1-component with a monosynaptic onset (3.2 ± 0.8 ms, $n = 12$) the activation of 2°VN (see Straka et al. 1997).

Disynaptic inhibitory components that overlapped with the monosynaptic excitatory responses were unmasked following bath application of the glycine receptor antagonist strychnine (1 μM; Fig. 1, *D1–F1*) as well as the $GABA_A$ receptor antagonist bicuculline (1 μM; Fig. 1, *D3–F3*). Strychnine increased the peak amplitudes of the control field potentials, gave rise to spike-like events (red arrows), and considerably delayed the return to the baseline (compare black and red traces in Fig. 1, *D1–F1*). Bicuculline also increased the peak amplitudes and triggered spike-like events (red arrows) but left the longer-latency components of the field potentials largely unaffected (Fig. 1, *D3–F3*).

Electronic subtraction of the traces recorded before and in the presence of strychnine or bicuculline revealed the magnitude and profile of the unmasked glycinergic (red areas in Fig. 1, *D2–F2*) and GABAergic inhibition (red areas in Fig. 1, *D4–F4*), respectively. The onset of the glycinergic (5.8 ± 1.8 ms, $n = 12$) and GABAergic component (5.9 ± 1.6 ms, $n = 12$) was delayed with respect to the monosynaptic N_1-component and complies with a disynaptic latency following stimulation of semicircular canal nerve branches (see Straka et al. 1997). Although the peak amplitudes of both inhibitory components were similar, the profile of the unmasked glycinergic component had a considerably longer time course compared with that of the GABAergic component (Figs. 1, *D, 2* and *4,* to *F, 2* and *4*, and 2*A, 1* and *2*). The area of the unmasked glycinergic component within the first 50 ms was more than twice as large as the GABAergic component ($P \leq 0.0001$) and suggests that EPSPs in individual 2°VN might be differently controlled by the two pharmacological types of inhibitory inputs.

Combined application of the NMDA receptor antagonist 7-Cl KYNA and strychnine or bicuculline was used to reveal a potential contribution of the NMDA receptor-mediated component to the increase of the field potentials in the presence of either one of the two inhibitory transmitter antagonists. Application of 7-Cl KYNA (10 μM) and strychnine (Fig. 1, *D1–F1*) or bicuculline (Fig. 1, *D3–F3*) reduced the peak amplitudes and facilitated the return to the baseline (green traces) of the field potentials that were increased beforehand by the two inhibitory transmitter antagonists (red traces). The relative effect of 7-Cl KYNA was similar for HC and AC, somewhat less for PC nerve-evoked field potentials, and generally larger in the presence of strychnine than in the presence of bicuculline (Fig. 1, *D, 2* and *4,* to *F, 2* and *4*). In addition, the spike-like events in the presence of strychnine or bicuculline (red arrows in Fig. 1, *D, 1* and *3,* to *F, 1* and *3*) were blocked completely. Electronic subtraction of the traces before and in the presence of 7-Cl KYNA (green areas in Fig. 1, *D, 2* and *4,* to *F, 2* and *4*) revealed a monosynaptic onset of the NMDA component (3.4 ± 1.7 ms; $n = 12$). These results indicate that a considerable proportion of the field potential in the presence of the inhibitory transmitter antagonists is mediated by NMDA receptors. This component is larger when compared with that in the absence of $GABA_A$ or glycine receptor blockers (Straka et al. 1996). Even though the interaction between the two different inhibitory and the excitatory component, respectively, is likely nonlinear, the larger unmasked NMDA component in the presence of strychnine compared with bicuculline (Fig. 1, *D, 2* and *4,* to *F, 2* and *4*) coincides with the longer time course of the glycinergic inhibitory component.

Characterization of frog phasic and tonic second-order semicircular canal neurons

The effect of strychnine and bicuculline on the monosynaptic EPSPs and the profile of the unmasked inhibitory compo-

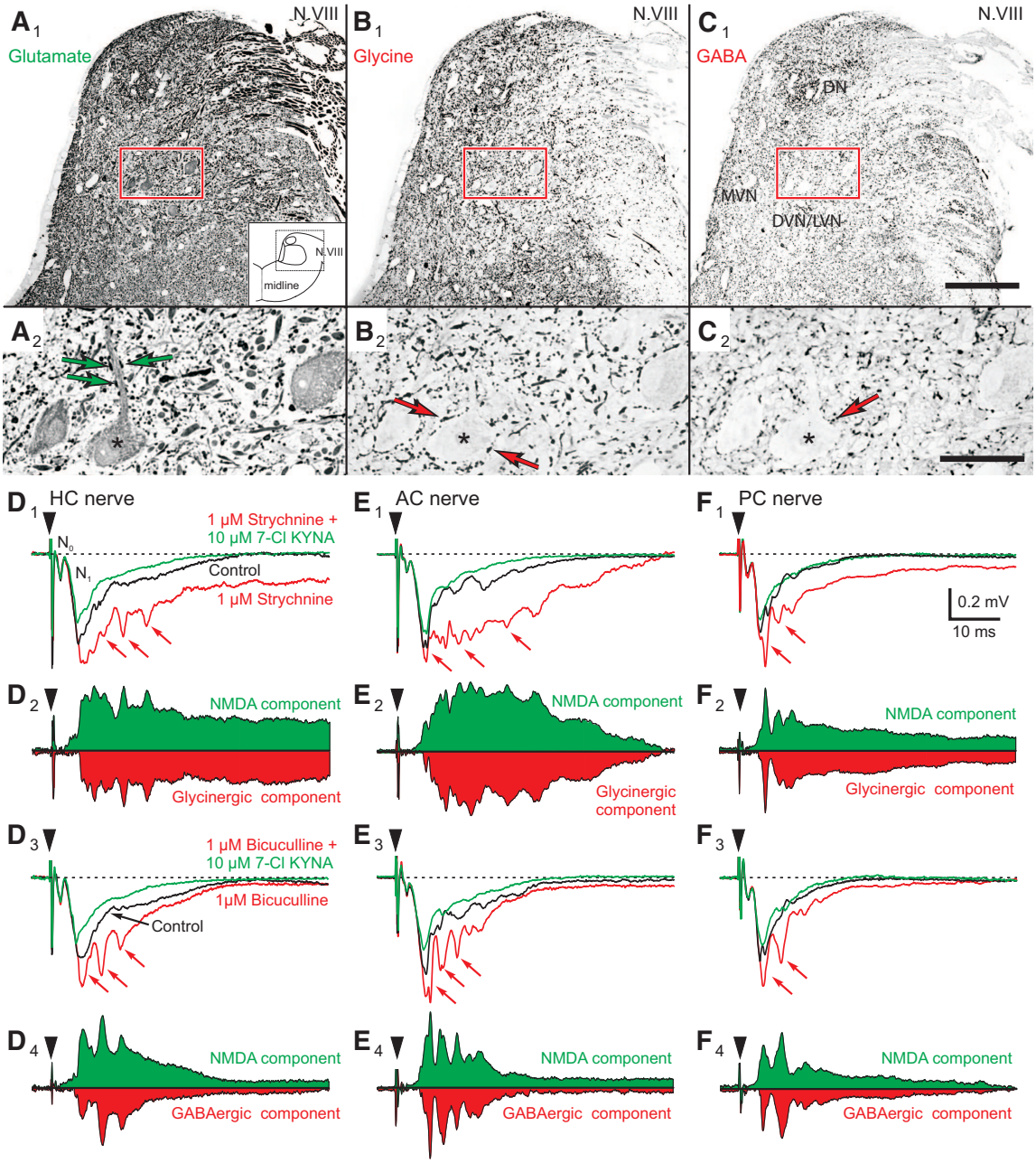

FIG. 1. Glutamate-, glycine-, and GABA-mediated neurotransmission in the vestibular nuclei. *A–C*: consecutive transverse semithin sections (0.5 μm thickness) through the dorsal hindbrain at the level of the VIII nerve, treated with antibodies against glutamate (*A*), glycine (*B*), and GABA (*C*). The outlined red area in *A1–C1* is shown at higher magnification in *A2–C2* (* in *A2–C2* indicates the same neuron). Green and red arrows mark glutamatergic (*A2*), glycinergic (*B2*), and GABAergic (*C2*) terminal-like structures. Calibration bars in *C, 1* and *2,* are 200 and 50 μm and apply also to *A, 1* and *2,* and *B, 1* and *2,* respectively. *D–F*: field potentials evoked by separate electrical stimulation (at 4 × T) of the ipsilateral horizontal (HC, *D*), anterior (AC, *E*), and posterior vertical semicircular canal (PC, *F*) nerve were recorded in the descending/lateralvestibular nuclei (DVN/LVN) and consisted of a pre- (N_0) and a postsynaptic (N_1) component, respectively. Control field potentials (black traces) increased in the presence (red traces) of the glycine receptor antagonist strychnine (*D1–F1*) or the $GABA_A$ receptor antagonist bicuculline (*D3–F3*). The enhanced responses (red traces) decreased after additional application of the *N*-methyl-D-aspartate (NMDA) receptor antagonist 7-chloro-kynurenic acid (7-Cl KYNA; green traces; *D, 1* and *3,* to *F, 1* and *3*). Electronic subtraction of red and black traces revealed the profile of the glycinergic and GABAergic components (red areas in *D, 2* and *4,* to *F, 2* and *4*), respectively; electronic subtraction of the red and green traces revealed the NMDA components (green areas in *D, 2* and *4,* to *F, 2* and *4*). Red arrows indicate spike-like events. Arrowheads in *D–F* mark stimulus onset and dashed horizontal line the baseline; records are the average of 30 individual responses; calibration bars in *F1* apply to all other traces. DN, dorsal auditory nucleus; MVN, medial vestibular nucleus.

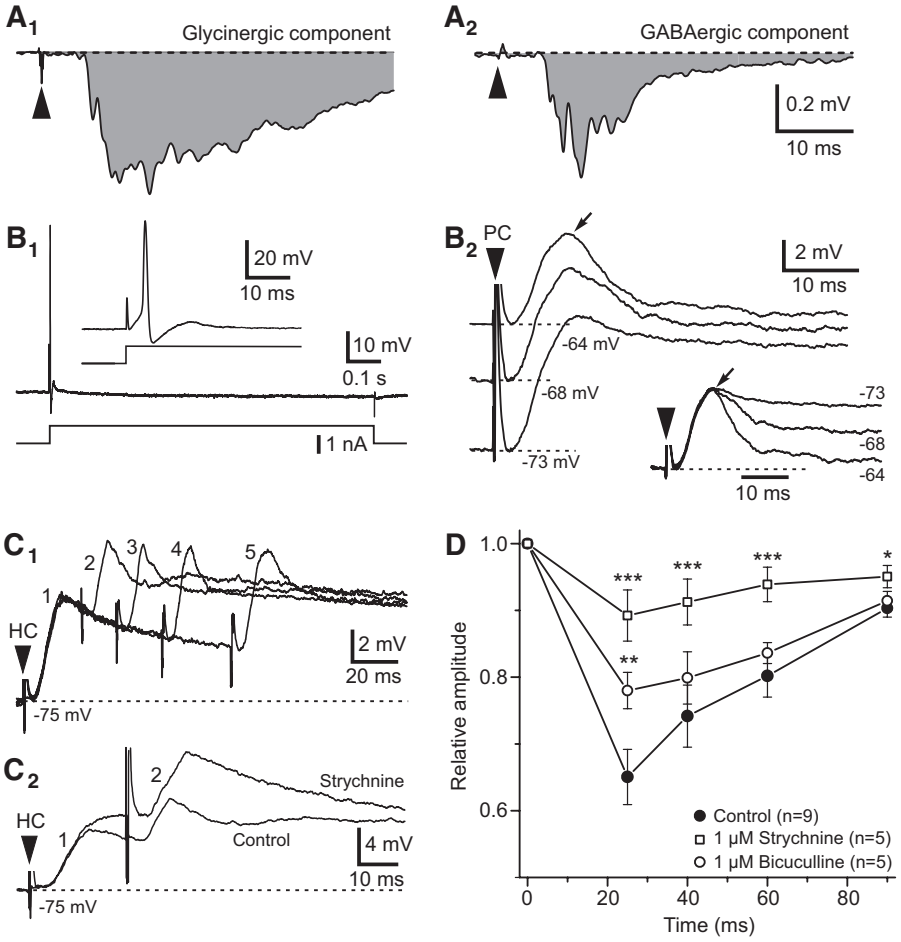

FIG. 2. Glycinergic and GABAergic inhibitory responses superimposed on semicircular canal nerve-evoked monosynaptic EPSPs. *A*: averages ($n = 12$) of horizontal (HC), anterior (AC), and posterior vertical semicircular canal (PC) nerve-evoked glycinergic (*A1*) and GABAergic (*A2*) field potentials components unmasked by application of strychnine or bicuculline differ in response profile. *B*: monosynaptic EPSPs in a phasic 2°PC neuron. Single spikes evoked by injection of a long positive current step (1 nA) characteristic for phasic 2°VN (*B1*); the *inset* in *B1* shows the single spike at an extended time scale. Monosynaptic EPSPs evoked by electrical stimulation of the PC nerve at 2.9 × T recorded at 3 membrane potentials (*B2*); EPSP decay time after the peak (↓) decreased with depolarization; normalization of the peak amplitudes (*inset* in *B2*) facilitated a comparison of the EPSP profiles recorded at the 3 membrane potentials. *C*: EPSPs evoked by double shock stimulation of the HC nerve in a phasic 2°VN. Overlay of EPSPs after double shock stimulation at 2.3 × T (*C1*) with the 2nd pulse separated by 25 ms (2), 40 ms (3), 60 ms (4), or 90 ms (5) from the 1st pulse (1). In the presence of strychnine (1 μM), the amplitude of the EPSPs to the 1st (1) and 2nd pulse after 25 ms (2) were increased (*C2*). *D*: relative amplitudes of the 2nd EPSP after double shock stimulation as a function of the delay between the 1st and the 2nd pulse in controls ($n = 9$) and in the presence of 1 μM strychnine ($n = 5$) or bicuculline ($n = 5$). The amplitude of the 2nd EPSP was calculated as the difference between the membrane potential before EPSP onset and EPSP peak and was normalized to the amplitude of the 1st EPSP in controls or in the presence of one of the antagonists, respectively. Significance of difference with respect to controls: $*P \leq 0.05$, $**P \leq 0.01$, $***P \leq 0.001$ (Mann-Whitney *U* test). ▼ in *A–C* mark stimulus onset; - - -, baseline (*A*) or resting membrane potentials (*B* and *C*); the trace in *B1* is a single sweep and in *B2* and *C* the average of 24 individual responses, respectively. Calibration bars in *A2* apply also to *A1*.

nents were studied in 60 intracellularly recorded 2°VN. Based on the differences of the responses to intracellular injection of long positive current pulses, all neurons were characterized as either phasic or tonic as in earlier studies (Beraneck et al. 2007; Straka et al. 2004). The response of most neurons ($n = 54$; 90%) consisted of a short burst of one to three spikes within the first 50 ms and the absence of a subsequent continuous discharge (Figs. 2*B1* and 3*A*), characteristic for phasic frog 2°VN. In contrast, a continuous discharge (Fig. 4*A*) with a frequency that increased with current amplitude following the injection of a long positive current pulse, typical for tonic 2°VN was encountered in few neurons ($n = 6$; 10%). As in earlier studies, the presence, as opposed to the lack of a continuous discharge during positive current steps unequivocally distinguished tonic from phasic 2°VN (Beraneck et al. 2007; Straka et al. 2004). The difference in the discharge pattern evoked by the current step was paralleled by a significant difference ($P \leq 0.001$; Mann Whitney *U* test) in the input resistance between phasic (12.6 ± 4.3 MΩ; $n = 54$) and tonic 2°VN (23.7 ± 5.4 MΩ; $n = 6$). In contrast, the resting membrane potential of the two neuronal types was similar (phasic 2°VN: -67 ± 5 mV, $n = 54$; tonic 2°VN: -68 ± 7 mV, $n = 6$).

All recorded neurons were identified as 2°VN by the presence of a monosynaptic EPSP (Fig. 2, *B2* and *C, 1* and *2*) after electrical stimulation of a particular ipsilateral semicircular canal nerve branch (Straka et al. 1997). The majority of 2°VN (88%) received the monosynaptic afferent input from only one of the three semicircular canals that originated in similar

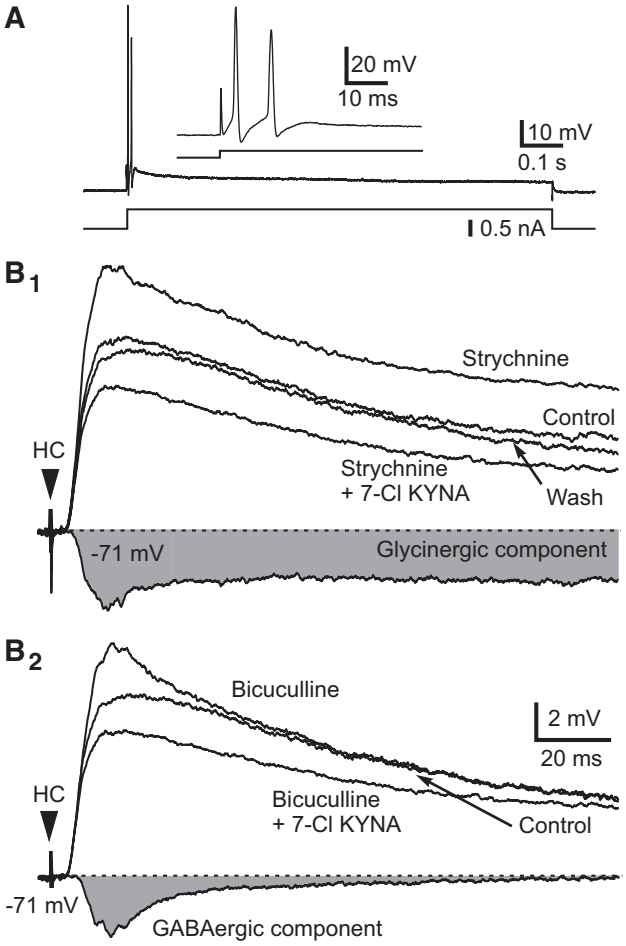

FIG. 3. Effects of glycine, GABA, and *N*-methyl-D-aspartate (NMDA) receptor antagonists on monosynaptic EPSPs in a phasic 2°VN. *A*: a short burst of 2 spikes evoked by injection of a long positive current step (1 nA) characteristic for phasic 2°VN; the *inset* shows the 2 spikes at an extended time scale. *B*: monosynaptic EPSPs evoked by electrical stimulation of the horizontal semicircular canal (HC) nerve at 2.7 × T. Disynaptic glycinergic and GABAergic inhibitory postsynaptic potentials (IPSPs) superimposed on monosynaptic EPSPs were unmasked by consecutive application of 1 μM strychnine (*B1*) and 1 μM bicuculline (*B2*). Electronic subtraction of the responses before (control) and in the presence of the inhibitory transmitter blockers revealed the different profiles (▨ in *B, 1* and *2*) of the unmasked glycinergic and GABAergic components, respectively. Application of the NMDA antagonist 7-chloro kynurenic acid (7-Cl KYNA; 10 μM) in the presence of one of the inhibitory transmitter blockers, respectively, decreased EPSP amplitudes below control values. ▼, stimulus onset; - - -, resting membrane potential of −71 mV; the trace in *A* is a single sweep and in *B* the average of 24 individual responses, respectively. Calibration bars in *B2* apply also to *B1*.

proportions from the HC ($n = 14$), the AC ($n = 19$), or the PC nerve ($n = 20$). In the remaining seven neurons (12%), a monosynaptic response was evoked by stimulation of two or all three ipsilateral canal nerves. The monosynaptic onset latency (3.4 ± 1.5 ms; $n = 70$) was similar for EPSPs evoked from the different semicircular canals.

Differential effects of strychnine and bicuculline on monosynaptic EPSPs in phasic 2°VN

The activation of a disynaptic inhibitory component superimposed on the monosynaptic EPSP was usually not detected without pharmacological block of glycine or $GABA_A$ receptors. Occasionally, however, the membrane potential of phasic 2°VN ($n = 4$) could be depolarized with DC currents. This caused a small reduction of the EPSP peak amplitude but more importantly a change in the shape due to a faster decay (Fig. 2*B2*). The shortening of the decay time is compatible with the activation of a delayed IPSP at the EPSP peak (↓ in Fig. 2*B2* and *inset*) that increased in amplitude with depolarization. The latency for this component (6.3 ± 1.2 ms; $n = 4$) is compatible with a disynaptic onset after electrical stimulation of the ipsilateral semicircular canal nerve. Because the cerebellum was removed in all experiments, this inhibition is likely mediated by inhibitory neurons in the ipsilateral vestibular nuclei as described earlier (Straka and Dieringer 1996).

The effect of the inhibitory responses on subsequent monosynaptic EPSPs in phasic 2°VN was revealed by stimulation of a semicircular canal nerve with two electrical pulses at different interstimulus intervals (Fig. 2, *C* and *D*). EPSPs evoked at various intervals after a preceding EPSP had smaller peak amplitudes (see 1–5 in Fig. 2*C1*). More precisely, the amplitude of the second EPSP depended on the interval between the two stimuli and was reduced by 35% if the two stimuli were

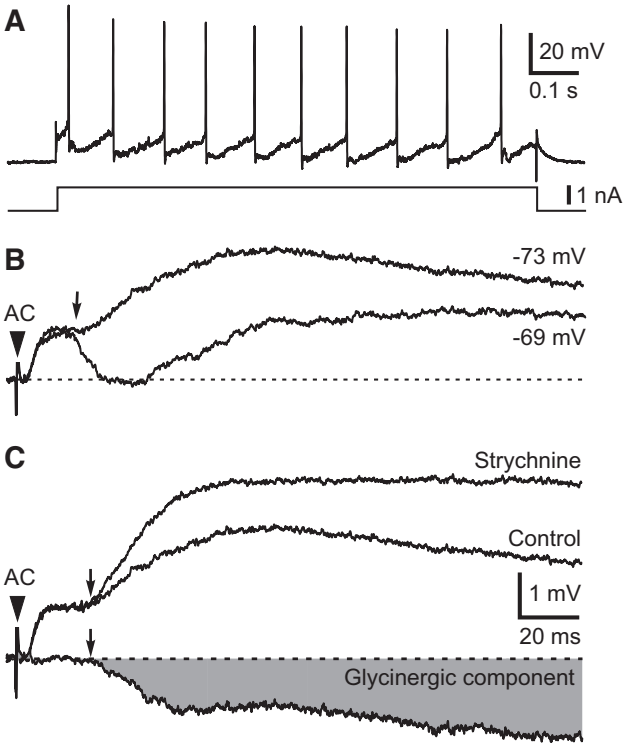

FIG. 4. Inhibitory responses superimposed on monosynaptic EPSPs in a tonic 2°VN. *A*: continuous discharge evoked by injection of a long positive current step (1.2 nA) characteristic for tonic 2°VN. *B*: overlay of monosynaptic responses; EPSPs were evoked by electrical stimulation of the anterior vertical semicircular canal (AC) nerve at 2.6 × T and were recorded at 2 different membrane potentials; note that a pronounced long-latency inhibitory component (↓) appears at the depolarized membrane potential. *C*: AC nerve-evoked monosynaptic EPSPs in the same tonic 2°VN before (control) and in the presence of 1 μM strychnine. Electronic subtraction of the responses revealed a glycinergic component (▨) with a long-latency onset (↓). ▼, stimulus onset; - - -, base line in *B* and the resting membrane potential of −73 mV in *C;* the trace in *A* is a single sweep and in *B* and *C,* the average of 24 individual responses, respectively. Calibration bars in *C* apply also to *B*.

separated by 25 ms (Fig. 2*D*). With larger interstimulus intervals, the reduction became gradually smaller and EPSPs evoked ~200 ms after the first had the same amplitude. This reduction in amplitude of the second EPSP was significantly less pronounced in the presence of 1 μM strychnine (1 and 2 in Fig. 2*C2*) or 1 μM bicuculline. Application of strychnine increased the amplitudes of both the first and the second EPSPs (Fig. 2*C2*); however, the second EPSP was disproportionately larger relative to the first. Accordingly, the marked reduction in amplitude of the second EPSP in controls (35 ± 4%; $n = 10$) was only 11 ± 4% ($n = 5$) in the presence of strychnine and 22 ± 3% ($n = 5$) in the presence of bicuculline (see amplitudes of EPSPs separated by 25 ms in Fig. 2*D*). Combined application of strychnine and bicuculline was attempted in few 2°VN ($n = 4$) but regularly caused a DC depolarization >20 mV that did not allow a study of the combined effects of both blockers. This depolarization is likely a consequence of increased continuous excitatory drive due to the functional neuronal circuitry in the isolated frog brain. A contribution of a persistent Na-conductance to this depolarization is unlikely because the membrane properties of phasic 2°VN are dominated by powerful voltage-dependent K conductances that effectively counteract the possible activation of a persistent Na conductance (Beraneck et al. 2007). The increase in amplitude of the second EPSP in the presence of either one of the two inhibitory transmitter blockers corroborates the activation of an inhibition by the first stimulus pulse that caused a reduction of the amplitude of the second EPSP in controls. However, the different time course of the effects of strychnine and bicuculline (Fig. 2*D*) suggest that glycinergic IPSPs are larger and last longer than GABAergic IPSPs.

The profiles of pharmacologically unmasked glycinergic and GABAergic inhibitory components were studied in 36 phasic 2°VN, including five neurons where the effect of strychnine as well as bicuculline was tested by sequential application of the two blockers in the same 2°VN (see Fig. 3*B, 1* and *2*). To facilitate a comparison of the amplitudes and profiles of disynaptic inhibitory components in phasic 2°VN, semicircular canal nerves were stimulated with a similar current pulse intensity (2.3 × T ± 0.3; $n = 36$). Application of either strychnine or bicuculline increased the amplitude of the monosynaptic EPSPs in all phasic 2°VN (e.g., Fig. 3*B, 1* and *2*). Electronic subtraction of the traces before and in the presence of the inhibitory transmitter blockers indicated that the unmasked glycinergic and GABAergic component have similar disynaptic onset latencies (~6.2 ms) and times to peak (~8.1 ms; Table 1). However, the unmasked glycinergic component had a larger peak amplitude and a longer duration than the GABAergic component as revealed by the sequential application of strychnine and bicuculline in the same phasic 2°VN (compare ▨ in Fig. 3*B,1* and *2*). Calculation of the area of the unmasked inhibitory components in all recorded phasic 2°VN indicated that this is a general feature of the glycinergic inhibition (Table 1). The larger area after normalization (Table 1) confirms the notion that a longer time course rather than a larger peak amplitude is the cause of the larger contribution of the glycinergic compared with the GABAergic component. Thus the extent of the ipsilateral disynaptic inhibition in phasic 2°VN depends on the pharmacological profile of the mediating population of interneurons, given the fact that only a small population of vestibular neurons has glycine and GABA co-localized (Reichenberger et al. 1997). In the five neurons where strychnine and bicuculline were applied sequentially, both antagonists revealed a superimposed disynaptic IPSP. This suggests that any given phasic 2°VN receives a glycinergic as well as a GABAergic inhibitory component.

Application of 7-Cl KYNA (10 μM) in the presence of either strychnine or bicuculline reduced the increased EPSPs slightly below control values, respectively (Fig. 3*B, 1* and *2*). This is compatible with the results of semicircular canal nerve-evoked field potentials (Fig. 1, *D–F*) and indicates that the increase in EPSP amplitudes provoked by inhibitory transmitter antagonists is caused to a considerable extent by a NMDA receptor-mediated component. However, at present it is unclear how much of the increase due to the block of the inhibition is caused by a concomitant increase of the non-NMDA (α-amino-3-hydroxy-5-methyl-4-isoxazolepropionic acid; AMPA) receptor-mediated response, which comprises the major component of vestibular nerve afferent-evoked EPSPs (Straka and Dieringer 1996). Because the proportion of the AMPA and NMDA response depends on the afferent fiber spectrum that activates the two components (Straka et al. 1996), it is at present not possible to precisely determine how much of each component is affected by the disynaptic inhibition.

Effects of strychnine and bicuculline on monosynaptic EPSPs in tonic 2°VN

The presence of superimposed inhibitory components on monosynaptic EPSPs in tonic 2°VN (Fig. 4, *B* and *C*) after electrical stimulation (at 2.3 × T) of the AC ($n = 2$), HC ($n = 1$), and PC ($n = 3$) nerves was studied after application of strychnine ($n = 3$) or bicuculline ($n = 3$). The limited number of recorded neurons is due to their relatively smaller percentage in the total population of 2°VN (~20%) (Beraneck et al. 2007; Straka et al. 2004) as well as to the limited period of stable recordings necessary for the pharmacological experiments. Nonetheless an inhibitory response superimposed on

TABLE 1. *Parameters of unmasked glycinergic and GABAergic inhibitory components superimposed on monosynaptic semicircular canal nerve-evoked EPSPs in phasic 2°VN*

	Latency, ms	Peak Amplitude, mV	Time to Peak, ms	Amplitude 80 ms After Onset of IPSP, mV	Area of IPSP Between Onset and 80 ms, mVms	Normalized Area of IPSP, ms
Glycinergic IPSP ($n = 20$)	6.16 ± 1.23	1.50 ± 0.22	8.07 ± 1.34	1.02 ± 0.13	84.44 ± 10.76	55.92 ± 3.92
GABAergic IPSP ($n = 21$)	6.12 ± 1.31 (NS)	1.08 ± 0.18 (‡)	8.35 ± 1.13 (NS)	0.47 ± 0.15 (**)	31.07 ± 3.83 (***)	29.99 ± 3.68 (***)

The normalized area was calculated as the absolute area (mV × ms) divided by the peak amplitude of the inhibitory postsynaptic potentials (IPSPs, mV), respectively. Values represent the means ± SD; significance of difference between parameters of glycinergic and GABAergic IPSPs: $*P \leq 0.05$, $**P \leq 0.01$, $***P \leq 0.001$ (Mann-Whitney *U*-test); NS, not significant. EPSP, excitatory postsynaptic potential.

monosynaptic EPSPs was encountered in tonic 2°VN. In a few neurons, the inhibitory component became visible after depolarization of the membrane potential (Fig. 4*B*).The small notch following the peak of the monosynaptic EPSP at a resting membrane potential of −73 mV (Fig. 4*B,* ↓), was facilitated at −69 mV and truncated the monosynaptic EPSP, compatible with a delayed inhibition. The onset of this component (21.3 ± 3.4 ms; $n = 3$), however, was much longer than that of the inhibitory components in phasic 2°VN.

Application of 1 μM strychnine (Fig. 4*C*) or bicuculline increased the EPSP of tonic 2°VN and unmasked inhibitory components with amplitudes of 0.8–3 mV. No difference was encountered between the amplitude and time course of the unmasked glycinergic and GABAergic IPSP. The onset of the inhibitory component (Fig. 4*C,* ▨) had an average latency of 23.2 ± 4.1 ms ($n = 6$) and was similar for the two pharmacological types of IPSPs. At higher stimulus intensities (>4 × T; $n = 4$), the number of synaptically-evoked action potentials superimposed on the longer-latency components of the EPSPs increased in the presence of both strychnine and bicuculline from approximately two to three to six spikes in different neurons (not shown). Unfortunately, the small sample size of tonic 2°VN ($n = 6$) did not allow a detailed analysis of possible differences of glycinergic and GABAergic IPSP profiles and corresponding changes in spike discharge pattern and timing. Nonetheless, the long latency of the inhibitory responses excludes a disynaptic origin of this component in tonic 2°VN.

Differential control of the spike discharge in phasic 2°VN by strychnine and bicuculline

Electrical stimulation of semicircular canal nerves at intensities >2.5 × T usually triggered action potentials on top of the monosynaptic EPSPs in phasic 2°VN (Fig. 5, *A, 1* and *4,* to *C, 1* and *4*). The average number of evoked spikes per stimulus pulse (spikes/pulse) increased with current intensity, saturated at stimulus intensities of 4–4.5 × T and was limited to approximately two spikes in most phasic 2°VN (mean: 2.06 spikes/pulse; Table 2). With increasing stimulus intensities the onset latency of the first spike as well as the first interspike interval became gradually shorter and less variable.

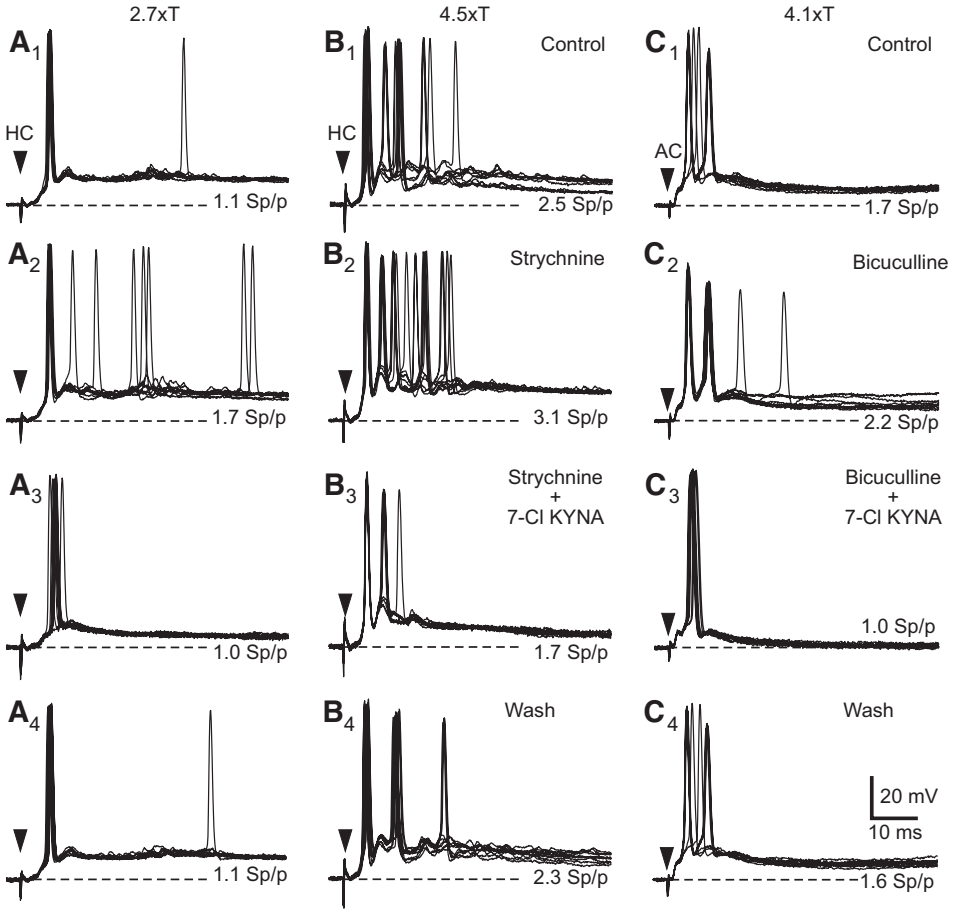

FIG. 5. Effects of glycine, $GABA_A$, and NMDA receptor antagonists on semicircular canal nerve-evoked spike discharge in 2 phasic 2°VN. *A* and *B*: HC nerve-evoked monosynaptic EPSPs and superimposed action potentials at 2 stimulus intensities (2.7 × T in *A,* 4.5 × T in *B*) in a phasic 2°HC neuron. *C*: AC nerve-evoked monosynaptic EPSPs and superimposed action potentials at a stimulus intensity of 4.1 × T in a phasic 2° AC neuron. Overlay of 10 individual responses, respectively, before (control, *A1–C1*), in the presence of 1 μM strychnine (*A2* and *B2*) or 1 μM bicuculline (*C2*), in the presence of 10 μM 7-Cl KYNA and 1 μM strychnine (*A3* and *B3*) or 10 μM 7-Cl KYNA and 1 μM bicuculline (*C3*) and after washout of the 2 transmitter blockers (wash, *A4–C4*), respectively. The average number of spikes per stimulus pulse (sp/p) of the 10 responses is indicated. ▼ in *A–C* mark stimulus onset; - - -, resting membrane potential at −70 mV in *A* and *B* and −69 mV in *C;* calibration bars in *C4* apply to all other traces.

TABLE 2. *Effects of strychnine, bicuculline, and 7-chloro kynurenic acid (7-CI KYNA) on the parameters of semicircular canal nerve-evoked spike discharge in phasic 2°VN*

	No. of Spikes	Latency of the First Spike, ms	Variability of the Latency of the First Spike, ms	Spike Interval Between First and Second Spike, ms	Variability of the First Spike Interval, ms
Control (n = 13)	2.11 ± 0.41	5.99 ± 0.31	0.22 ± 0.05	5.81 ± 0.67	0.30 ± 0.12
Strychnine	3.23 ± 0.73 (^{**1})	5.49 ± 0.28 (^{***1})	0.16 ± 0.04 (^{**1})	4.76 ± 0.39 (^{**1})	0.19 ± 0.07 (^{*1})
Strychnine + 7-CI KYNA	1.92 ± 0.44 (^{**2})	6.17 ± 0.33 (^{***2})	0.25 ± 0.05 (^{**2})	5.78 ± 0.63 (^{*2})	0.33 ± 0.09 (^{*2})
Control (n = 14)	2.02 ± 0.33	6.09 ± 0.50	0.26 ± 0.07	5.38 ± 0.42	0.25 ± 0.06
Bicuculline	2.41 ± 0.44 (^{*1})	5.51 ± 0.50 (^{***1})	0.18 ± 0.04 (^{*1})	4.96 ± 0.37 (^{*1})	0.16 ± 0.04 (^{*1})
Bicuculline + 7-CI KYNA	1.75 ± 0.47 (^{**2})	6.29 ± 0.61 (^{***2})	0.33 ± 0.06 (^{***2})	5.56 ± 0.43 (^{*2})	0.39 ± 0.05 (^{*2})

Spikes were evoked at stimulus intensities of 4–4.5 × T; values represent the means ± SD; significance of difference ($^{*1}P \leq 0.05$, $^{**1}P \leq 0.01$, $^{***1}P \leq 0.001$; Wilcoxon signed-rank test for paired parameters) between parameters of controls and in the presence of strychnine or bicuculline and ($^{*2}P \leq 0.05$, $^{**2}P \leq 0.01$, $^{***2}P \leq 0.001$; Wilcoxon signed-rank test for paired parameters) between the parameters of the latter and in the presence of the inhibitory transmitter blockers, respectively and 7-CI KYNA.

Application of 1 μM strychnine increased in all phasic 2°VN the average number of evoked spikes (Fig. 5, *A2* and *B2*) to reach a maximum of more than 3 spikes/pulse at saturation (Table 2). Application of 1 μM bicuculline also increased the average number of evoked spikes (Fig. 5*C2*); however, the increase was less pronounced (~2.4 spikes/pulse) compared with that provoked by strychnine (Table 2) and only occurred in ~70% of the phasic 2°VN (10 of 14 neurons). This differential effect of strychnine and bicuculline complies with the different time courses of the glycinergic and GABAergic IPSPs at subthreshold stimulus intensities (Fig. 3*B, 1* and *2*).

In contrast to the differential increase of the average spike number per stimulus pulse by strychnine and bicuculline, both antagonists equally affected the timing of the first spike (Table 2). The latency of this spike as well as the first interspike interval in controls (~6 and ~5.5 ms, respectively) decreased to a similar extent in the presence of either one of the two blockers (Table 2). In addition, both transmitter antagonists reduced the variability of the latency of the first spike and the interval of the first two spikes (Table 2), leading to a higher synchronization of the synaptically evoked discharge.

The increase in average spike numbers per stimulus pulse in phasic 2°VN in the presence of the glycine or $GABA_A$ receptor antagonist was reversed beyond control values after application of 10 μM 7-Cl KYNA to the bath (Fig. 5, *A3* to *C3*). At lower stimulus intensities, only the first spike was activated in the presence of the NMDA receptor antagonist (Fig. 5*A3*), whereas the average number of spikes decreased below 2 spikes/pulse at saturation intensities of >4 × T (Fig. 5*B3;* Table 2). In addition, the onset latency of the first spike and the duration of the first interspike interval as well the variability of the latter increased significantly after application of 7-Cl KYNA (Table 2). This is compatible with the idea that the effects of the inhibitory transmitter blockers were mediated in part by an afferent nerve-evoked NMDA component.

DISCUSSION

Semicircular canal nerve-evoked monosynaptic EPSPs in phasic but not in tonic frog 2°VN are superimposed by disynaptic glycinergic and GABAergic IPSPs that differ in their response profiles. The longer duration of the glycinergic compared with the GABAergic IPSPs reduced the amplitude of the monosynaptic EPSPs and the number of evoked spikes for a longer period. These differences in the inhibitory response profiles are in agreement with the overall larger number of glycinergic as opposed to GABAergic terminal-like structures on vestibular neurons. Both pharmacological types of IPSPs control the magnitude and timing of the monosynaptic excitation in phasic 2°VN thereby promoting the processing of transient signals in this vestibular neuronal subtype.

Differential control of afferent excitation in phasic and tonic 2°VN by ipsilateral inhibitory circuits

The activation of semicircular canal nerve-evoked disynaptic IPSPs superimposed on the labyrinthine nerve-evoked monosynaptic EPSPs in phasic but not tonic 2°VN suggests that the afferent excitation in the two types of vestibular neurons is differently controlled by ipsilateral inhibitory circuits. Because the cerebellum was removed in all experiments, the feed-forward inhibition in phasic 2°VN (Fig. 6) is likely mediated by interneurons in the vestibular nuclei on the same side (Straka and Dieringer 1996). Recurrent collaterals of inhibitory vestibular neurons such as those reported in squirrel monkey (McCrea et al. 1987) could further contribute to the disynaptic inhibition. However, because a disynaptic inhibition is present even in the absence of action potentials, the inhibitory inputs must originate from neurons other than the recorded one. The delayed onset of the inhibition with respect to the monosynaptic EPSP, promotes the processing of transient inputs by limiting the duration of the afferent activation, especially at more depolarized membrane potentials (see Fig. 2*B2*). In conjunction with the specific intrinsic membrane properties of phasic 2°VN that make these neurons particularly suitable for signal detection (Beraneck et al. 2007; Straka et al. 2004), the transformation of higher frequency vestibular nerve afferent inputs is enhanced. Thus the effect of the disynaptic inhibition on temporal aspects of evoked afferent synaptic responses in phasic 2°VN acts synergistically with their intrinsic membrane properties.

The absence of an inhibition with a disynaptic onset in frog tonic 2°VN suggests that the vestibular circuit that mediates a feed-forward inhibition to phasic 2°VN is specific and does not relay its signals onto all 2°VN. However, the presence of an ipsilateral inhibition with longer latency in tonic 2°VN indicates that IPSPs are not generally absent in these neurons, compatible with the presence of glycinergic and GABAergic terminal-like structures on virtually every frog central vestibular neuron (Fig. 1, *B* and *C*) (see Reichenberger et al. 1997). Even though both tonic and phasic 2°VN receive monosynaptic EPSPs from the thickest vestibular nerve afferents (Straka

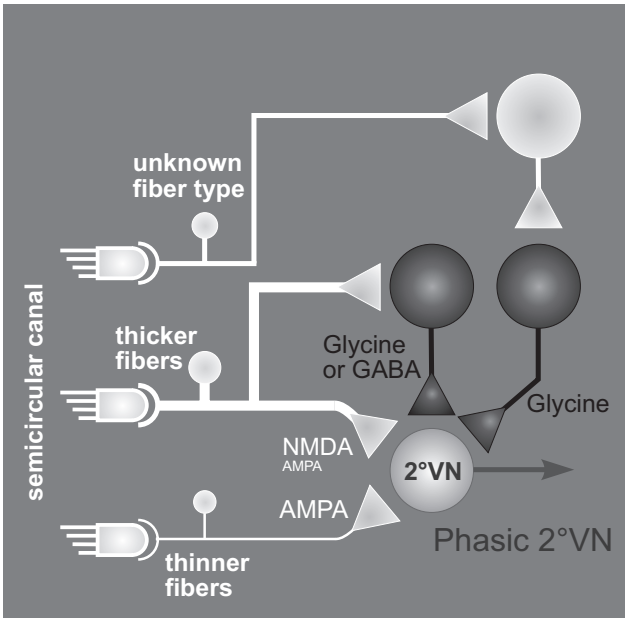

FIG. 6. Schematic diagram illustrating the presumed connectivity of ipsilateral inhibitory circuits and phasic 2°VN. Phasic 2°VN are monosynaptically activated by thicker as well as thinner semicircular canal nerve afferent fibers that differentially activate AMPA and NMDA receptors. Thicker afferent nerve fibers from the same semicircular canal activate inhibitory interneurons that mediate glycinergic and/or GABAergic IPSPs with a disynaptic onset. In addition, a polysynaptic glycinergic IPSP is presumably mediated through intermediary excitatory interneurons that are activated by unknown afferent fiber types. White neurons are excitatory, black neurons are inhibitory.

et al. 2004), the disynaptic inhibition that originates from the same fiber spectrum (Straka and Dieringer 2000) is present only in phasic 2°VN. This suggests that the control of afferent inputs from the thickest vestibular nerve fibers by a feed-forward inhibition (Fig. 6) is not a general feature of vestibular signal processing. Rather the differential organization of the inhibition selectively occurs in conjunction with the intrinsic membrane properties and synaptic response dynamics of phasic and tonic frog 2°VN and promotes the idea of parallel pathways for high and low dynamic vestibular signal transformation (Beraneck et al. 2007; Straka et al. 2004).

Differential profiles of glycinergic and GABAergic inhibitory responses

Disynaptic IPSPs in frog phasic 2° semicircular neurons are glycinergic as well as GABAergic (Fig. 6) (Straka and Dieringer 2000; Straka et al. 1997). The latter IPSPs are mediated only by $GABA_A$ but not by $GABA_B$ receptors (Straka and Dieringer 1996). Glycinergic IPSPs differ from GABAergic IPSPs by larger peak amplitudes and longer duration. The larger peak amplitude might be explained by an activation of more glycinergic synapses, compatible with larger numbers of glycinergic than GABAergic terminal-like structures on frog vestibular neurons (Fig. 1, *B* and *C*).

The longer duration of glycinergic IPSPs could be due to slower channel kinetics, additional activation of glycinergic synapses at longer latency, more distal synaptic termination sites, or a particular interaction with the excitatory inputs. Differences in ion channel activation kinetics or location of synapses are unlikely because the rise times of the glycinergic and GABAergic IPSPs (Straka et al. 1997) and the largely somatic location of the glycinergic and GABAergic terminal-like structures are similar (Reichenberger et al. 1997). More likely, an additional recruitment of glycinergic synapses at longer latency activated by higher-order inhibitory interneurons could cause a longer duration. This is also compatible with the generally larger number of glycinergic terminal structures on frog 2°VN. Alternatively, the longer duration of the glycinergic IPSPs might result from the larger peak amplitudes that more effectively reduce the monosynaptic EPSPs through the nonlinear interaction with the NMDA receptor-mediated component (see following text). A larger IPSP would cause a disproportionately larger reduction of the NMDA receptor component due to a nonproportional increase of the voltage-dependent Mg^{2+} block (Nowak et al. 1984). This would reduce a NMDA receptor-activated Ca^{2+} influx to a larger extent, and a block of the glycinergic IPSP would therefore unmask an inhibitory component with a longer duration.

Because only few frog vestibular neurons co-localize glycine and GABA (Reichenberger et al. 1997), separate subsets of inhibitory interneurons with different functional roles at multiple synaptic levels might be recruited following activation of ipsilateral semicircular canal afferents. Future experiments in the isolated whole brain employing more natural stimuli will reveal possible differences in the glycinergic and GABAergic feed-forward side-loops for the control of dynamic response parameters in 2°VN.

Disynaptic inhibition of different glutamate receptor-mediated components

The increase of the monosynaptic glutamatergic EPSP by glycinergic or GABAergic blockers in phasic 2°VN diminished after adding a NMDA blocker (Fig. 3). This indicates that the disynaptic inhibition exerts its effect in part by controlling the activation of the NMDA receptor-mediated component compatible with earlier results (Straka et al. 1996). This NMDA component is evoked only by the thickest vestibular nerve afferent fibers, whereas AMPA receptors are activated predominantly, although not exclusively, by thinner fibers (Straka and Dieringer 1996; Straka et al. 1996). Thus the monosynaptic NMDA component and the disynaptic inhibition originate from the same afferent fiber spectrum, i.e., the thickest vestibular afferent fibers (Straka and Dieringer 1996, 2000), compatible with the feed-forward side-loop model of Minor and Goldberg (1991).

The disynaptic inhibition when activated would reduce the magnitude of the NMDA receptor component in phasic 2°VN largely by two interrelated mechanisms. First, the evoked IPSPs decrease the input resistance by opening Cl^- channels that cause a shunt of all subsequent inputs (Fig. 2, *C* and *D*) and at depolarized membrane potentials, truncate the underlying monosynaptic EPSP (see Fig. 2*B, inset*). Second, the hyperpolarization due to the inhibition disfacilitates a NMDA receptor activation by reinforcing the voltage-dependent Mg^{2+} block thereby minimizing long-lasting depolarizations and active dendritic events. Thus a reduction of the NMDA component by ipsilateral glycinergic and GABAergic circuits together with the activation of voltage-dependent K^+ conductances (Beraneck et al. 2007) results in a limitation of long-lasting labyrin-

thine afferent activity in frog phasic 2°VN and particularly promotes transient inputs.

A concomitant decrease of the afferent nerve-evoked AMPA component by the disynaptic inhibition in phasic 2°VN is likely, although its magnitude might be smaller due to the absence of voltage-dependent activation requirements of this glutamate-receptor subtype. To compare the relative proportions of NMDA and AMPA receptor-mediated excitation, controlled by the disynaptic glycinergic and GABAergic feed-forward inhibition, the time courses and respective contribution of both components to the monosynaptic EPSP need to be determined. However, any attempt to study a differential control of the two glutamate receptor components by the inhibitory side-loop is constrained by the fact that the relative contribution of NMDA and AMPA components to the monosynaptic EPSP in frog 2°VN varies and depends on the activation of the presynaptic afferent fiber spectrum (Fig. 6) (Straka and Dieringer 1996, 2000; Straka et al. 1996).

The possibility that the disynaptic inhibition controls the afferent excitation in 2°VN through an interaction not only with the NMDA but also with the AMPA receptor-mediated component is not compromising the interpretation of the present results. According to the side-loop model of Minor and Goldberg (1991), the disynaptic feed-forward inhibition cancels the monosynaptic excitatory inputs from the same spectrum of thick afferent fibers. Assuming that this connectivity is in fact implemented in the frog vestibular circuitry, it is not surprising that the disynaptic inhibition would control both AMPA and NMDA components because the thickest vestibular nerve afferent fibers monosynaptically activate both receptor subtypes in 2°VN (Fig. 6) (Straka et al. 1996). However, the NMDA component considerably exceeds that of the AMPA component activated by these afferent fiber types (Straka et al. 1996). Future experiments on frog brain stem slice preparations with the VIIIth nerve attached and the local inhibitory network intact that allow reversible, repetitive application of AMPA, NMDA, glycine, and GABA receptor antagonists will reveal the precise cellular control mechanism of the ipsilateral disynaptic inhibition.

Common network circuitry underlying vertebrate central vestibular information processing

Based on intrinsic membrane properties and response dynamics, frog tonic and phasic 2°VN are functionally equivalent to rodent type A and type B MVN neurons (Bagnall et al. 2007; Beraneck et al. 2003, 2007; Johnston et al. 1994; Saito and Ozawa 2007; Sekirnjak and du Lac 2006; Takazawa et al. 2004; see Straka et al. 2005). Supported by neuronal modeling (Av-Ron and Vidal 1999; Quadroni and Knöpfel 1994), vestibular signal processing in separate frequency-tuned neuronal channels seems to be a common mechanism. Consequently, intrinsic membrane and emerging network properties of the different neuronal subtypes in mammals might also be co-adapted as in frogs (Beraneck et al. 2007). A differential insertion of vestibular neuronal subtypes into vestibular networks is substantiated by the differences in discharge regularity of type A and B MVN neurons in the guinea pig whole brain (Babalian et al. 1997) or of cat tonic and "kinetic" vestibular neurons (Shimazu and Precht 1965). The irregular resting activity of type B MVN neurons in the isolated whole brain (Babalian et al. 1997) as opposed to their regular discharge in brain slices is likely caused by considerable random spontaneous synaptic activity generated by inhibitory network circuitry. In fact, mouse type B MVN neurons (functionally equivalent to frog phasic 2°VN) receive more spontaneous glycinergic and GABAergic inputs from ipsilateral vestibular interneurons than type A MVN neurons (Camp et al. 2006). This predominance of IPSPs in one vestibular cell type complies with the activation of disynaptic IPSPs in only ~50% of vestibular neurons after electrical stimulation of vestibular nerve afferents in monkey (Goldberg et al. 1987). In mammals, a feed-forward inhibition that exerts its effect on type B MVN neurons might originate from the specific subset of GABAergic neurons in the parvocellular part of the MVN that differ in their physiology from vestibuloocular projection neurons (Bagnall et al. 2007; Gittis and du Lac 2006; Sekirnjak and du Lac 2006). The presence of a set of specific conductances in type B MVN neurons (Beraneck et al. 2003; Eugene et al. 2007; Johnston et al. 1994) render these neurons particularly sensitive to inhibitory synaptic inputs from, e.g., interneuronal connections. A modifiable gain of the inhibitory side-loop through inhibitory or excitatory inputs would allow short- and long-term adaptive changes for an independent and graded control of responses in type B MVN neurons suitable for a continuous fine tuning of the dynamics as suggested by the feed-forward side-loop model of Minor and Goldberg (1991).

ACKNOWLEDGMENTS

Thanks to Drs. M. Beraneck and P. P. Vidal for valuable comments on an earlier version of this manuscript and to Dr. L. E. Moore for critically reading the manuscript. The work was supported by funding from the Centre Nationale des Etudes Spatiales (CNES).

REFERENCES

Angelaki DE, Perachio AA. Contribution of irregular semicircular canal afferents to the horizontal vestibuloocular response during constant velocity rotation. *J Neurophysiol* 69: 996–999, 1993.

Av-Ron E, Vidal PP. Intrinsic membrane properties and dynamics of medial vestibular neurons: a simulation. *Biol Cybern* 80: 383–392, 1999.

Babalian A, Vibert N, Assié G, Serafin M, Mühlethaler M, Vidal PP. Central vestibular networks in the guinea pig: functional characterization in the isolated whole brain in vitro. *Neuroscience* 81: 405–426, 1997.

Bagnall MW, Stevens RJ, du Lac S. Transgenic mouse lines subdivide medial vestibular nucleus neurons into discrete, neurochemically distinct populations. *J Neurosci* 27: 2318–2330, 2007.

Beraneck M, Hachemaoui M, Idoux E, Ris L, Uno A, Godaux E, Vidal PP, Moore LE, Vibert N. Long-term plasticity of ipsilesional medial vestibular nucleus neurons after unilateral labyrinthectomy. *J Neurophysiol* 90: 184–203, 2003.

Beraneck M, Pfanzelt S, Vassias I, Rohregger M, Vibert N, Vidal PP, Moore LE, Straka H. Differential intrinsic response dynamics determine synaptic signal processing in frog vestibular neurons. *J Neurosci* 27: 4283–4296, 2007.

Biesdorf S, Straka H. Control of responses in frog second-order semicircular canal neurons by inhibitory and excitatory inputs. *Soc Neurosci Abstr* 30: 652.1, 2004.

Boyle R, Goldberg JM, Highstein SM. Inputs from regularly and irregularly discharging vestibular nerve afferents to secondary neurons in squirrel monkey vestibular nuclei. III. Correlation with vestibulospinal and vestibuloocular output pathways. *J Neurophysiol* 68: 471–484, 1992.

Camp AJ, Callister RJ, Brichta AM. Inhibitory synaptic transmission differs in mouse type A and B medial vestibular nucleus neurons in vitro. *J Neurophysiol* 95: 3208–3218, 2006.

Chen-Huang C, McCrea R, Goldberg JM. Contributions or regularly and irregularly discharging vestibular-nerve inputs to the discharge of central vestibular neurons in the alert squirrel monkey. *Exp Brain Res* 114: 405–422, 1997.

Eugene D, Deforges S, Guimont F, Idoux E, Vidal PP, Moore LE, Vibert N. Developmental regulation of the membrane properties of central vestibular neurons by sensory vestibular information in the mouse. *J Physiol* 583: 923–943, 2007.

Gittis AH, du Lac S. Firing properties of GABAergic versus non-GABAergic vestibular nucleus neurons conferred by a differential balance of potassium currents. *J Neurophysiol* 97: 3986–3996, 2006.

Goldberg JM. Afferent diversity and the organization of central vestibular pathways. *Exp Brain Res* 130: 277–297, 2000.

Goldberg JM, Highstein SM, Moschovakis AK, Fernández C. Inputs from regularly and irregularly discharging vestibular nerve afferents to secondary neurons in the vestibular nuclei of the squirrel monkey. I. An electrophysiological analysis. *J Neurophysiol* 58: 700–718, 1987.

Highstein SM, Goldberg JM, Moschovakis AK, Fernández C. Inputs from regularly and irregularly discharging vestibular nerve afferents to secondary neurons in the vestibular nuclei of the squirrel monkey. II. Correlation with output pathways of secondary neurons. *J Neurophysiol* 58: 714–739, 1987.

Johnston AR, MacLeod NK, Dutia MB. Ionic conductances contributing to spike repolarization and after-potentials in rat medial vestibular nucleus neurones. *J Physiol* 481: 61–77, 1994.

Luksch H, Walkowiak W, Muñoz A, ten Donkelaar HJ. The use of in vitro preparations of the isolated amphibian central nervous system in neuroanatomy and electrophysiology. *J Neurosci Methods* 70: 91–102, 1996.

McCrea RA, Strassman A, May E, Highstein SM. Anatomical and physiological characteristics of vestibular neurons mediating the horizontal vestibulo-ocular reflex of the squirrel monkey. *J Comp Neurol* 264: 547–570, 1987.

Minor LB, Goldberg JM. Vestibular nerve inputs to the vestibulo-ocular reflex: a functional ablation study in the squirrel monkey. *J Neurosci* 11: 1636–1648, 1991.

Nowak L, Bregestovski P, Ascher P, Herbert A, Prochiantz A. Magnesium gates glutamate-activated channels in mouse central neurons. *Nature* 307: 462–465, 1984.

Quadroni R, Knöpfel T. Compartmental models of type A and type B guinea pig medial vestibular neurons. *J Neurophysiol* 72: 1911–1924, 1994.

Reichenberger I, Dieringer N. Size-related colocalization of glycine and glutamate immunoreactivity in frog and rat vestibular afferents. *J Comp Neurol* 349: 603–614, 1994.

Reichenberger I, Straka H, Ottersen OP, Streit P, Gerrits NM, Dieringer N. Distribution of GABA, glycine and glutamate immunoreactivities in the vestibular nuclear complex of the frog. *J Comp Neurol* 377: 149–164, 1997.

Saito Y, Ozawa S. Membrane properties of rat medial vestibular nucleus neurons in vivo. *Neurosci Res* 59: 215–223, 2007.

Sekirnjak C, du Lac S. Physiological and anatomical properties of mouse medial vestibular nucleus neurons projecting to the oculomotor nucleus. *J Neurophysiol* 95: 3012–3023, 2006.

Shao M, Hirsch JC, Giaume C, Peusner KD. Spontaneous synaptic activity is primarily GABAergic in vestibular nucleus neurons of the chick embryo. *J Neurophysiol* 90: 1182–1192, 2003.

Shao M, Hirsch JC, Giaume C, Peusner KD. Spontaneous synaptic activity in chick vestibular nucleus neurons during the perinatal period. *Neuroscience* 127: 81–90, 2004.

Shimazu H, Precht W. Tonic and kinetic responses of cat's vestibular neurons to horizontal angular acceleration. *J Neurophysiol* 28: 991–1013, 1965.

Straka H, Beraneck M, Rohregger M, Moore LE, Vidal PP, Vibert N. Second-order vestibular neurons form separate populations with different membrane and discharge properties. *J Neurophysiol* 92: 845–861, 2004.

Straka H, Biesdorf S, Dieringer N. Canal-specific excitation and inhibition of frog second order vestibular neurons. *J Neurophysiol* 78: 1363–1372, 1997.

Straka H, Debler K, Dieringer N. Size-related properties of vestibular afferent fibers in the frog: differential synaptic activation of *N*-methyl-D-aspartate and non-*N*-methyl-D-aspartate receptors. *Neuroscience* 70: 697–707, 1996.

Straka H, Dieringer N. Electrophysiological and pharmacological characterization of vestibular inputs to identified frog abducens motoneurons and internuclear neurons in vitro. *Eur J Neurosci* 5: 251–260, 1993.

Straka H, Dieringer N. Uncrossed disynaptic inhibition of second-order vestibular neurons and its interaction with monosynaptic excitation from vestibular nerve afferent fibers in the frog. *J Neurophysiol* 76: 3087–3101, 1996.

Straka H, Dieringer N. Convergence pattern of uncrossed excitatory and inhibitory semicircular canal-specific inputs onto second-order vestibular neurons of frogs. *Exp Brain Res* 135: 462–473, 2000.

Straka H, Dieringer N. Basic organization principles of the VOR: lessons from frogs. *Prog Neurobiol* 73: 259–309, 2004.

Straka H, Vibert N, Vidal PP, Moore LE, Dutia MB. Intrinsic properties of vertebrate vestibular neurons: function, development and plasticity. *Prog Neurobiol* 76: 349–392, 2005.

Takazawa T, Saito Y, Tsuzuki K, Ozawa S. Membrane and firing properties of glutamatergic and GABAergic neurons in the rat medial vestibular nucleus. *J Neurophysiol* 92: 3106–3120, 2004.

4 Differential Dynamic Processing of Afferent Signals in Frog Tonic and Phasic Second-Order Vestibular Neurons

The Journal of Neuroscience, October 8, 2008 • 28(41):10349–10362 • 10349

Behavioral/Systems/Cognitive

Differential Dynamic Processing of Afferent Signals in Frog Tonic and Phasic Second-Order Vestibular Neurons

Sandra Pfanzelt,[1,2] Christian Rössert,[2] Martin Rohregger,[3] Stefan Glasauer,[2] Lee E. Moore,[1] and Hans Straka[1]

[1]Laboratoire de Neurobiologie des Réseaux Sensorimoteurs, Centre National de la Recherche Scientifique, UMR 7060, Université Paris Descartes, 75270 Paris Cedex 06, France, [2]Department of Neurology, Bernstein Center for Computational Neuroscience, Ludwig-Maximilians-Universität München, 81377 Munich, Germany, and [3]Department of Physiology, Ludwig-Maximilians-Universität München, 80336 Munich, Germany

The sensory–motor transformation of the large dynamic spectrum of head-motion-related signals occurs in separate vestibulo-ocular pathways. Synaptic responses of tonic and phasic second-order vestibular neurons were recorded in isolated frog brains after stimulation of individual labyrinthine nerve branches with trains of single electrical pulses. The timing of the single pulses was adapted from spike discharge patterns of frog semicircular canal nerve afferents during sinusoidal head rotation. Because each electrical pulse evoked a single spike in afferent fibers, the resulting sequences with sinusoidally modulated intervals and peak frequencies up to 100 Hz allowed studying the processing of presynaptic afferent inputs with *in vivo* characteristics in second-order vestibular neurons recorded *in vitro* in an isolated whole brain. Variation of pulse-train parameters showed that the postsynaptic compound response dynamics differ in the two types of frog vestibular neurons. In tonic neurons, subthreshold compound responses and evoked discharge patterns exhibited relatively linear dynamics and were generally aligned with pulse frequency modulation. In contrast, compound responses of phasic neurons were asymmetric with large leads of subthreshold response peaks and evoked spike discharge relative to stimulus waveform. These nonlinearities were caused by the particular intrinsic properties of phasic vestibular neurons and were facilitated by GABAergic and glycinergic inhibitory inputs from tonic type vestibular interneurons and by cerebellar circuits. Coadapted intrinsic filter and emerging network properties thus form dynamically different neuronal elements that provide the appropriate cellular basis for a parallel processing of linear, tonic, and nonlinear phasic vestibulo-ocular response components in central vestibular neurons.

Key words: **semicircular canal; phasic; tonic; afferent fibers; vestibular; macula**

Introduction

Processing of head movement-related signals in vestibulomotor networks occurs in parallel pathways that are organized as frequency-tuned channels from the sensory periphery to the motor plant (Lisberger et al., 1983; Minor et al., 1999; Goldberg, 2000; Straka and Dieringer, 2004). This parallel organization is necessary to transform sensory signals as diverse as static head deviation or high acceleration profiles that occur during rapid locomotion into dynamically adequate motor commands for gaze and posture control. Hair cells in vestibular end organs and vestibular afferent fibers appear to be organized as subpopulations of dynamically different neuronal elements with interrelated morphophysiological properties for the detection and coding of head motion (Baird, 1994a,b; Eatock et al., 1998; Goldberg, 2000; Straka and Dieringer, 2004).

At the level of central vestibular neurons distinct subpopulations of second-order vestibular neurons (2°VNs) with different intrinsic membrane properties have been observed in various vertebrate species (Serafin et al., 1991; Johnston et al., 1994; du Lac and Lisberger, 1995; Peusner and Giaume, 1997; Straka et al., 2005). Although cellular properties of 2°VNs may vary between vertebrate species, the different neuronal subgroups form specific filter elements, respectively (Straka et al., 2005). If appropriately adapted to the dynamics of the sensory afferent inputs, these central vestibular populations could separately mediate linear (tonic) and nonlinear (phasic) vestibulomotor components (Minor et al., 1999; Clendaniel et al., 2002).

Based on specific differences in intrinsic membrane properties, frog 2°VNs subdivide into two distinct neuronal subtypes (Straka et al., 2004; Beraneck et al., 2007). Tonic 2°VNs behave like low-pass filters, whereas phasic 2°VNs show a pronounced resonance behavior for subthreshold membrane polarization and spike discharge, thereby generating potential-dependent band-pass filters (Beraneck et al., 2007). The different impedance behavior during membrane polarization makes the two subtypes most suitable for amplification (tonic 2°VNs) and differentiation (phasic 2°VNs) of vestibular inputs (Beraneck et al., 2007). A different insertion of the two neuronal subtypes into local inhib-

Received July 8, 2008; revised Aug. 22, 2008; accepted Aug. 28, 2008.

This work was supported by the French Centre National de la Recherche Scientifique and Centre National d'Etudes Spatiales. S.P. received funding from a Marie-Curie Training Sites contract HPMT-CT-2000-00008 (France), the Deutscher Akademischer Austauschdienst D/05/40377 (Germany), and the Graduiertenkolleg 1091 (Orientation and Motion in Space); C.R. received a PhD grant from the Bayerische Forschungsstiftung. We thank Dr. Mathieu Beraneck for critically reading this manuscript and Dr. Isabelle Vassias for excellent processing and photographing of the histological material shown in Figure 2*A*.

Correspondence should be addressed to Dr. Hans Straka, Laboratoire de Neurobiologie des Réseaux Sensorimoteurs, Centre National de la Recherche Scientifique, UMR 7060, Université Paris Descartes, 45 rue des Saints-Pères, 75270 Paris Cedex 06, France. E-mail: hans.straka@univ-paris5.fr.

DOI:10.1523/JNEUROSCI.3368-08.2008

 0270-6474/08/2810349-14$15.00/0

itory networks as indicated by the presence of ipsilateral disynaptic feedforward IPSPs in phasic but not tonic 2°VNs (Biesdorf et al., 2008) concurs with the highly transient intrinsic properties of the former neurons. The distinctly different filter properties and their differential effect on single monosynaptic afferent EPSPs in phasic and tonic 2°VNs suggests that more complex synaptic inputs similar to those that occur during natural head movements would be the appropriate test to reveal the different modes of signal processing of the two subtypes.

The present study uses the isolated brain of adult frogs to investigate the synaptic responses of tonic and phasic 2°VNs after activation of labyrinthine nerve afferents by trains of single electrical pulses with a timing that was obtained from the spike discharge of afferent fibers during head movements. For this purpose, the spike activity of frog vestibular nerve afferents during sinusoidal head rotation *in vivo* (Blanks and Precht, 1976) was transformed into a sequence of single electrical pulses for the activation of individual labyrinthine nerve branches *in vitro*.

Preliminary results have been published previously in abstract form (Pfanzelt et al., 2004).

Materials and Methods

In vitro experiments were performed on the isolated brains of 47 grass frogs (*Rana temporaria*) and complied with the *Principles of Animal Care* (publication No. 86-23, revised in 1985 by the National Institutes of Health). Permission for these experiments was granted by the government of Oberbayern (211-2531-31/95). As described in previous studies (Straka and Dieringer, 1993), the animals were deeply anesthetized with 0.1% MS-222 (3-aminobenzoic acid ethyl ester), and perfused transcardially with iced Ringer's solution [(in mM) 75 NaCl, 25 $NaHCO_3$, 2 $CaCl_2$, 2 KCl, 0.5 $MgCl_2$, 11 glucose, pH 7.4]. Thereafter, the skull and bony labyrinth were opened by a ventral approach. After dissecting the three semicircular canals on each side, the brain was removed with all labyrinthine end organs attached to the eighth nerve. Subsequently, the brain was submerged in iced Ringer's and the dura, the labyrinthine end organs, and the choroid plexus covering the fourth ventricle were removed. In all experiments, the forebrain was removed. Brains were used up to 4 d after their isolation and were stored overnight at 6°C in continuously oxygenated Ringer's solution (carbogen, 95% O_2, 5% CO_2) with a pH of 7.5 ± 0.1. For the experiments, the brainstem was glued with cyanoacrylate to a plastic mesh, which was fixed with insect pins to the Sylgard floor of a chamber (volume, 2.4 ml). The chamber was continuously perfused with oxygenated Ringer's solution at a rate of 1.3–2.1 ml/min. The temperature was electronically controlled and maintained at 14 ± 0.1°C.

Intracellular recordings were obtained from vestibular nerve afferent fibers ($n = 27$) and central vestibular neurons ($n = 110$). Vestibular nerve afferents were recorded in the eighth nerve between Scarpa's ganglion and the entry of the nerve into the brainstem. The peripheral origin of individual afferent fibers was determined by the presence of short-latency all-or-nothing antidromic responses (<0.8 ms) after separate electrical stimulation of the three semicircular canal nerves or the lagenar nerve branch. Central neurons in the vestibular nuclei were identified as 2°VNs by their monosynaptic responses to separate stimulation of the nerve branches. For electrical activation of the nerve branches, single constant current pulses (duration, 0.2 ms; threshold, 1.5–3.1 μA) were applied across individually adjusted suction electrodes (diameter, 120–150 μm). The use of this electrode type facilitated the isolation of the individual nerve branches without current spread to other labyrinthine nerve branches. Pulses were produced by a stimulus isolation unit (World Precision Instruments A 360).

Glass microelectrodes used for extracellular and intracellular recordings were made with a horizontal puller (P-87 Brown/Flaming). Electrodes for extracellular field potential recordings were beveled (30°, ~20 μm tip diameter) and filled with a 2 M solution of sodium chloride (~1 MΩ final resistance). Electrodes for intracellular recordings were filled with a mixture of 2 M potassium acetate and 3 M potassium chloride (10:1), which gave a final resistance of ~90–110 MΩ. Neuronal recordings were made in bridge mode (SEC-05L; NPI Electronic).

At the beginning of each experiment, presynaptic and postsynaptic field potentials evoked by separate stimulation of the labyrinthine nerve branches were recorded at a standard reference site in the vestibular nuclei to optimize the position of the stimulus electrodes and to determine the stimulus threshold (T) for each nerve branch (Straka et al., 1997, 2002). Stimulus intensities were indicated as multiples of the threshold values for the postsynaptic field potentials. Vestibular neurons were recorded in all vestibular subnuclei (lateral, superior, descending, and medial), except the most medial parts of the medial vestibular nucleus. Based on the differential discharge patterns during long positive current steps, frog 2°VNs were distinctly distinguished into phasic or tonic vestibular neurons (Straka et al., 2004; Beraneck et al., 2007). As reported previously, most of the vestibular neurons in the isolated frog brain had no spontaneous discharge at resting membrane potential (Straka and Dieringer, 2004; Straka et al., 2005). Only neurons with a membrane potential more negative than −55 mV were included in this study.

A differential processing of synaptic signals in phasic and tonic type 2°VNs was studied by applying stimulus trains of single current pulses to the labyrinthine nerve branch, which were as close as possible to naturally occurring vestibular afferent input patterns. The trains consisted of individual pulses with interstimulus frequencies that were sinusoidally modulated up to a variable maximal frequency. The timing of the single pulses in the train and the maximal peak frequency was obtained from the discharge pattern of frog horizontal canal afferent fibers during sinusoidal vertical axis rotation (see Fig. 1*A*) (Blanks and Precht, 1976). The imitation of a natural vestibular afferent discharge by an electrical stimulus train applied to labyrinthine nerve branches in the isolated whole brain *in vitro* is an approximation and restricted by differences in the synchronicity of the evoked discharge in the population of recruited afferent fibers and the activated fiber spectrum compared with the *in vivo* situation. However, this particular stimulus paradigm provides an excellent way to bridge the gap between *in vivo* studies of vestibulo-ocular functionality and *in vitro* single-cell studies of intrinsic membrane properties of 2°VNs.

For the transformation of the afferent activity *in vivo* into a stimulus train, the discharge of an afferent fiber to sinusoidal head acceleration at 0.2 Hz (±20°) was fitted with a sine wave function (see Fig. 1A_1). Because the resting discharge of this as of most other vestibular nerve afferent fibers in frog is very low (<2–10 spikes/s) (Blanks and Precht, 1976; Dieringer and Precht, 1977), the sine wave was only fitted for the activation half cycle. This sine wave function was transformed into a sequence of single events with sinusoidally modulated intervals and peak frequencies of 40, 70, 100, 150, or 200 Hz for different sets of experiments (see Fig. 1A_2). This sequence was applied during the first half cycle of a sine wave and was followed by a second half cycle without stimuli (see Fig. 1A_3). These electrical pulse trains were applied multiple times (8–20 cycles) to those semicircular canal or the lagena nerve branches that were monosynaptically connected to the recorded 2°VNs. In the following, this stimulation will be denoted as "sinusoidal pulse train."

Each single pulse generated one spike in afferent fibers and evoked monosynaptic EPSPs in 2°VNs. Synaptic compound responses in phasic and tonic 2°VNs were formed by the temporal summation of the evoked individual monosynaptic EPSPs. These compound responses were characterized by several stimulus parameters, such as stimulus peak frequency (40, 70, or 100 Hz), half-cycle length (0.25, 0.5, 1, or 2.5 s), and single-pulse intensity (1.2 to 5× T). Amplitude and timing of the evoked responses were quantified in smoothed fits of the compound responses (see Fig. 2*D*,*E*, red lines). A compound response peak advance (+) or lag (−) relative to stimulus peak frequency was determined as the time between compound response peak and stimulus peak frequency and converted into degrees. The conversion allowed comparing the results obtained at different half-cycle lengths.

A contribution of glycinergic and GABAergic inhibitory circuits to the processing of synaptic signals in 2°VNs was studied by bath application of strychnine (Sigma; 1 μM) and bicuculline (Sigma; 1–5 μM). Surgical removal of the cerebellum or pressure injection of 100–150 nl of lidocaine (Sigma; 2–5% in Ringer's solution) through a beveled injection

electrode (30°, 10–15 μm tip diameter) into the ipsilateral cerebellar peduncle was used to reveal a contribution of the cerebellum to the processing of afferent signals in 2°VNs.

Single sweeps of the responses were digitized (CED 1401; Cambridge Electronic Design), stored on computer, and analyzed off-line (Signal, Cambridge Electronic Design; and Matlab, MathWorks). Synaptic potentials were analyzed from averages of 8–20 single sweeps after electronic subtraction of the extracellular field potential recorded in the vicinity. Statistical differences in parameters were calculated according to the Mann–Whitney *U* test (unpaired parameters) and the Wilcoxon signed rank test (paired parameters; Prism, Graphpad Software). All averaged results are expressed as mean ± SE. Graphical presentations were made with the aid of commercially available computer software (Origin, Microcal Software; Corel Draw, Corel).

Retrograde labeling of vestibular projection neurons and anterograde tracing of vestibular nerve afferent fibers (see Fig. 2*A*) helped to determine the location of neurons within the vestibular nuclear boundary in the isolated frog brain based on external landmarks. To outline the location of central vestibular neurons and the termination of vestibular nerve afferent fibers, crystals of Alexa Fluor 488 (green) or 546 dextran (red) were inserted unilaterally into the oculomotor nucleus or the upper spinal cord, or were placed on particular vestibular nerve branches in the periphery in isolated frog brains *in vitro*. After 48 h of survival at 9°C, brains were fixed in 4% paraformaldehyde in 0.1 M phosphate buffer (PB) for 24 h and stored overnight in 15 and 30% sucrose in 0.1 M PB. All brains were cut transversally in 60 μm sections on a cryostat. Sections were mounted on slides, coverslipped with Vectashield (Vector Laboratories; Biovalley), and analyzed by laser scanning confocal microscopy (Zeiss LSM 510) at a wavelength of 488 or 543 nm. Stacks of 10–20 confocal images were generated with a 20×/0.5 objective and a plan Apochromat 40×/1.3 oil-immersion objective. Images for Figure 2*A* were produced by horizontal projection of the entire stack.

Modeling of the synaptic processing in tonic and phasic 2°VNs was performed by extending previously described intrinsic neuronal models (Borg-Graham, 1991; Moore et al., 1995) with conductance-based synapses. Parameter estimation was based on frequency responses of representative phasic and tonic 2°VNs (Beraneck et al., 2007). The estimation was done by a compartmental admittance formulation, which consisted of an active soma and one active dendrite with three compartments. All passive and active parameters were assumed to be uniformly distributed (Moore et al., 1995; Murphey et al., 1995). Parameters were estimated using a compartmental admittance formulation in Matlab (MathWorks). Real-time compartmental models were simulated in NEURON (Carnevale and Hines, 2006) (for a detailed description, see the supplemental material, available at www.jneurosci.org).

Dual-exponential conductance-based synapses were added to the intrinsic single-cell compartmental models using the following equation: $I_{sb} = g_{sb} F [\exp(-t/\tau_2) - \exp(-t/\tau_1)](V_i - V_{sb})$ with τ_1 as rise and τ_2 as fall time constant (Johnston and Wu, 1994). The peak conductance for a single synaptic event was defined by g_{sb}; V_{sb} indicates the reversal potential and V_i the current compartmental membrane potential. The scaling factor F is defined such that the peak of the dual exponential is 1. These synapses were implemented by the function "exp2syn" in the NEURON simulation environment, extended by an absolute synaptic refractory period (Hjelmstad et al., 1997). The values of the reversal potentials for excitatory ($V_{sE} = 0$ mV) and inhibitory synapses ($V_{sI} = -75$ mV) were obtained from Hille (2001). Two different parameter sets for synaptic innervation were used: the "*E* compartmental model" consisted of one excitatory synapse at the last dendritic compartment with the following parameters: $\tau_1 = 5$ ms, $\tau_2 = 97$ ms, $g_{sE} = 16.8$ nS. To mimic the monosynaptic excitation, a delay of 3.4 ms (Biesdorf et al., 2008) from the stimulus to the onset of the excitation was used. For the "*E*/*I* compartmental model" the *E* compartmental model was extended by two inhibitory synapses at the soma: glycine ($\tau_1 = 2$ ms, $\tau_2 = 200$ ms, $g_{sI} = 22.5$ nS) and $GABA_A$ ($\tau_1 = 2$ ms, $\tau_2 = 91$ ms, $g_{sI} = 16.8$ nS). All synaptic time constants and conductances were obtained by fitting published experimental data (Biesdorf et al., 2008). The inhibition for the stimulation paradigms 70 Hz/2.5 s (peak frequency/half-cycle length) in the model was activated by detected spike events of phasic or tonic neurons, using a synaptic delay of 1.8 ms (Straka et al. 1997). For all other computations, the spike discharge of tonic 2°VNs has been generated from the 70 Hz/2.5 s stimulation paradigm.

Results

Discharge of vestibular nerve afferent fibers

Vestibular nerve afferent fibers ($n = 27$) during sinusoidal pulse-train stimulation of individual labyrinthine nerve branches (Fig. 1A_3) were recorded intracellularly to determine the maximal peak frequency at which each single pulse in the train was still able to evoke spikes. Recorded afferent fibers originated from the horizontal canal (HC; $n = 4$), the anterior vertical canal (AC; $n = 4$), the posterior vertical canal (PC; $n = 12$), or the lagena (LA; $n = 7$). Spikes were elicited by electrical pulse intensities between ~1.2 and 3× *T* of the afferent nerve-evoked field potential recorded in the vestibular nuclei (threshold, 1.5–3.1 μA). All pulses of the stimulus train evoked single spikes up to a peak frequency of ~100 Hz (Fig. 1B_1,B_2,*C*, inset for 40 and 100 Hz). Because each individual pulse evoked only one spike, the discharge in the afferent fibers had the same frequency modulation as the stimulus train. At a higher peak frequency, increasingly more single pulses of the train failed to evoke spikes (Fig. 1B_3,*C*, inset for 200 Hz). Although some fibers responded with an action potential to each single pulse up to peak frequencies of 150 Hz, the discharge reliability of the population of recorded afferent neurons decreased progressively for stimulus trains with peak frequencies >100 Hz (Fig. 1*C*).

Because intracellular recordings of axons were likely biased toward larger fibers, the upper frequency for reliable firing during pulse trains are likely dominated by the results from the thickest vestibular nerve afferents. However, the amplitude of labyrinthine nerve-evoked presynaptic field potentials in the vestibular nuclei remained unchanged for stimulus frequencies up to 100 Hz *in vitro* (Biesdorf and Straka, 2004), indicating that most afferents can sustain a discharge up to this frequency, compatible with *in vivo* data (Blanks and Precht, 1976). Therefore, the maximal stimulus peak frequency was limited to 100 Hz in the present study to assure the faithful activation of spikes in all afferent fibers by each electrical pulse of the stimulus train. Because afferent fibers in our *in vitro* study were silent at rest, this electrical stimulus generated a defined presynaptic activity pattern in all afferents that terminate on a particular vestibular neuron. Thus, this electrical stimulus paradigm, which is based on the timing of the spike discharge of a vestibular nerve afferent fiber during a head movement *in vivo*, is well suited to reveal the dynamic processing of vestibular sensory signals in the different neuronal subtypes. Because frog phasic and tonic vestibular neurons receive monosynaptic inputs from a similar afferent fiber spectrum (Straka et al., 2004) any differences in the dynamics of the synaptic processing are unlikely to result from different afferent termination patterns on the two neuronal subtypes, but rather are caused by differences in intrinsic membrane and/or emerging network properties.

Identification and classification of frog vestibular neurons

Central vestibular neurons ($n = 110$) were recorded in the isolated frog brain throughout the rostrocaudal extent of the vestibular nuclei. Retrogradely labeled vestibulo-ocular (Fig. 2A_1,A_2) and vestibulospinal neurons after application of Alexa Fluor 546 dextran in the oculomotor nucleus, or the upper spinal cord and the labeled terminal field of vestibular nerve afferent fibers (Fig. 2A_3) outlined the location of the vestibular neurons in the dorsal hindbrain. Data on afferent and efferent vestibular connections

10352 • J. Neurosci., October 8, 2008 • 28(41):10349–10362

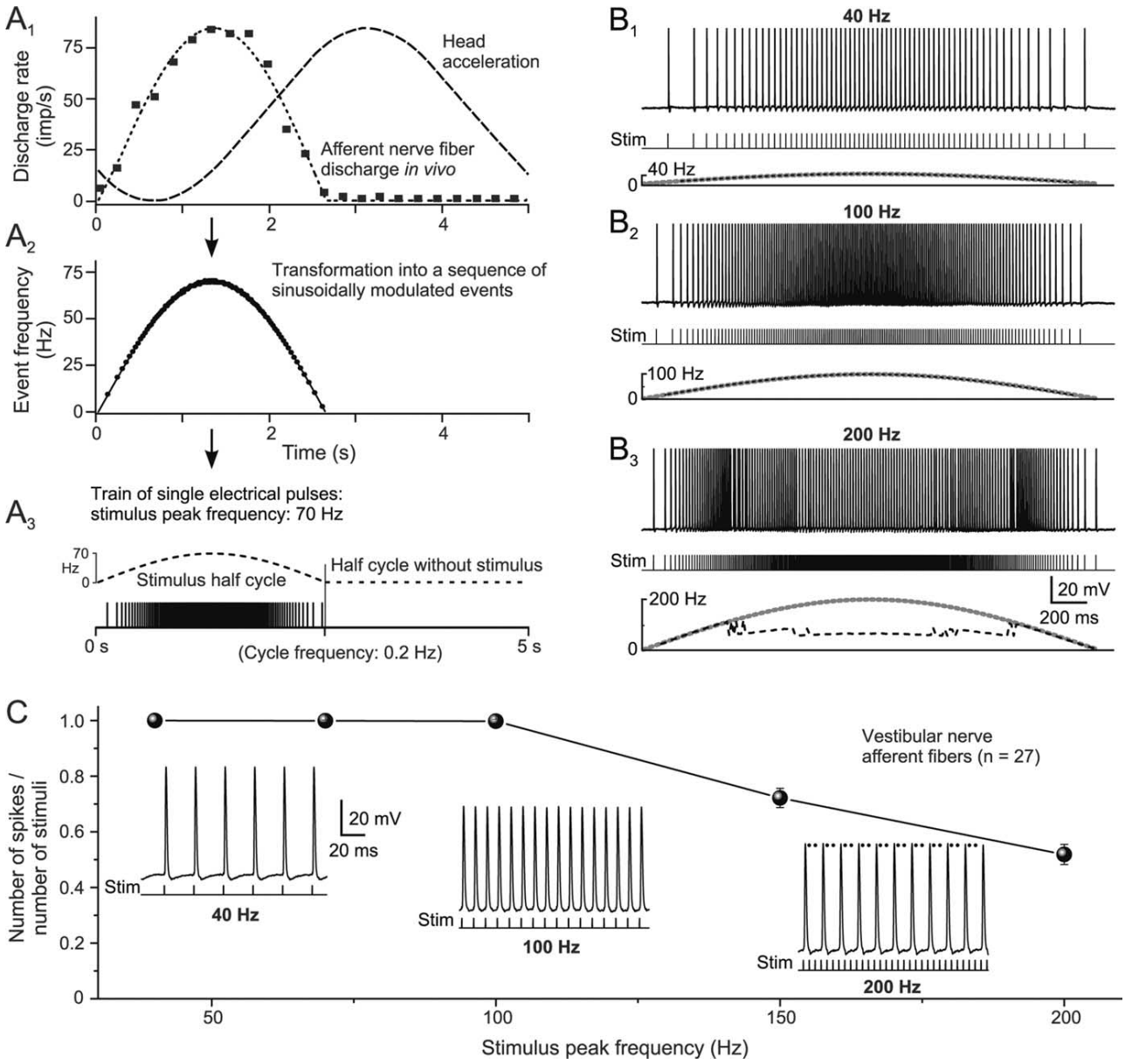

Figure 1. Discharge of vestibular nerve afferent fibers evoked by trains of single electrical pulses (sinusoidal pulse train). ***A1–A3***, The discharge of a horizontal semicircular canal afferent fiber (■) recorded during a 0.2 Hz (±20°) sinusoidal rotation in frog *in vivo* (Blanks and Precht, 1976) was fitted with a sine wave function (dashed line in ***A1***), transformed into sinusoidally modulated sequences of events with modifiable peak frequencies (***A2***, ●), and used as a template for pulse trains to electrically stimulate individual labyrinthine nerve branches (***A3***). Because of the low resting discharge, only one half cycle was used for stimulation. ***B1–B3***, Intracellular recorded spike discharge of a posterior vertical canal afferent fiber evoked by a sinusoidal pulse train (Stim) with peak frequencies of 40 (***B1***), 100 (***B2***), and 200 Hz (***B3***); bottom traces in ***B1–B3*** indicate pulse trains, stimulus frequency (dotted gray line), and discharge rate (dashed black line). The calibration in ***B3*** also applies to ***B1*** and ***B2***. ***C***, Ratio between the number of spikes and stimulus pulses (mean ± SE) as a function of peak frequency (1 indicates that each single pulse of a train evokes one single spike). Insets, Spike discharge of the afferent fiber shown in ***B1–B3*** at peak frequencies of 40, 100, and 200 Hz at an extended time scale; at a peak frequency of 200 Hz, two of three stimuli failed to evoke spikes (black dots). The calibration for the trace at 40 Hz applies to all insets.

(Straka and Dieringer, 1991; Birinyi et al., 2001), as well as the location of vestibular projection neurons and the termination of vestibular nerve afferent fibers relative to external landmarks (e.g., entry of the eighth nerve into the brainstem; dorsal apex), served as clues for localizing the recording area for 2°VNs in the isolated frog brain.

Based on intrinsic membrane properties and discharge behavior in response to intracellular current injection, central VNs were classified as phasic or tonic neurons (Straka et al., 2004). As described previously, during injection of long positive current steps, tonic VNs ($n = 15$; 13.6%) exhibited a continuous discharge throughout the current step (Fig. 2*B*) (Straka et al., 2004; Beraneck et al., 2007). In contrast, the larger population of phasic VNs ($n = 95$; 86.4%) responded with a short, high-frequency burst of one to three spikes within the first 50 ms (Fig. 2*C*), which unequivocally separated these neurons from tonic VNs. The difference in the evoked discharge pattern was paralleled by a significant difference ($p \leq 0.0001$; Mann–Whitney *U* test) in the input resistance between phasic (11.8 ± 3.1 MΩ; $n = 42$) and tonic neurons (21.5 ± 3.9 MΩ; $n = 11$). In contrast, the resting mem-

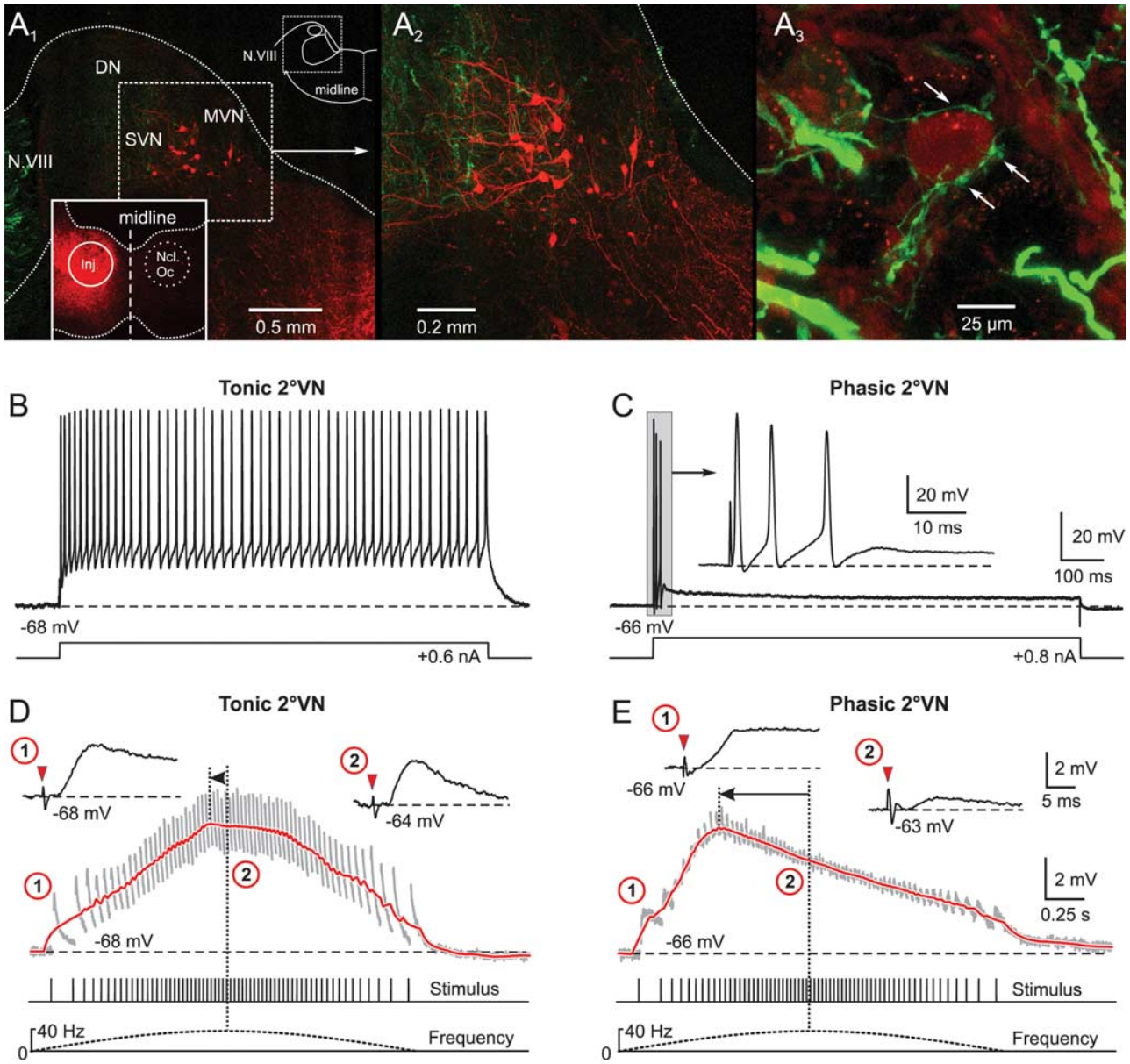

Figure 2. Synaptic compound responses evoked by pulse-train stimulation of semicircular canal nerves in identified central vestibular neurons. ***A*$_1$**, The location of retrogradely labeled vestibulo-ocular neurons in the superior vestibular nucleus (SVN) and MVN after injection of Alexa Fluor 546 dextran (red) into the ipsilateral oculomotor nucleus (Ncl Oc; inset) help determine the area for the recordings in the isolated frog brain. ***A*$_2$**, Higher magnification of labeled SVN and MVN vestibulo-ocular neurons located in the outlined area in ***A*$_1$**. ***A*$_3$**, AC afferent fibers, labeled in green from the periphery with Alexa Fluor 488 dextran, contact the soma (arrows) of a neuron in the SVN. ***B***, ***C***, A continuous discharge (***B***) and a short burst of three spikes (***C***) evoked by intracellular injection of long positive current steps (bottom traces) characterized tonic (***B***) and phasic 2°VNs (***C***), respectively. The inset in ***C*** shows the short initial burst (gray area) of the phasic 2°VN at an extended time scale. ***D***, ***E***, Compound responses formed by temporal summation of individual EPSPs (gray traces) after pulse-train stimulation of the AC nerve with a peak frequency of 40 Hz in the same tonic (***D***) and phasic 2°VN (***E***) as shown in ***B*** and ***C***, respectively. The bottom traces indicate pulse train and stimulus frequency. Insets in ***D*** and ***E*** show EPSPs evoked by the first single pulse of the train (1) and by the single pulse at peak frequency (2) at an extended time scale; horizontal dashed lines in ***B–E*** indicate the membrane potential (−68 mV in ***B***, ***D***; −66 mV in ***C***, ***E***). Red arrowheads in insets in ***D*** and ***E*** indicate the single pulses. Red traces in ***D*** and ***E*** are smoothed fits of the compound responses; horizontal arrows indicate the advance of the compound response peak with respect to stimulus peak frequency (vertical dotted lines). Records in ***B*** and ***C*** are single sweeps, and in ***D*** and ***E*** are the average of 12 responses. Calibrations in ***C*** and ***E*** apply to ***B*** and ***D***, respectively. DN, Dorsal auditory nucleus.

brane potential of the two subtypes were similar (phasic, −68.4 ± 12.3 mV, $n = 95$; tonic, −69.2 ± 9.2 mV, $n = 15$).

Recorded neurons in the vestibular nuclei were identified as second-order by an EPSP with a monosynaptic onset after electrical stimulation of a particular ipsilateral semicircular canal or the lagenar nerve (Fig. 2 *D*, *E*, inset 1). This monosynaptic EPSP is the physiological correlate of the morphologically visualized synaptic connection between vestibular nerve afferent fibers and central vestibular neurons (Fig. 2 A_3, arrows). The criteria for the timing of monosynaptic responses have been described previously in detail (Straka and Dieringer, 1997). Accordingly, semicircular canal or lagenar nerve-evoked EPSPs with onset latencies between 2.7 and 4.5 ms were considered as monosynaptic. Based on this definition, the recorded 2°VNs could be distinguished as 2°HC ($n = 28$), 2°AC ($n = 32$), 2°PC ($n = 33$) and 2°LA ($n = 17$) neurons. Although many of these neurons received, in addition,

inputs with disynaptic or oligosynaptic latencies from one or more ipsilateral labyrinthine nerve branches, only the monosynaptic inputs were considered for further investigation.

Activation of second-order vestibular neurons with sinusoidal pulse trains

The responses of tonic and phasic 2°VNs to electrical stimulation of a particular vestibular nerve branch with a sinusoidal pulse train consisted of a temporal summation of the individual monosynaptic EPSPs evoked by each single pulse (Fig. 2*D*,*E*, gray traces). In tonic 2°VNs ($n = 14$), compound responses were rather symmetric with a slow rise and decay and an overall waveform that was approximately aligned with the stimulus frequency modulation (Fig. 2*D*, compare red solid and dashed lines below stimulus). Thus, the compound response peak in this neuronal type (Fig. 2*D*, vertical dotted lines, horizontal arrow) approximately matched the stimulus peak frequency or was slightly advanced (Fig. 2*D*, vertical dotted lines, arrowhead). In contrast, phasic 2°VNs ($n = 67$) showed a relatively rapid rise and an early decay of the compound response that created a considerable peak advance (Fig. 2*E*, vertical dotted lines, horizontal arrow) relative to the stimulus peak frequency (Fig. 2*E*, compare red solid and dashed lines below stimulus). This pronounced difference in compound response dynamics and response peak timing relative to stimulus waveform of tonic and phasic 2°VNs was characteristic and suggested a different postsynaptic signal processing in the two neuronal subtypes.

The different dynamics of compound responses in tonic and phasic 2°VNs were paralleled by differences in the behavior of the individual monosynaptic EPSPs during the pulse train (Fig. 2*D*,*E*, insets 1, 2). Compared with the first EPSP, the amplitudes of those evoked by the subsequent single pulses in tonic 2°VNs were moderately reduced during the stimulus train (Fig. 2*D*, compare insets 1, 2). In contrast, in phasic 2°VNs, the amplitudes of the individual EPSPs decreased considerably during the pulse train compared with the first EPSP (Fig. 2*E*, compare insets 1, 2) and reached a minimum at stimulus peak frequency. This difference is compatible with the differential impedance behavior of the two vestibular subtypes during membrane polarization (Beraneck et al., 2007). In particular, the marked reduction of the EPSP amplitude in phasic 2°VNs at stimulus peak frequency (Fig. 2*E*, inset 2) complies with the marked impedance decrease of these neurons during depolarization.

In the following, several parameters of the stimulus pulse train, such as peak frequency, cycle length, or single-pulse intensity were varied to reveal the postsynaptic response dynamics in 2°VNs during different labyrinthine afferent activity patterns. Although the activity in vestibular nerve afferents, evoked by the different stimulus pulse trains, is an approximation with respect to the synchronicity of the afferent activity pattern during natural head motion *in vivo* (Ramachandran and Lisberger, 2006; Hospedales et al., 2008), by its defined timing it facilitates the characterization of the neuronal mechanisms underlying a parallel processing of afferent signals in separate populations of central vestibular neurons.

Effect of stimulus train peak frequency

Compound responses in both tonic and phasic 2°VNs evoked by stimulus trains with successively larger peak frequencies (40, 70, and 100 Hz) had similar peak amplitudes but exhibited progressively larger peak advances when the peak frequency was augmented from 40 Hz to 70 and 100 Hz (Fig. 3A_1–A_3,B_1–B_3; Table 1). The mean advance of the response peak relative to stimulus peak frequency increased to a similar extent in both types of 2°VNs (Fig. 3*E*; Table 1). However, independent of stimulus peak frequency, the advance was always significantly larger in phasic compared with tonic 2°VNs (Fig. 3*E*; Table 1). In most phasic 2°VNs, the compound response had a more pronounced truncation during pulse trains with higher peak frequencies (Fig. 3B_2,B_3, open triangles). This further accentuated the asymmetry of the compound responses and indicates that these neurons have a highly nonlinear synaptic processing of repetitive afferent vestibular inputs. Construction of the population mean responses (Fig. 3*C*) and smoothed fits (*D*) from the recordings of phasic ($n = 67$) and tonic 2°VNs ($n = 14$), respectively, confirmed the clear differences in postsynaptic signal processing of the two neuronal subpopulations.

Increasing the stimulus peak frequency from 40 Hz to 70 and 100 Hz did not only change the time course of the compound responses but also caused an increasingly larger reduction of the individual EPSP size in both tonic and phasic 2°VNs (Fig. 3A_1–A_3,B_1–B_3,*F*, gray traces; Table 1). This reduction was particularly prominent in phasic 2°VNs (Fig. 3F_1,F_2, compare plots) because EPSPs evoked by the single pulses at peak frequency of 100 Hz were on average <10% of the amplitude of the first EPSP (Fig. 3F_2; Table 1). This suggests the presence of powerful shunting mechanisms for afferent synaptic inputs, preferentially at high stimulus peak frequencies. This shunting likely contributes to the observed truncation of the compound response (Fig. 3B_2,B_3, open triangles) and the increased peak advance at higher peak frequencies. Although some shunting of single EPSPs was also observed in tonic 2°VNs, the maximal reduction (at 100 Hz peak frequency) was significantly less than in phasic 2°VNs (Fig. 3F_1,F_2; Table 1). Except for stimulus peak frequencies of 40 Hz the shunting effect on single EPSP size was always more pronounced in phasic compared with tonic 2°VNs (Table 1).

Effect of stimulus train length

Using stimulus train length as a variable but keeping peak frequency constant revealed a different dependency of both amplitude and timing of the compound response from this parameter in tonic and phasic 2°VNs (Fig. 4*A*,*B*). Compatible with the relatively linear transformation of presynaptic afferent activity into postsynaptic compound responses in tonic 2°VNs, the response peak almost doubled in amplitude when the stimulus train length (half cycle) was increased from 0.25 s to 2.5 s (Fig. 4A_1–A_4, C_1, open circles). This finding indicates that the temporal summation of individual EPSPs in tonic 2°VNs gradually increases with continuously larger numbers of single pulses in the train and confirms the notion of a mostly linear input–output relationship in this vestibular neuronal subtype. The substantial increase in compound response peak amplitude with increasing train length is accompanied by a considerable change in the timing of the response peak. Notably, the large peak lag of approximately −45° at a half-cycle length of 0.25 s changes into a peak advance of ~20° at a half-cycle length of 2.5 s (Fig. 4C_2, open circles). Accordingly, the compound response peak in tonic 2°VNs would be aligned with peak frequency at a half-cycle length of ~1.5 s (Fig. 4C_2, dotted arrow to bottom axis).

In phasic 2°VNs, the amplitude of the compound response evoked during a stimulus half cycle of 2.5 s increased only by ~25% compared with the response evoked with a stimulus half cycle of 0.25 s (Fig. 4*B*,C_1). This small increment in amplitude during a 10-fold extension in stimulus half-cycle length contrasts with the almost twofold increase in tonic 2°VNs (Fig. 4C_1). This is because of the relatively larger responses in phasic 2°VNs (75%)

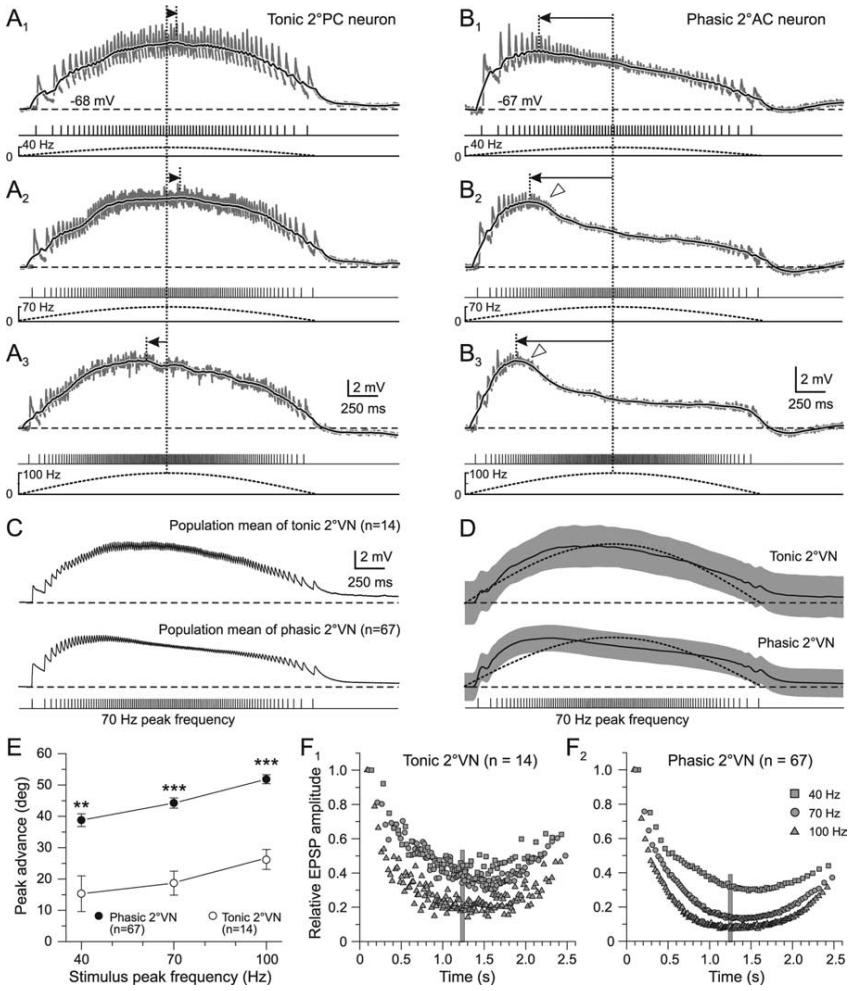

Figure 3. Compound synaptic responses as a function of stimulus train peak frequency in phasic and tonic 2°VNs. ***A*$_1$*–B*$_3$**, Compound responses formed by summation of single EPSPs (gray traces) in a tonic 2°PC (***A*$_1$*–A*$_3$**) and a phasic 2°AC (***B*$_1$*–B*$_3$**) neuron after pulse-train stimulation with a peak frequency of 40 (***A*$_1$**, ***B*$_1$**), 70 (***A*$_2$**, ***B*$_2$**), and 100 Hz (***A*$_3$**, ***B*$_3$**). The black traces are smoothed fits of the compound responses; bottom traces show pulse trains (half-cycle duration, 2.5 s) and stimulus frequency modulation (dashed lines), respectively; horizontal dashed lines indicate the resting membrane potential (−68 mV in ***A***; −67 mV in ***B***) and horizontal arrows the lag/advance of the compound response peak with respect to stimulus peak frequency (vertical dotted lines). Synaptic responses in ***A*$_1$*–B*$_3$** are the averages of 12 single sweeps. Calibrations in ***A*$_3$** and ***B*$_3$** apply to ***A*$_1$**, ***A*$_2$** and ***B*$_1$**, ***B*$_2$**, respectively; open arrowheads in ***B*$_2$** and ***B*$_3$** mark the truncation of the compound response. ***C***, ***D***, Population mean of compound responses (***C***) and smoothed fits (***D***) evoked by pulse trains with 70 Hz peak frequency and 2.5 s half-cycle length in tonic ($n = 14$) and phasic 2°VNs ($n = 67$). The gray bands in ***D*** indicate ±SE of the mean, the dotted curves indicate the stimulus modulation and the horizontal dashed lines the mean resting membrane potential of −69 mV in tonic and −68 mV in phasic 2°VNs. ***E***, Advance (in degrees) of the compound response peak relative to stimulus peak frequency (mean ± SE) in phasic (●) and tonic 2°VNs (○) as a function of stimulus peak frequency. $^{**}p \leq 0.001$, $^{***}p \leq 0.0001$, significant difference between tonic and phasic 2°VNs (Mann–Whitney *U* test). ***F*$_1$**, ***F*$_2$**, Average amplitude of individual EPSPs evoked by the single pulses of the train with peak frequencies of 40 (□), 70 (○), and 100 Hz (△) in tonic (***F*$_1$**) and phasic 2°VNs (***F*$_2$**). Amplitudes were normalized to the size of the first EPSP. Plots of ±SE were omitted for clarity; vertical gray bars mark the timing of the stimulus peak frequency.

at a half-cycle length of 0.25 s compared with tonic 2°VNs (55%) (Fig. 4C_1). The larger amplitudes in phasic 2°VNs during short stimulus trains (0.25 s) and the rather small increment with increasing train length can be explained by the relatively rapid rise of the compound response generating the considerable peak advance (Figs. 2*E*, 3*B*). This small increase in peak amplitudes for half-cycle lengths between 0.25 and 2.5 s, however, is contrasted by a large simultaneous change of peak timing, which exceeded that of tonic 2°VNs (Fig. 4C_2). The considerable response peak lag of approximately −35° at a half-cycle length of 0.25 s changed into a peak advance of ~45° at a half-cycle length of 2.5 s (Fig. 4C_2, filled circles). Calculation of the stimulus half-cycle length at which compound responses in phasic 2°VNs were aligned with stimulus peak frequency yielded a value of ~0.7 s (Fig. 4C_2, dotted arrow to the bottom axis). This time is considerably shorter than that in tonic 2°VNs (~1.5 s) and again attributable to the faster slope of the compound response during the first few stimuli of the train (Figs. 2*E*, 3*B*). Moreover, it complies with the notion that phasic 2°VNs are particularly suitable for the detection of short, high-frequency components, whereas tonic 2°VNs are better suited to the processing of low-dynamic head motion components.

Effect of single stimulus pulse intensity

Higher-intensity single current pulses applied to the vestibular nerve branches recruit increasingly more afferent fibers. This recruitment causes larger amplitudes of all individual monosynaptic EPSPs (Fig. 5*A–F*, inset 1) and consequently compound responses with larger peak amplitudes in both tonic (Fig. 5*A–C*) and phasic 2°VNs (Fig. 5*D–F*). With larger intensities of all single pulses of a train [1.3× T (Fig. 5*A*), 1.8× T (*B*), and 3.1× T (*C*)], the compound responses evoked by stimulus trains with low-intensity single pulses increased and action potentials were triggered in tonic 2°VNs as soon as the spike threshold was reached. The number of evoked spikes during the train stimulation depended on the subthreshold compound response amplitude but consistently was largest around peak stimulus frequency (Fig. 5*B*,*C*, insets 2). This indicates that in tonic 2°VNs ($n = 10$) the evoked discharge is rather linearly related to the underlying synaptic membrane depolarization as for intracellular injected currents (Straka et al., 2004). This effect became more evident when the relative spike discharge rate during the stimulus train (peak frequency, 70 Hz; train half-cycle length, 2.5 s; single-pulse intensity, >2.5× T) was plotted as a function of time (Fig. 5G_1). The maximal spike discharge rate occurs slightly before stimulus train peak frequency (Fig. 5G_1, arrow) and corresponds with the peak advance of the subthreshold compound response (Fig. 3*C*). Thus, the spike discharge in these neurons that more or less mirrors the stimulus frequency modulation has a rather tight correlation with the synaptic depolarization.

In phasic 2°VNs, stimulus-train-evoked compound responses changed from a symmetric waveform at low-intensity single pulses [e.g., 1.4× T (Fig. 5*D*)] to a skewed response at high-intensity single pulses [2.0× T (Fig. 5*E*) and 3.2× T (*F*)]. Most importantly however, in all phasic 2°VNs ($n = 31$), only a small number of action potentials (approximately one to six) were evoked during the first 10–15 single pulses of the stimulus train

10356 • J. Neurosci., October 8, 2008 • 28(41):10349–10362

Table 1. Timing of the compound response peak and reduction of amplitudes of single EPSPs during pulse-train stimulation in phasic and tonic 2°VN

	Tonic 2°VNs		Phasic 2°VNs	
Stimulus peak frequency	Peak advance relative to stimulus peak frequency	Relative size of single EPSPs at stimulus peak frequency	Peak advance relative to stimulus peak frequency	Relative size of single EPSPs at stimulus peak frequency
40 Hz	15 ± 5° (9)*	46 ± 10%, n.s. (9)	38 ± 2° (36)	35 ± 2% (36)
70 Hz	19 ± 3° (14)*	38 ± 9% (14)*	44 ± 2° (67)	14 ± 1% (67)
100 Hz	26 ± 3° (9)*	23 ± 3% (9)**	53 ± 1° (40)	8 ± 1% (40)

Single EPSP amplitudes at stimulus peak frequencies (40, 70, and 100 Hz) are indicated as a percentage (mean ± SE) of the EPSP evoked by the first pulse in the stimulus train. The timing of the compound response peak is indicated relative to the peak frequency. n.s., Not significant. The number of neurons (*n*) is shown in parentheses.

*$p \leq 0.01$; **$p \leq 0.001$, significant difference (Mann–Whitney *U* test) between parameters of phasic and tonic 2°VN.

(Fig. 5*E*,*F*, insets 2). Even with larger single-pulse intensity (>5× *T*) no further increase in spike number or spiking after the first 15 pulses was observed. This is illustrated by plotting the relative spike discharge rate during the stimulus train (Fig. 5G_2). The likelihood for spike triggering is maximal at the third single pulse of the train (Fig. 5G_2, arrow). This temporal limitation of evoked spikes is compatible with the pronounced peak advance of the subthreshold compound response (Fig. 3*E*) and is likely related to the substantial shunting of single EPSPs after the response peak is reached (Fig. 3F_2).

The differential temporal pattern of synaptically evoked spikes in phasic and tonic 2°VNs (Fig. 5G_3) was quantified by calculating the stimulus cycle frequency at which the maximal discharge rate (Fig. 5G_1,G_2, arrows) coincides with the stimulus peak. The maximal discharge rate matches the stimulus peak frequency at a cycle frequency of ~1 Hz in phasic and ~0.25 Hz in tonic 2°VNs (Fig. 5G_1,G_2). Accordingly, the differential synaptic spike discharge behavior in phasic and tonic 2°VNs (Fig. 5G_3) is compatible with the different intrinsic filter properties and suggests a preferential processing of high- and low-dynamics vestibular afferent signals in the two neuronal subtypes, respectively (Beraneck et al., 2007).

Inhibitory neuronal circuits control afferent synaptic signal processing in phasic 2°VNs

The early truncation of the compound responses and the marked reduction of single EPSP amplitudes that likely contributes to the peak advance in phasic 2°VNs might not only be caused by prominent voltage-dependent potassium conductances (Beraneck et al., 2007), but also by inhibitory synaptic inputs superimposed on the afferent-evoked monosynaptic excitation (Biesdorf et al., 2008). A potential contribution of glycinergic and GABAergic IPSPs to the nonlinear characteristics of compound responses in phasic 2°VNs was studied by bath application of the respective transmitter antagonists (Fig. 6*A*,*C*). Appli-

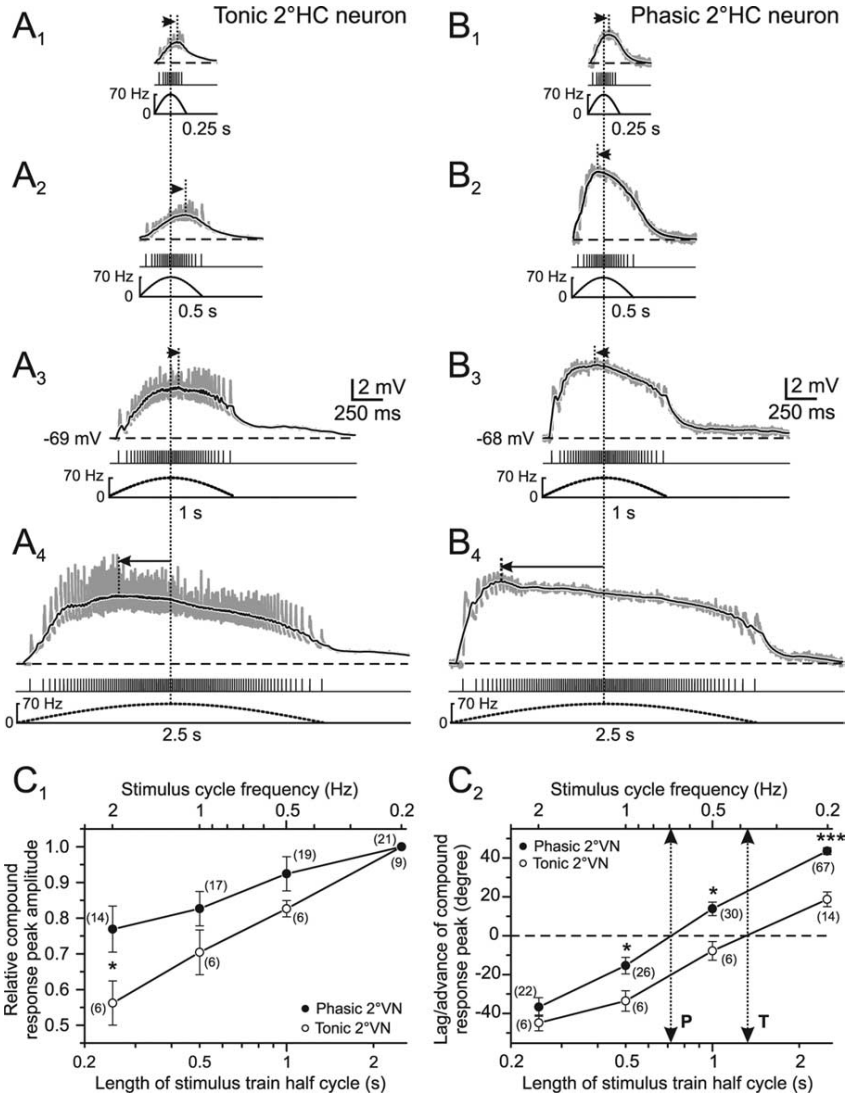

Figure 4. Compound synaptic responses as a function of stimulus pulse train length in phasic and tonic 2°VNs. ***A*$_1$–*A*$_4$**, Compound responses of single EPSPs (gray traces) in a tonic (***A*$_1$–*A*$_4$**) and a phasic (***B*$_1$–*B*$_4$**) 2°HC neuron after pulse-train stimulation with 0.25 (***A*$_1$**, ***B*$_1$**), 0.5 (***A*$_2$**, ***B*$_2$**), 1 (***A*$_3$**, ***B*$_3$**), and 2.5 s (***A*$_4$**, ***B*$_4$**) half-cycle length. The peak frequency was 70 Hz and pulse intensity was 1.8× *T* in ***A*** and 1.7× *T* in ***B***. Black traces are smoothed fits of the compound responses; bottom traces show pulse trains and stimulus frequency (dashed lines), respectively; horizontal dashed lines indicate the membrane potential (−69 mV in ***A***; −68 mV in ***B***) and horizontal arrows indicate the lag/advance in degree of the compound response peak with respect to stimulus peak frequency (vertical dotted lines). All records are the average of 12 responses. Calibrations in ***A*$_3$** and ***B*$_3$** apply to all other traces. ***C*$_1$**, ***C*$_2$**, Mean (±SE) of compound response peak amplitude (***C*$_1$**) and peak lag/advance relative to stimulus peak frequency (***C*$_2$**) of tonic (○) and phasic 2°VNs (●) as a function of stimulus half-cycle length (bottom axis) and corresponding full stimulus cycle frequency (top axis). Amplitudes in ***C*$_1$** were normalized to those obtained at a stimulus half-cycle length of 2.5 s; dotted two-sided arrows indicate half-cycle length and corresponding full-cycle frequency where response peak and stimulus peak frequency are aligned (0°; dashed horizontal line) in tonic (T) and phasic (P) 2°VNs. The number of neurons is indicated in parentheses. *$p \leq 0.05$, ***$p \leq 0.0001$, significance of difference between tonic and phasic neurons (Mann–Whitney *U* test).

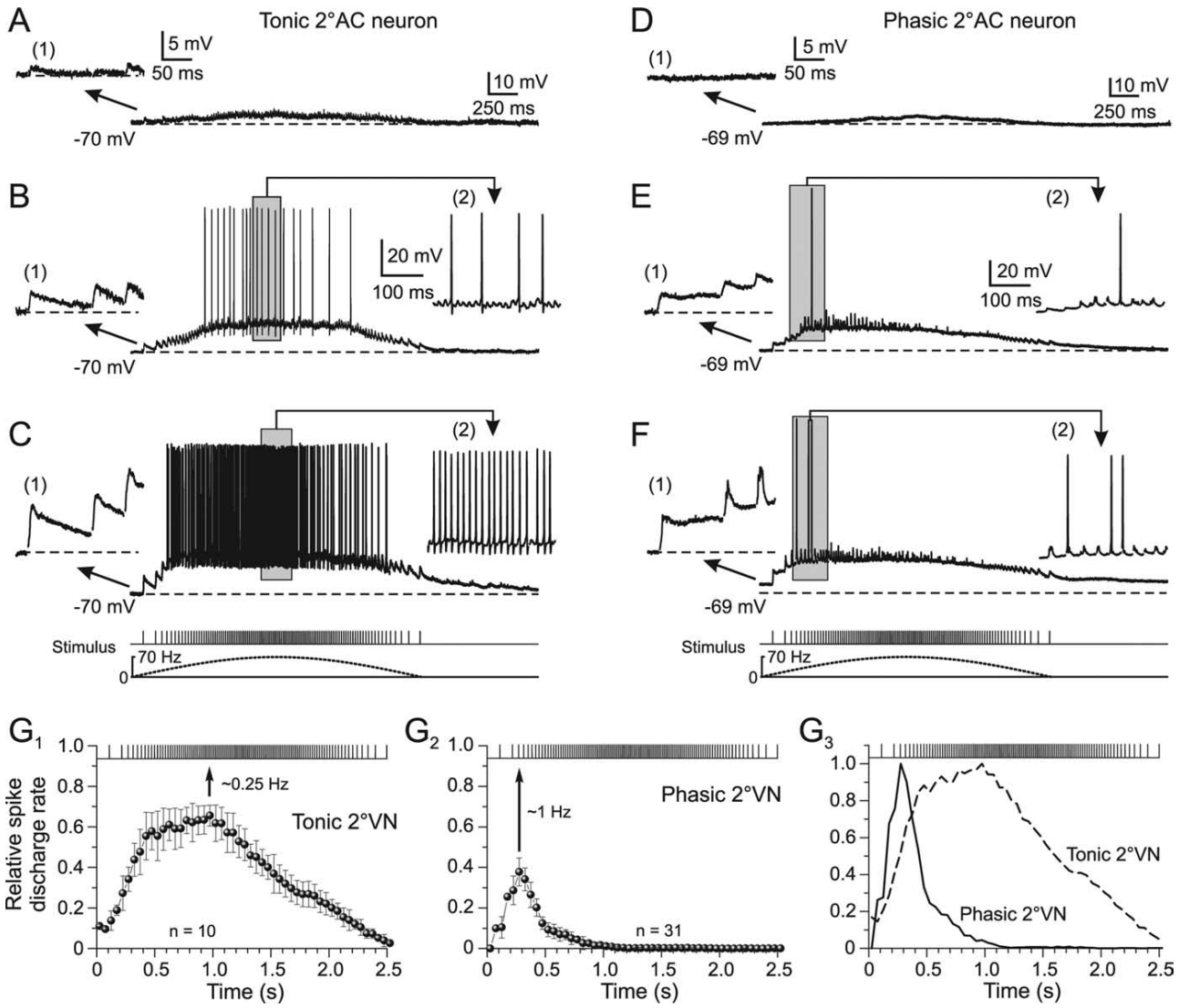

Figure 5. Synaptic discharge dynamics as a function of stimulus pulse intensity in phasic and tonic 2°VNs. ***A–F***, Compound responses and superimposed spikes in a tonic (***A–C***) and a phasic (***D–F***) 2°AC neuron after stimulation with sinusoidal pulse trains at a peak frequency of 70 Hz. The intensities for the single pulses were in the tonic 2°AC (***A***, 1.3× *T*; ***B***, 1.8× *T*; ***C***, 3.1× *T*) and in the phasic 2°AC neuron (***D***, 1.4× *T*; ***E***, 2.0× *T*; ***F***, 3.2× *T*); the first three single EPSPs of the train (1) and during the indicated period (gray area) of spike discharge (2) in ***A–F*** are shown at an extended time and amplitude scale; bottom traces in ***C*** and ***F*** show pulse trains (half-cycle duration, 2.5 s) and stimulus frequency (dashed lines) that also apply to ***A***, ***B*** and ***D***, ***E***, respectively. Horizontal dashed lines indicate the membrane potential (−70 mV in ***A–C***; −69 mV in ***D–F***); records in ***B***, ***C*** and ***E***, ***F*** are single sweeps and in ***A*** and ***D***, the average of 12 responses, respectively. Calibrations in ***A*** and ***D*** and insets (1) therein apply also to ***B***, ***C*** and ***E***, ***F***, respectively; calibration in insets (2) in ***B*** and ***E*** apply also to insets (2) in ***C*** and ***F***, respectively. G_1–G_3, Relative rate of evoked spike discharge (mean ± SE) during pulse trains with peak frequencies of 70 Hz in tonic (G_1) and phasic 2°VNs (G_2) at single-pulse intensity >2.5× *T*. The relative rate was calculated from the number of spikes in each cell during the stimulus train in 50 ms bins and divided by the number of stimuli within the respective bin. The discharge in phasic 2°VNs is confined to the first 10–15 single pulses of the train (G_3, solid line), whereas in tonic 2°VNs it is more aligned with the frequency modulation of the single pulses (G_3, dashed line). Curves in G_3 were obtained by normalization to the peaks in G_1 and G_2, respectively. Peak discharge rate in tonic and phasic 2°VNs (G_1, G_2, arrows) corresponds to a full stimulus cycle of ~0.25 and ~1 Hz, respectively.

cation of the glycine receptor antagonist strychnine (1 μM; $n = 7$) or the $GABA_A$ receptor antagonist bicuculline (1–5 μM; $n = 8$) caused a significant reversible increase of the compound response amplitude by ~2 mV and a decrease of the mean peak advance by >20° compared with controls (Fig. 6*A*,*C*,*H*,*I*). Moreover, the observed reduction of single EPSP amplitudes during the stimulus train in controls became smaller after application of both transmitter antagonists (Fig. 6*B*,*D*). Although, this effect was significant only after blocking the GABAergic transmission (Fig. 6*D*, asterisk), it suggests that at least part of the observed shunting during the stimulus train was caused by inhibitory inputs. Probable neuronal candidates for mediating the glycinergic and GABAergic inhibition are ipsilateral vestibular inhibitory interneurons (Straka and Dieringer, 1996) that have been shown to activate disynaptic IPSPs in phasic, but not in tonic 2°VNs after electrical stimulation of vestibular nerve afferent fibers (Biesdorf et al., 2008). An ipsilateral origin was confirmed by the recordings of several phasic 2°VNs ($n = 6$) in isolated frog brains in which the midline was completely transected from the optic tectum to the obex. The peak advance of the compound responses of these neurons was identical to those of controls, thereby excluding commissural connections as the source of the inhibition.

The larger effect of bicuculline with respect to strychnine on the shunting of single EPSP amplitude during the pulse-train stimulus suggests that GABAergic inputs might be either more effective or more numerous. However, GABAergic IPSPs from

10358 • J. Neurosci., October 8, 2008 • 28(41):10349–10362

inhibitory vestibular interneurons have shorter time constants than glycinergic IPSPs (Biesdorf et al., 2008), suggesting that additional GABAergic circuits might be recruited by the pulse-train stimulation in the present study. Because all experiments were performed in the isolated frog brain in which the cerebellum was attached (Fig. 6*G*), it is possible that the activation of vestibular nerve afferent fibers recruits the cerebellar circuitry and thereby evokes Purkinje-cell-mediated GABAergic IPSPs (Magherini et al., 1975) in phasic 2°VNs. Pressure injection of 100–150 nl of 2% lidocaine ($n = 16$) into the ipsilateral cerebellar peduncle (Fig. 6*G*) that blocks the activation of the cerebellar circuitry provoked, in some of the phasic 2°VNs ($n = 7$ of 16), a reversible increase of the compound response amplitude by ~1 mV as well as a reduction of the peak advance by ~25° compared with controls (Fig. 6*E*,*H*,*I*), but had no effect in others ($n = 9$ of 16). The accompanying reduction of the shunt of single EPSP amplitudes during the stimulus pulse train, however, was not significant (Fig. 6*F*). A spread of pressure-injected lidocaine from the cerebellum into the vestibular nuclei as a potential explanation of the effect was ruled out because the amplitude of the monosynaptic EPSPs in the 2°VNs ($n = 16$), as well as of presynaptic and postsynaptic vestibular afferent field potential components (verified in control experiments) after single electrical pulse stimulation did not decrease. This amplitude constancy served as an indication that no block of action potentials in vestibular afferent fibers occurred within the vestibular nuclei. The effects on the compound response after injection of lidocaine into the cerebellum were confirmed in experiments where phasic 2°VNs ($n = 18$) were recorded in isolated whole brains ($n = 4$) in which the cerebellum was removed. In fact, the peak advance of compound responses in phasic 2°VNs recorded in these preparations was significantly reduced by ~20° in 12 of the 18 neurons compared with controls (Fig. 6*I*).

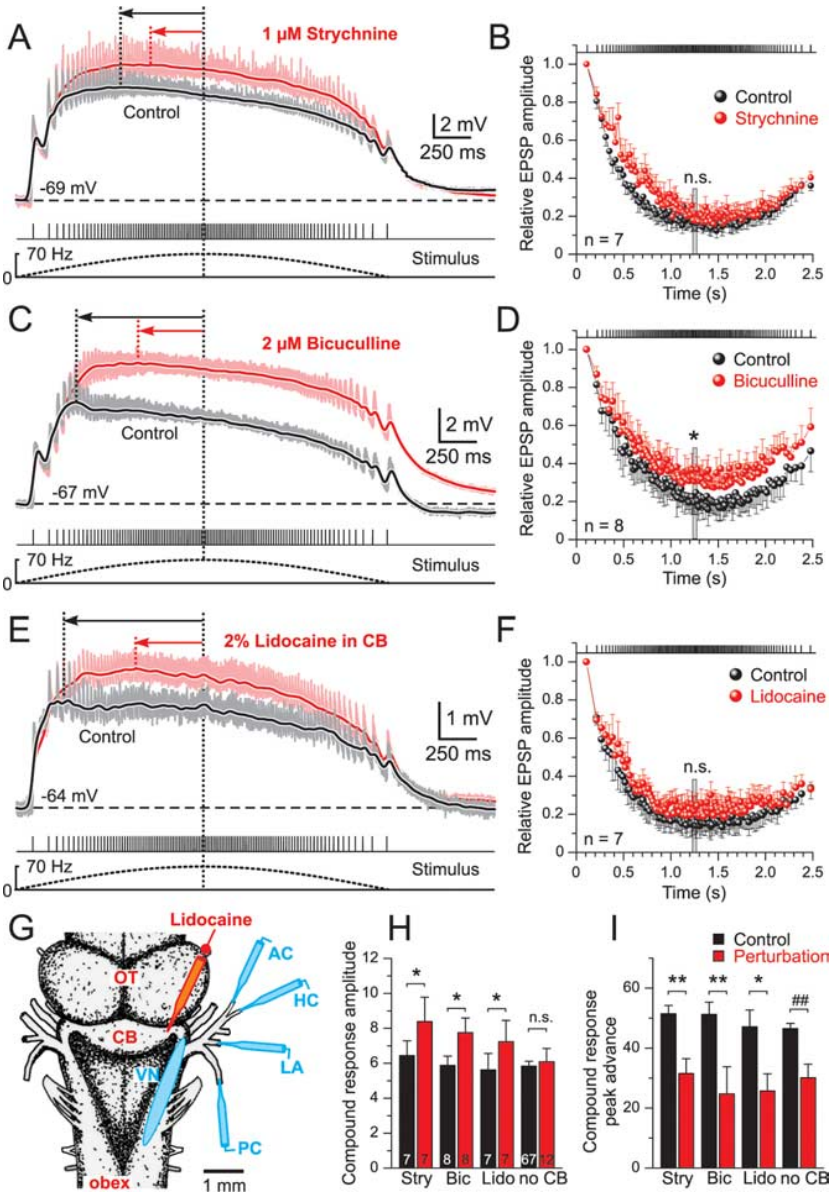

Figure 6. Inhibitory control of compound synaptic responses in phasic 2°VNs. ***A***, ***C***, ***E***, Effect of blocking the glycinergic (strychnine, ***A***) and GABAergic transmission (bicuculline, ***C***) and the cerebellar output (100–150 nl of lidocaine in CB, ***E***) on amplitude and timing of the compound responses in three different phasic 2°VNs. Responses were evoked by stimulation of the anterior vertical (***A***, ***E***) or horizontal semicircular canal nerves (***C***) with sinusoidal pulse trains of 70 Hz peak frequency. The black and red traces are smoothed fits of the compound responses (gray and pink traces); bottom traces show pulse trains (half-cycle duration, 2.5 s) and stimulus frequency (dashed lines), respectively; horizontal dashed lines indicate membrane potentials (−69 mV in ***A***; −67 mV in ***C***; −64 mV in ***E***), and black and red horizontal arrows the peak advance relative to stimulus peak frequency (vertical dotted lines). All records are the average of 12 responses. ***B***, ***D***, ***F***, Amplitudes (mean ± SE) of individual EPSPs evoked by single pulses of the train before (black) and after (red) drug application; amplitudes were normalized to the first EPSP, respectively. Vertical gray bars mark the timing of stimulus peak frequency. ***G***, Schematic drawing illustrating the stimulation of individual vestibular nerve branches, the vestibular nuclei, and the site for injection of lidocaine into the ipsilateral cerebellar peduncle. ***H***, ***I***, Amplitude (***H***) and timing (***I***) of the compound response peak (mean ± SE) before and after application of strychnine (Stry), bicuculline (Bic), pressure injection of lidocaine (Lido) into the ipsilateral cerebellar peduncle, or after surgical removal of the cerebellum (no CB). $^{*}p \leq 0.05$, $^{**}p \leq 0.01$, significance of difference before and after drug application (Wilcoxon signed-rank test); $^{\#\#}p \leq 0.01$ (Mann–Whitney *U* test), significance between controls and 2°VNs recorded after the removal of the cerebellum. n.s., Not significant; CB, cerebellum; OT, optic tectum.

Modeling approach to reveal cellular and network contributions for signal processing in 2°VNs

To differentiate between contributions of intrinsic membrane properties and the properties of network circuitry in shaping postsynaptic signals in 2°VNs, a modeling approach was used. Minimal models consisting of a soma and a three compartmental dendrite with uniformly distributed conductances were generated from frequency domain data of tonic and phasic 2°VNs (Fig. 7) (for details, see the supplemental material, available at www.jneurosci.org). Compatible with previous results (Beraneck et al., 2007), a noninactivating sodium conductance was required to obtain the observed increase in impedance with depolarization in tonic 2°VNs (Fig. 7*A*). In contrast, for

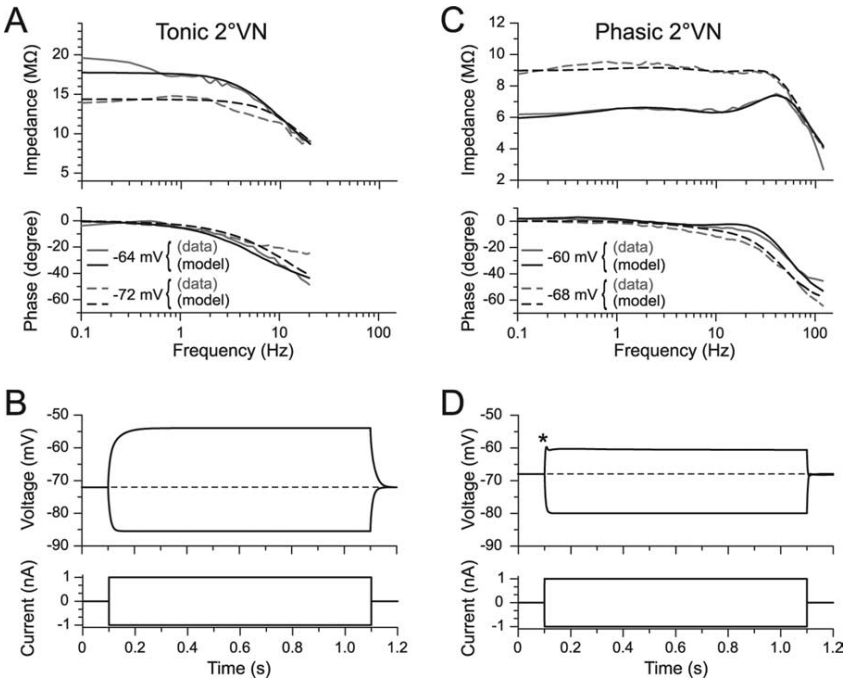

Figure 7. Frequency responses of tonic and phasic compartmental models of 2°VNs superimposed on magnitude and phase data used for parameter estimation. ***A***, ***C***, Impedance and phase functions of tonic (***A***) and phasic 2°VNs (***C***) at two different membrane potentials, computed from published data (Beraneck et al., 2007). Gray curves indicate data and black curves are tonic and phasic neuronal model fits using parameter estimation methods described previously (Saint Mleux and Moore, 2000). For cell parameter values, see the supplemental material (available at www.jneurosci.org as supplemental material). ***B***, ***D***, Reconstruction of real-time current step responses of the tonic (***B***) and the phasic model neuron (***D***) using the compartmental models with respective parameters; the asymmetry between depolarizing and hyperpolarizing responses of the phasic neuron model (***D***) as well as the characteristic initial transient in response to positive current steps (***D***, asterisk) matches the real data (Straka et al., 2004).

phasic 2°VNs, an inactivating potassium conductance (Bekkers and Delaney, 2001) as well as a delayed rectifier was required to quantitatively describe the particular potential dependence of the resonance behavior (Fig. 7*C*). Using parameters derived from the impedance data, simulations with the three compartment cable model (Fig. 7*B*,*D*) adequately predicted membrane potential responses to current steps, including a depolarization-induced damped oscillation in phasic 2°VNs (Fig. 7*D*, asterisk). The similar responses of model and frog phasic 2°VNs supports the particular role of the potassium conductances in generating the distinct resonance and the dynamic response pattern of this neuronal vestibular subtype (Straka et al., 2004; Beraneck et al., 2007).

The role of intrinsic cellular properties in causing the observed dynamics of synaptic compound responses was tested by extending the "single-neuron models" of tonic and phasic 2°VNs by excitatory conductance-based synapses (*E* compartmental model) (for parameters, see Material and Methods). This allowed mimicking the repetitive synaptic excitation of 2°VNs by vestibular nerve afferent fibers as performed in the present study. Calculation of the synaptic compound response characteristics as a function of different stimulus parameters shows that these extended single-neuron models yield results (Fig. 8A_1,A_2, filled circles, open circles) that were at least qualitatively similar to the obtained data, illustrating the functional consequences of the different dynamic properties of phasic and tonic 2°VNs. Therefore, the characteristic intrinsic cellular properties contribute to some extent to the observed differences in compound response peak timing of the two vestibular neuronal subtypes (Fig. 8A_1,A_2, filled circles, open circles). However, the assumed cellular properties in the model were not sufficient to account for the precise response characteristics as e.g., the large peak advance seen in phasic 2°VNs (Figs. 3*C*, 4C_2).

Based on the experimental results concerning inhibitory inputs from ipsilateral vestibular networks in phasic but not tonic 2°VNs after electrical nerve stimulation (Biesdorf et al., 2008), a combination of excitatory and superimposed inhibitory synapses was added to the single-neuron model (*E*/*I* compartmental model). All parameters related to amplitude and time course of monosynaptic afferent excitation and disynaptic GABAergic and glycinergic inhibition (for details, see Material and Methods and supplemental material, available at www.jneurosci.org) have been adapted to values obtained from empiric experiments (Biesdorf et al., 2008). This procedure allowed the generation of model fits of single-pulse-activated afferent monosynaptic EPSPs and superimposed disynaptic GABAergic and glycinergic IPSPs (Fig. 8*B*). The estimated EPSP and IPSP parameters were used to reconstruct compound responses after pulse-train stimulation at a stimulus peak frequency of 70 Hz and half-cycle length of 2.5 s (Fig. 8C_1). The assumption of conductance-based inhibitory synapses yielded model response values similar to those of real frog phasic 2°VNs (compare Fig. 8A_1,A_2, filled squares, with 3*E*, 4C_2). After turning off the glycinergic and GABAergic inhibition, the reconstructed model compound responses show that these components are particularly important for the timing of the response in phasic 2°VNs and considerably enhance the peak advance caused by the intrinsic cellular properties (Fig. 8C_1). This indicates that the particular response dynamics of this neuronal subtype originate from both the intrinsic membrane properties as well as the emerging properties of the inhibitory synaptic circuitry in which these neurons are embedded.

Previous studies have shown that the disynaptic GABAergic and glycinergic IPSPs in phasic 2°VNs are mediated by inhibitory neurons in the ipsilateral vestibular nucleus (Straka and Dieringer 1996, 2000; Biesdorf et al., 2008). To obtain realistic reconstructions of control model responses of phasic 2°VNs after pulse-train stimulation (compare Fig. 8C_1, control, with 3*C*), it was necessary to assume that both GABAergic and glycinergic inhibitory neurons fire spikes during pulse-train stimulation with a pattern typical for tonic 2°VNs (Fig. 8D_1). Using the alternative assumption, i.e., that the disynaptic inhibition is exclusively mediated by neurons with discharge patterns typical for phasic 2°VNs (Fig. 8D_2), the resulting model compound response exhibited a dynamics (Fig. 8C_2, black trace) that is incompatible with the experimental data (compare Fig. 8C_1, control). The delayed rapid increase in the response amplitude (Fig. 8C_2, arrowhead) was caused by the restricted effect of the inhibition in the model response attributable to the temporally limited discharge of the hypothetical phasic inhibitory neurons (Fig. 8D_2).

The testable prediction from this modeling approach in future studies thus is that tonic ipsilateral vestibular neurons mediate the observed disynaptic inhibition onto phasic 2°VNs.

Discussion

Frequency-modulated electrical pulse-train stimulation of individual vestibular nerve branches activated synaptic responses in frog tonic and phasic 2°VNs with distinctly different profiles. The mostly linear transformation of the presynaptic afferent activity into postsynaptic responses in tonic 2°VNs complies with the linear intrinsic properties and low-pass filter characteristics of these neurons and suggests an implication in the processing of low-dynamic, tonic components of head motion. In contrast, responses of phasic 2°VNs exhibited highly asymmetric profiles because of distinct bandpass filter properties and the impact of inhibitory inputs from vestibular and cerebellar circuits. Accordingly, phasic 2°VNs form adequate central vestibular elements optimized for processing of high-dynamic, nonlinear head motion components.

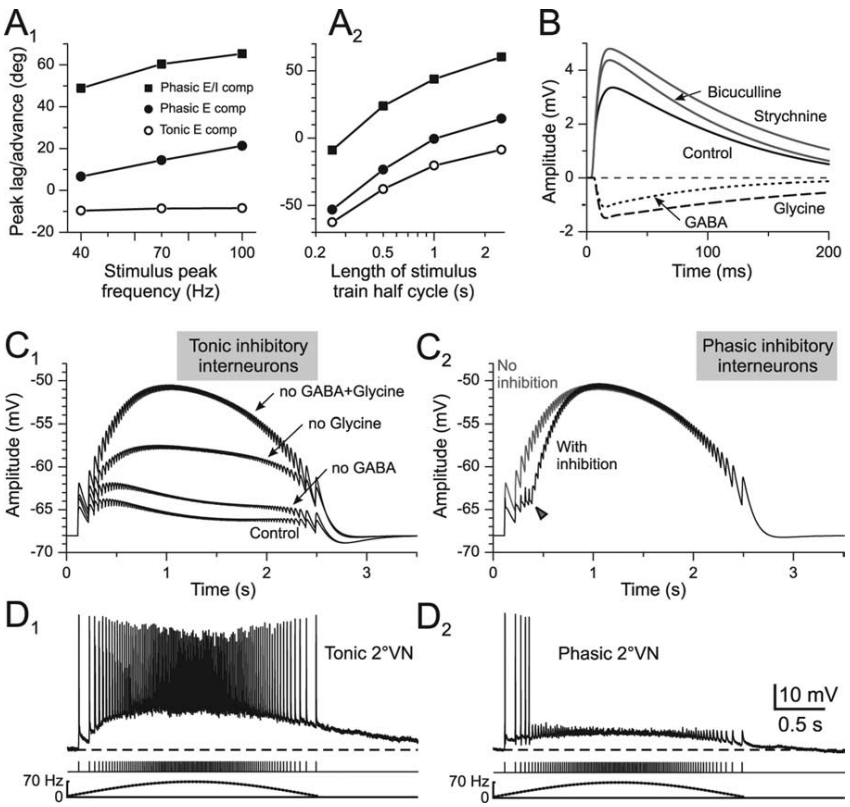

Figure 8. Compound responses generated from intrinsic compartmental models extended by excitatory (*E* compartmental model) or excitatory and inhibitory synaptic conductances (*E*/*I* compartmental model). ***A*$_1$, *A*$_2$,** Peak lag/advance as a function of stimulus peak frequency (***A*$_1$**) or half-cycle length (***A*$_2$**) of model compound responses reconstructed from tonic (○) and phasic (●) E compartmental models; appropriate conductances that mimic the disynaptic inhibition (*E*/*I* compartmental model) cause the peak advance (■) observed in phasic 2°VNs. ***B***, Fitted average responses of the *E*/*I* compartmental model mimicking labyrinthine nerve-evoked monosynaptic EPSPs before (control) and after application of bicuculline or strychnine in phasic 2°VNs; subtraction from control responses reveals the differential time courses of disynaptic GABAergic (dotted line) and glycinergic (dashed line) IPSPs [fit based on data from the study by Biesdorf et al. (2008)]. ***C*$_1$–*D*$_2$,** Model compound responses of a phasic 2°VN (peak frequency, 70 Hz) based on the *E*/*I* compartmental model assuming that inhibitory interneurons exhibit either a discharge like a real tonic (***D*$_1$**) or a real phasic 2°VN (***D*$_2$**); model compound responses before (control) and after blocking disynaptic GABAergic, glycinergic, or both components are shown in ***C*$_1$**; the arrowhead in ***C*$_2$** indicates the increase of the model response amplitude attributable to the termination of the limited discharge (***D*$_2$**) if the inhibitory interneurons were phasic type 2°VNs; recordings in ***D*$_1$** and ***D*$_2$** are single sweeps; dashed lines indicate the resting membrane potential (−66 mV in ***D*$_1$**; −62 mV in ***D*$_2$**). The calibration in ***D*$_2$** applies to ***D*$_1$**; bottom traces in ***D*$_1$** and ***D*$_2$** show pulse trains and stimulus frequency (dotted lines).

Limitations of the stimulus paradigm

Vestibular afferent fibers cover a broad spectrum of response dynamics during head rotation (Goldberg, 2000). The heterogeneity in afferent spiking during natural activation causes an asynchronous postsynaptic input in 2°VNs that is important for the high-fidelity linear response behavior of the vestibulo-ocular reflex (VOR) (Ramachandran and Lisberger, 2006; Hospedales et al., 2008). The sinusoidally modulated electrical pulse trains in the present study cause mainly synchronized vestibular afferent activity. Thus, imitation of head motion-related afferent discharge *in vitro* is an approximation with respect to presynaptic discharge timing and recruited fiber spectrum. However, it facilitates investigating the transformation of well-defined presynaptic vestibular afferent activity into postsynaptic responses of tonic and phasic 2°VNs. Thus, the use of *in vivo* discharge patterns as a template for electrical stimulation *in vitro* is well suited to understand the cellular basis for a differential processing of vestibular sensory signals in 2°VNs.

Coadaptation of intrinsic membrane and emerging network properties of 2°VNs

The different, oppositely oriented response properties of frog tonic and phasic 2°VNs (Beraneck et al., 2007) and the differential insertion into inhibitory synaptic circuits (Biesdorf et al., 2008) suggest that intrinsic membrane and emerging network properties are functionally coadapted. Together with the different dynamics of pulse train-evoked compound responses, this supports the idea that each of the two subtypes is optimally adapted for a particular role in vestibular sensory–motor transformation. Accordingly, tonic 2°VNs as low-pass filters are well suited for the processing of low-frequency head motion components with a relatively linear transformation of presynaptic afferent activity patterns into postsynaptic responses. In contrast, phasic 2°VNs are most suitable for processing transient, high-frequency components with an input–output function that is rather nonlinear as evidenced by the timing of peak discharge rate (Fig. 5*G*$_2$). The large nonlinearity of the latter neuronal subtype is caused by a fast and efficient EPSP summation and a subsequent shunting of the input, particularly during high-frequency presynaptic afferent activity (Fig. 3*B*). The shunting is mostly attributable to the combined effect of voltage-dependent potassium conductances (Beraneck et al., 2007) and a potent disynaptic inhibition after the monosynaptic EPSP (Biesdorf et al., 2008). Although the experimental data do not allow a distinction between relative contributions of intrinsic and network properties in shaping the synaptic responses, our modeling approach suggests that the feedforward inhibition contributes considerably to the generation of the highly asymmetric response profile in phasic 2°VNs, thus facilitating the effects of the intrinsic cellular characteristics.

The distinct differences of pulse-train evoked synaptic re-

sponses in frog tonic and phasic 2°VNs is suitable to form the cellular basis for a processing of VOR signals in parallel, frequency-tuned channels that mediate linear (tonic) and nonlinear (phasic) components, respectively (Minor et al., 1999). Separate information channels occur at the sensory periphery (Goldberg, 2000) as well as at the extraocular motor level as evidenced by the presence of functional elements with different morphophysiological properties (Büttner-Ennever, 2005; Spencer and Porter, 2005). In frog, this is evidenced by the presence of abducens motoneurons with different response profiles (Dieringer and Precht, 1986). The large advance and nonlinear pattern of the discharge in phasic 2°VNs during sinusoidal pulse-train stimulation of semicircular canal nerves (Fig. 5*E*,*F*,G_2) concurs with the particular contribution of eye movements to gaze stabilization in frogs (Dieringer, 1987). During sinusoidal head rotation, compensatory eye motion consists of a rapid, transient eye velocity peak followed by a rather stable eye position. Although the eye velocity shows a transient profile during sinusoidal table rotation, combined eye/head movements generate perfect compensatory gaze movements. The observed different dynamic eye motion components are coherent with an activation of extraocular motoneurons by a combination of signals from phasic and tonic 2°VNs (Fig. 5G_1–G_3) stimulated with the same cycle length of table rotation as *in vivo* (Blanks and Precht, 1976; Dieringer, 1987). Given that both tonic and phasic 2°VNs project directly to extraocular targets (Straka et al., 2004), the discharge patterns of the two vestibular cell types are well suited to generate the necessary premotor commands for the different dynamic eye motion components during gaze stabilization in frog.

Common principles of vertebrate central vestibular information processing

The independent adaptive control of different dynamic aspects of angular VOR suggests that the mediation of linear and nonlinear components in separate sensory–motor channels (Lisberger et al., 1983; Minor et al., 1999; Lasker et al., 2000; Clendaniel et al., 2002; Ramachandran and Lisberger, 2006) is a general feature of vertebrate vestibular information processing. Such a parallel processing requires that different dynamic aspects of head motion-related vestibular signals are not only coded in separate vestibular sensory (Goldberg, 2000) and extraocular motor channels (Büttner-Ennever, 2005; Spencer and Porter, 2005) but are also processed centrally within separate populations of 2°VNs. In frog, tonic and phasic 2°VNs are ideally suited for a separate central processing of linear and nonlinear components. Appropriate homologues for a respective parallel processing in mammals might be tonic and "kinetic" vestibular neurons described in cat (Shimazu and Precht, 1965) or rodent type A and B medial vestibular nucleus (MVN) neurons (Babalian et al., 1997). The latter types exhibit adequate cellular properties necessary for differential signal processing (Straka et al., 2005) mostly based on differences in potassium conductances (Gittis and du Lac, 2007).

In frog, the differential tuning of synaptic response dynamics in 2°VNs depends on intrinsic membrane properties as well as on inhibitory side loops. The connectivity of these circuits is likely not a particularity of frogs but rather a common vertebrate feature. The similarities of vestibular network organization in different vertebrates (Straka and Dieringer, 2004) suggest that the sensory–motor transformation of head motion-related signals in mammals is also controlled by similarly organized side loops (Minor and Goldberg, 1991). Thus, a differential insertion of, for example, rodent type A and B MVN neurons into inhibitory and excitatory circuits is likely and might allow an independent adaptation and modification of particular dynamic aspects. Given a fundamental functional equivalence of central vestibular neurons in different vertebrates (Straka et al., 2005), intrinsic membrane and emerging network properties of mammalian vestibular subgroups might be coadapted as in frogs.

Inhibitory control of vestibular responses

An ipsilateral disynaptic GABAergic and glycinergic inhibition that facilitates nonlinear response components in frog phasic 2°VNs (Biesdorf et al., 2008) is likely also present in a subgroup of mammalian central vestibular neurons. Mouse type B MVN neurons, functional homologues of frog phasic 2°VNs, receive considerably more spontaneous glycinergic and GABAergic inputs from ipsilateral vestibular interneurons than type A MVN neurons (Camp et al., 2006). A feedforward side loop that mediates an inhibition on type B MVN neurons could originate from a subset of type-A-like GABAergic neurons in the parvocellular part of the MVN (Bagnall et al., 2007; Gittis and du Lac, 2007, 2008). This putative organization in mouse matches with our modeling predictions (Fig. 8*B*,*C*) and suggests that vestibular inhibitory interneurons are tonic 2°VNs, which are equivalent to mammalian type A MVN neurons (Straka et al., 2005). Thus, a conserved intrinsic vestibular circuitry exists that allows a continuous fine tuning of the response dynamics in a particular type of 2°VNs (Minor and Goldberg, 1991; Straka and Dieringer, 1996).

In all vertebrates, a subpopulation of central vestibular neurons receives a Purkinje cell-mediated GABAergic inhibition (Straka and Dieringer, 2004). Although this inhibition seems to be weak in frog (Magherini et al., 1975; Dieringer and Precht, 1979), a cerebellar lesion increased the gain of the abducens motoneuronal discharge during sinusoidal head rotation by ~50% (Straka and Dieringer, 2004). This complies with the increase of semicircular canal nerve-evoked compound response amplitudes in phasic 2°VNs after a block of the cerebellar circuit (Fig. 6*E*). The presence of a cerebellar inhibition in some phasic 2°VNs makes these neurons equivalent to mammalian floccular target neurons (FTN) in the MVN (De Zeeuw et al., 1994; Lisberger, 1998). In rodents, these neurons were shown to form a specific subpopulation of type B MVN neurons (Babalian and Vidal, 2000; Sekirnjak et al., 2003). Thus, a differentially organized Purkinje cell-mediated inhibition in equivalent subpopulations of vestibular neurons seems to be another conserved feature of vertebrate vestibular signal processing. The particular role of mammalian FTN in VOR plasticity and the flexibly controlled synaptic signal processing in frog phasic 2°VNs suggests that these neurons are part of a modifiable pathway that enables plastic adaptations of vestibulomotor responses (Lisberger, 1998; Minor et al., 1999; Boyden et al., 2004; Gittis and du Lac, 2006; Ramachandran and Lisberger, 2006, 2008).

References

Babalian A, Vibert N, Assie G, Serafin M, Mühlethaler M, Vidal PP (1997) Central vestibular networks in the guinea-pig: functional characterization in the isolated whole brain in vitro. Neuroscience 81:405–426.

Babalian AL, Vidal PP (2000) Floccular modulation of vestibuloocular pathways and cerebellum-related plasticity: an in vitro whole brain study. J Neurophysiol 84:2514–2528.

Bagnall MW, Stevens RJ, du Lac S (2007) Transgenic mouse lines subdivide medial vestibular nucleus neurons into discrete, neurochemically distinct populations. J Neurosci 28:2318–2330.

Baird RA (1994a) Comparative transduction mechanisms of hair cells in the bullfrog utriculus. I. Responses to intracellular current. J Neurophysiol 71:666–684.

Baird RA (1994b) Comparative transduction mechanisms of hair cells in the

bullfrog utriculus. II. Sensitivity and response dynamics to hair bundle displacement. J Neurophysiol 71:685–705.

Bekkers JM, Delaney AJ (2001) Modulation of excitability by alpha-dendrotoxin-sensitive potassium channels in neocortical pyramidal neurons. J Neurosci 21:6553–6560.

Beraneck M, Pfanzelt S, Vassias I, Rohregger M, Vibert N, Vidal PP, Moore LE, Straka H (2007) Differential intrinsic response dynamics determine synaptic signal processing in frog vestibular neurons. J Neurosci 27:4283–4296.

Biesdorf S, Straka H (2004) Control of responses in frog second-order semicircular canal neurons by inhibitory and excitatory inputs. Soc Neurosci Abstr 30:652.1.

Biesdorf S, Malinvaud D, Reichenberger I, Pfanzelt S, Straka H (2008) Differential inhibitory control of semicircular canal nerve afferent-evoked inputs in second-order vestibular neurons by glycinergic and GABAergic circuits. J Neurophysiol 99:1758–1769.

Birinyi A, Straka H, Matesz C, Dieringer N (2001) Location of dye-coupled second order and of efferent vestibular neurons labeled from individual semicircular canal or otolith organs in the frog. Brain Res 921:44–59.

Blanks RH, Precht W (1976) Functional characterization of primary vestibular afferents in the frog. Exp Brain Res 25:369–390.

Borg-Graham L (1991) Modelling the non-linear conductances of excitable membranes. In: Cellular neurobiology: a practical approach (Chad J, Wheal H, eds). Oxford: IRL at Oxford UP.

Boyden ES, Katoh A, Raymond JL (2004) Cerebellum-dependent learning: the role of multiple plasticity mechanisms. Annu Rev Neurosci 27:581–609.

Büttner-Ennever JA (2005) The extraocular motor nuclei: organization and functional neuroanatomy. Prog Brain Res 151:95–125.

Camp AJ, Callister RJ, Brichta AM (2006) Inhibitory synaptic transmission differs in mouse type A and B medial vestibular nucleus neurons in vitro. J Neurophysiol 95:3208–3218.

Carnevale NT, Hines ML (2006) The NEURON book. Cambridge, UK: Cambridge UP.

Clendaniel RA, Lasker DM, Minor LB (2002) Differential adaptation of the linear and nonlinear components of the horizontal vestibuloocular reflex in squirrel monkeys. J Neurophysiol 88:3534–3540.

De Zeeuw CI, Wylie DR, DiGiorgi PL, Simpson JI (1994) Projections of individual Purkinje cells of identified zones in the flocculus to the vestibular and cerebellar nuclei in the rabbit. J Comp Neurol 349:428–447.

Dieringer N (1987) The role of compensatory eye and head movements for gaze stabilization in the unrestrained frog. Brain Res 404:33–38.

Dieringer N, Precht W (1977) Modification of synaptic input following unilateral labyrinthectomy. Nature 269:431–433.

Dieringer N, Precht W (1979) Mechanisms of compensation for vestibular deficits in the frog. II. Modification of the inhibitory pathways. Exp Brain Res 36:329–357.

Dieringer N, Precht W (1986) Functional organization of eye velocity and eye position signals in abducens motoneurons of the frog. J Comp Physiol 158:179–194.

du Lac S, Lisberger SG (1995) Cellular processing of temporal information in medial vestibular nucleus neurons. J Neurosci 15:8000–8010.

Eatock RA, Rüsch A, Lysakowski A, Saeki M (1998) Hair cells in mammalian utricles. Otolaryngol Head Neck Surg 119:172–181.

Gittis AH, du Lac S (2006) Intrinsic and synaptic plasticity in the vestibular system. Curr Opin Neurobiol 16:385–390.

Gittis AH, du Lac S (2007) Firing properties of GABAergic versus non-GABAergic vestibular nucleus neurons conferred by a differential balance of potassium currents. J Neurophysiol 97:3986–3996.

Gittis AH, du Lac S (2008) Similar properties of transient, persistent, and resurgent Na currents in GABAergic and non-GABAergic vestibular nucleus neurons. J Neurophysiol 99:2060–2065.

Goldberg JM (2000) Afferent diversity and the organization of central vestibular pathways. Exp Brain Res 130:277–297.

Hille B (2001) Ion channels of excitable membranes, Ed 3. Sunderland, MA: Sinauer.

Hjelmstad GO, Nicoll RA, Malenka RC (1997) Synaptic refractory period provides a measure of probability of release in the hippocampus. Neuron 19:1309–1918.

Hospedales TM, van Rossum MC, Graham BP, Dutia MB (2008) Implications of noise and neural heterogeneity for vestibulo-ocular reflex fidelity. Neural Comput 20:756–778.

Johnston D, Wu SM (1994) Foundations of cellular neurophysiology (Bradford Books). Cambridge, MA: MIT.

Johnston AR, MacLeod NK, Dutia MB (1994) Ionic conductances contributing to spike repolarization and after-potentials in rat medial vestibular nucleus neurones. J Physiol 481:61–77.

Lasker DM, Hullar TE, Minor LB (2000) Horizontal vestibuloocular reflex evoked by high-acceleration rotations in the squirrel monkey. III. Responses after labyrinthectomy. J Neurophysiol 83:2482–2496.

Lisberger SG (1998) Physiologic basis for motor learning in the vestibulo-ocular reflex. Otolaryngol Head Neck Surg 119:43–48.

Lisberger SG, Miles FA, Optican LM (1983) Frequency-selective adaptation: evidence for channels in the vestibulo-ocular reflex? J Neurosci 3:1234–1244.

Magherini PC, Giretti ML, Precht W (1975) Cerebellar control of vestibular neurons of the frog. Pflugers Arch 356:99–109.

Minor LB, Goldberg JM (1991) Vestibular nerve inputs to the vestibulo-ocular reflex: a functional ablation study in the squirrel monkey. J Neurosci 11:1636–1648.

Minor LB, Lasker DM, Backous DD, Hullar TE (1999) Horizontal vestibuloocular reflex evoked by high-acceleration rotations in the squirrel monkey. I. Normal responses. J Neurophysiol 82:1254–1270.

Moore LE, Buchanan JT, Murphey CR (1995) Localization and interaction of N-methyl-D-aspartate and non-N-methyl-D-aspartate receptors of lamprey spinal neurons. Biophys J 68:96–103.

Murphey CR, Moore LE, Buchanan JT (1995) Quantitative analysis of electrotonic structure and membrane properties of NMDA-activated lamprey spinal neurons. Neural Comp 7:486–506.

Peusner KD, Giaume C (1997) Ontogeny of electrophysiological properties and dendritic pattern in second-order chick vestibular neurons. J Comp Neurol 384:621–633.

Pfanzelt S, Rohregger M, Moore LE, Straka H (2004) Differential dynamics of labyrinthine nerve afferent-evoked responses in tonic and phasic frog second-order vestibular neurons. Soc Neurosci Abstr 30:652.2.

Ramachandran R, Lisberger SG (2006) Transformation of vestibular signals into motor commands in the vestibuloocular reflex pathways of monkeys. J Neurophysiol 96:1061–1074.

Ramachandran R, Lisberger SG (2008) Neural substrate of modified and unmodified pathways for learning in monkey vestibulo-ocular reflex. J Neurophysiol, in press.

Saint Mleux B, Moore LE (2000) Active dendritic membrane properties of *Xenopus* larval spinal neurons analyzed with a whole cell soma voltage clamp. J Neurophysiol 83:1381–1393.

Sekirnjak C, Vissel B, Bollinger J, Faulstich M, du Lac S (2003) Purkinje cell synapses target physiologically unique brainstem neurons. J Neurosci 23:6392–6398.

Serafin M, de Waele C, Khateb A, Vidal PP, Mühlethaler M (1991) Medial vestibular nucleus in the guinea-pig. I. Intrinsic membrane properties in brainstem slices. Exp Brain Res 84:417–425.

Shimazu H, Precht W (1965) Tonic and kinetic responses of cat's vestibular neurons to horizontal angular acceleration. J Neurophysiol 28:991–1013.

Spencer RF, Porter JD (2005) Biological organization of the extraocular muscles. Prog Brain Res 151:43–80.

Straka H, Dieringer N (1991) Internuclear neurons in the ocular motor system of frogs. J Comp Neurol 312:537–548.

Straka H, Dieringer N (1993) Electrophysiological and pharmacological characterization of vestibular inputs to identified frog abducens motoneurons and internuclear neurons in vitro. Eur J Neurosci 5:251–260.

Straka H, Dieringer N (1996) Uncrossed disynaptic inhibition of second-order vestibular neurons and its interaction with monosynaptic excitation from vestibular nerve afferent fibers in the frog. J Neurophysiol 76:3087–3101.

Straka H, Dieringer N (2000) Convergence pattern of uncrossed excitatory and inhibitory semicircular canal-specific inputs onto second-order vestibular neurons of frogs. Exp Brain Res 135:462–473.

Straka H, Dieringer N (2004) Basic organization principles of the VOR: lessons from frogs. Prog Neurobiol 73:259–309.

Straka H, Biesdorf S, Dieringer N (1997) Canal-specific excitation and inhibition of frog second order vestibular neurons. J Neurophysiol 78:1363–1372.

Straka H, Holler S, Goto F (2002) Patterns of canal and otolith afferent input convergence in frog second order vestibular neurons. J Neurophysiol 88:2287–2301.

Straka H, Beraneck M, Rohregger M, Moore LE, Vidal PP, Vibert N (2004) Second-order vestibular neurons form separate populations with different membrane and discharge properties. J Neurophysiol 92:845–861.

Straka H, Vibert N, Vidal PP, Moore LE, Dutia MB (2005) Intrinsic membrane properties of vertebrate vestibular neurons: function, development and plasticity. Prog Neurobiol 76:349–392.

5 Discussion

The identification and characterization of neuron types within circuits is crucial to understanding their role in behavior. In frog, tonic and phasic neurons in the vestibular nuclei are likely to code slow, low-frequent and rapid, high-frequent components of head movement-related signals, respectively. Intrinsic membrane properties confer low-pass filter-like characteristics to tonic and band-pass characteristics to phasic neurons. The band-pass filter behavior of the latter subtype is due to the activation of at least two potassium conductances, an I_D potassium channel (Beraneck et al., 2007) as well as the TEA-sensitive delayed rectifier (unpublished). Depolarization leads to an increase in input resistance in tonic neurons, while the input resistance in phasic neurons decreases. This oppositely directed response behavior makes tonic and phasic neurons well-suited for amplification of synaptic signals or event detection. Response dynamics to continuous synaptic inputs, however, do not only depend on neuronal intrinsic properties but also on the synaptic contributions of various local circuits. Labyrinthine-evoked monosynaptic EPSPs in phasic but not in tonic second-order vestibular neurons (2°VN) are superimposed by disynaptic glycinergic and GABAergic IPSPs with different response profiles (Biesdorf et al., 2008). Glycinergic compared to GABAergic IPSPs reduce the amplitude of monosynaptic EPSPs for a longer period. Both pharmacological types of IPSPs, though, shorten the magnitude and duration of the monosynaptic excitation in phasic 2°VN. They thus boost the processing of transient signals in this neuronal subtype. The different insertion of tonic and phasic neurons in inhibitory circuits is consistent with their different filter properties and indicates a co-adaptation of intrinsic and emerging network properties. To investigate how head movement-related signals are processed in tonic and phasic 2°VN, labyrinthine nerve fibers were electrically stimulated with frequency-modulated pulse trains (Pfanzelt et al., 2008). This stimulus reproduces the discharge in an afferent fiber during rotational movements. The application of this stimulus yields compound synaptic responses with different profiles in frog tonic and phasic 2°VN. The

mainly linear transformation of presynaptic labyrinthine activity into postsynaptic potentials in tonic neurons concurs with their low-pass filter properties. Phasic neurons exhibit highly asymmetric profiles that can be assigned to their resonant currents as well as to their insertion into inhibitory disynaptic circuits. Thus, the co-adaptation of intrinsic and network properties establishes two different neuronal types that are well-suited for a parallel processing of head movement-related signals with different dynamics.

5.1 Membrane conductances in central vestibular neurons

Neurons show a variety of activity patterns that are in part due to the number and type of voltage-gated ion channels in their membrane. The differential neuronal properties are critically influenced by the type and density of voltage-gated channels. Variations of these parameters can lead to changes in firing frequency and threshold, and might even switch neurons from one kind of activity mode, such as tonic firing, into, for instance, a burst-like activity mode. Such a turning point in the response pattern exists in chicken tangential vestibular neurons during embryonic development (Peusner and Giaume, 1997). These neurons are central relay neurons of the vestibulo-ocular reflex (VOR) pathway. The major cell population, the principal cells, gradually acquires the ability of non-accommodating firing of action potentials during chick embryonic development. Up to a critical moment in development, principal cells accommodate after a single action potential, whereas in the hatchling these neurons show a tonic firing behavior upon a depolarizing current step (Peusner and Giaume, 1997). Suppression of a dendrotoxin-sensitive potassium channel was sufficient to transform accommodating cells into non-accommodating cells (Gamkrelidze et al., 1998).

Tonic and phasic second-order vestibular neurons in frog mediate different aspects of head movement-related signals to extraocular and spinal targets. To learn more about their distinct roles in the VOR circuit, it was crucial to reveal the conductances, which confer to frog tonic and phasic neurons their typical response characteristics. Passive membrane properties of neurons in general create filter characteristics that are typical for low-pass filters (Hutcheon and Yarom, 2000): current inputs at low frequencies result in relatively large voltage responses whereas higher frequency inputs are dampened. Injection of oscillatory frequency-modulated currents

into frog tonic 2°VN revealed that these neurons behaved like low-pass filters (Beraneck et al., 2007). This concurs with the notion that the input-output behavior of these neurons is approximately linear. The impedance increase with depolarization in this type of neuron, however, was suggestive for the activation of a non-inactivating sodium conductance (I_{NaP}). The established tonic cellular model (Pfanzelt et al., 2008) further affirmed the need of such a non-inactivating steady-state conductance to reproduce the impedance increase. I_{NaP} conductance is activated at potentials ∼10 mV below spike threshold (Crill, 1996). The characteristics of I_{NaP}, thus, convey tonic neurons the ability to enhance excitatory and inhibitory synaptic inputs (Vervaeke et al., 2006). The ability of frog tonic 2°VN to amplify small synaptic signals suggests that these neurons are particularly suitable for integration of synaptic signals. In addition, an increased responsiveness provides a more precise representation of the amplitude and time course of the input signal (McCormick et al., 2003). Altogether, the low-pass filter behavior and the enhanced sensitivity to synaptic inputs confer to frog tonic 2°VN properties, which render them appropriate for long-lasting activity and synaptic integration. Assuming that the signals of these neurons are mediated to extraocular targets, they would be excellently suitable for premotor commands that drive slow-tonic eye muscles in order to keep eccentric eye positions (Dieringer and Precht, 1986).

In contrast to the low-pass filter behavior of tonic neurons, frog phasic 2°VN typically show a resonance upon stimulation with oscillatory frequency-modulated currents. Such resonances constrain neurons to respond most powerfully to inputs at biologically important frequencies. Resonance typically results from an interaction between active and passive membrane properties (Wu et al., 2001). The low-pass filter dynamics of the passive membrane properties weakens responses to inputs arriving at higher frequencies. An additional conductance that attenuates voltage responses to inputs occurring at low frequencies and that reinforces those at mid-frequencies results in a neuron with band-pass filter-like behavior. The response pattern of non-accommodating and accommodating cells in the chicken tangential nucleus is very much reminiscent of that of tonic and phasic neurons upon a depolarizing current step (Peusner and Giaume, 1997). This resemblance might be attributed to similar sets of ion channels in chicken tangential and frog vestibular neurons. The application of low doses of the specific potassium channel blocker 4-AP indeed revealed that an I_D potassium channel contributed to the resonant

behavior (Beraneck et al., 2007). Such an ion channel is activated above spike threshold and is hence able to oppose longer-lasting membrane depolarizations (Wu et al., 2001). Pharmacological blocking of this channel in frog phasic 2°VN resulted in an impedance increase during low-frequency responses and also abolished the resonance in these neurons. In contrast to the chicken tangential neurons, however, this voltage-gated current alone could not switch a phasic into a tonic neuron. Firing after blocking this channel was extended to lower frequencies but was never encountered at frequencies below ∼10 Hz. Thus, an additional conductance must be involved in generating the resonant behavior in phasic neurons. Preliminary results showed that in fact a delayed rectifier potassium channel, which could be blocked by low concentrations of tetraethylammonium (TEA), is involved in shaping the response properties of frog phasic vestibular neurons. Modeling of frog phasic 2°VN approved the necessity of a non-inactivating potassium channel, in addition to the inactivating low-threshold I_D conductance. This channel, like the I_D conductance, was activated above threshold, but was endowed with slower activation kinetics. Model responses upon depolarizing current steps yielded similar response characteristics compared to real data. It is thus very likely that several potassium conductances are involved in shaping the resonance of frog phasic neurons. Unlike tonic neurons, phasic neurons decrease their impedance upon depolarization, which keeps these neurons close to the resting potential. This stabilization close to the resting membrane potential is caused by the resonant currents, which tend to shunt the membrane potential. This, in combination with their preference for higher frequencies make them suitable to function as event detectors since any synaptic input will likely cause a single action potential or at maximum a short burst-like discharge.

Thus, the differential filter properties of frog central vestibular neurons are likely to be linked with different functional roles in the processing of vestibular inputs. The presence of neuronal subsets with different dynamic properties is not a peculiarity of frog central vestibular neurons but seems to be a common principle among vertebrates (see Straka et al., 2005). Rodent type A and type B MVN (medial vestibular nucleus) neurons are the functional correlates of frog tonic and phasic neurons, respectively. These correlates, however, differ in a number of aspects from frog vestibular neurons, such as spontaneous discharge and composition of ion channels. Nevertheless, type A MVN neurons are like tonic neurons in that they are better suited to linearly process synaptic inputs. This is due to their ability to modulate their discharge over a

wider frequency range than type B MVN neurons. At higher frequencies type B MVN neurons synchronize their discharge with the depolarizing phase of the stimulus. They exhibit linear responses only over a small low-frequency range, but are the only cells that are able to respond to high-frequency and high-amplitude signals by working as an event detector (Ris et al., 2001; Beraneck et al., 2003). Vestibular neurons with a purely phasic discharge pattern and highly transient response profiles, as frog 2°VN, are absent in other adult vertebrate species. This might be linked with another particularity of frog vestibular neurons, which is the virtual absence of a spontaneous discharge in central vestibular neurons in the *in vitro* preparation. Since also afferent fibers in the frog show highly phasic response properties (Precht et al., 1971; Lowenstein and Saunders, 1975) repetitive firing in frog vestibular neurons depends on constant synaptic input, mainly from the labyrinthine endorgans. As a consequence, the spontaneous discharge rate of central vestibular neurons *in vivo* reflects the discharge of afferent fibers, which is rather low (1–10 Hz; Dieringer and Precht, 1977).

Adult guinea pig MVN neurons subdivide in about equal proportions of type A and B neurons (Beraneck et al., 2003). A recent study (Eugène et al., 2007) has shown that similar proportions of MVN neurons are found in adult mice. Rat MVN neurons differ somewhat in their distribution; they exhibit $\frac{1}{3}$ of type A and $\frac{2}{3}$ of type B MVN neurons (Johnston et al., 1994; Him and Dutia, 2001). In the frog, in contrast, only 10-20 % of all the recorded neurons are of the tonic type, whereas 80-90 % are identified as phasic neurons (Beraneck et al., 2007; Pfanzelt et al., 2008). However, it cannot be excluded that there is a sampling bias towards phasic neurons because tonic neurons might be smaller and thereby more difficult to impale. The highly accommodating properties of frog phasic 2°VN, their preponderance over tonic 2°VN, the phasic response behavior of afferent nerve fibers and the rather negative resting membrane potential result in the absence of a spontaneous discharge in the *in vitro* preparation. This absence reflects the tuning of vestibular information processing in frogs to much more phasic dynamics compared to the dynamics in rodents. What might be the functional explanation of such an adjustment to phasic dynamics in frog? Such differences represent presumably adaptations to different, ecological habitats and lifestyle. The highly phasic dynamics in frogs could be required because of their particular movement strategy, as seen for instance, during prey catching. Their prey catching behavior is characterized by long periods of immobility (Schneider, 1954) that are

interrupted by brief and rapid orienting movements towards the prey. For such a "wait, turn and snap" behavior, a system with highly phasic neurons that serve as event detectors seem to be the most suited. The absence of a continuously modulated synaptic input from the labyrinth suggests that the maintenance of a high resting discharge is less important for the movement strategy of the frog. The purely phasic response behavior of 2°VN might be considered as an energy-saving mechanism. The smaller number of tonic neurons would serve to stabilize gaze and posture during the long phases of immobility or during slow movements. Locomotion in guinea pigs or rats, in contrast, is largely marked by continuous and smooth body movements. In this case, a modulated input from the labyrinth is best processed by neurons with a rather high resting discharge to obtain a larger range of linearity and an increased sensitivity.
To date it is unclear if the classification into neuronal subtypes of *in vitro* recordings can be brought in line with the classification defined in *in vivo* recordings. Experiments *in vivo* established several classes of neurons according to their activity during behavior. In cat, neurons that respond with an increased discharge to ipsilateral head rotation have been further subdivided into tonic and kinetic neurons based on the regularity of their spontaneous discharge rate (Shimazu and Precht, 1965). Babalian et al. (1997) suggested that type B MVN neurons might correspond to the irregular discharging, kinetic neurons and type A MVN neurons to tonic-type, regular discharging neurons in the cat. The *in vitro* whole brain preparation might help to consolidate *in vitro* and *in vivo* schemes. The application of a stimulus that mimics a head movement can provide a link between *in vitro* defined classes of neurons and their functional relevance during behavior.

5.2 Synaptic processing in central vestibular neurons

Frog central vestibular neurons subdivide into tonic and phasic neurons. The different filter properties of these two subtypes could be tuned to the activity patterns of different types of labyrinthine nerve fibers during naturally occurring body motion. Consequently, tonic neurons should be adjusted to the input of thin, regular firing fibers that are concerned with the processing of slow head movements or static head deviations. Filter properties of phasic neurons, in contrast, should be adapted to the input of thick, irregularly firing fibers that encode high-

dynamic components of a head movement (Goldberg, 2000). To test if frog tonic and phasic 2°VN differ in how they process labyrinthine afferent signal components, it was necessary to analyze if these two subtypes differentially transform the presynaptic inputs into postsynaptic responses. To reveal differences in their response dynamics afferent nerve fibers, were electrically stimulated with a frequency-modulated pulse train (pulse train stimulation). As described in detail (Pfanzelt et al., 2008) the stimulus was designed to simulate the discharge rate of afferent fibers recorded *in vivo* during rotational acceleration (Blanks and Precht, 1976). Since in the *in vitro* frog preparation all central connectivity remains functional, it represents a link between the differential intrinsic membrane properties and their functional role during synaptic signal processing. Pulse train stimulation of labyrinthine nerve branches led to different response profiles in tonic and in phasic 2°VN. Tonic neurons exhibited a largely linear transformation of presynaptic inputs into postsynaptic responses. This result corroborates the notion of these neurons having membrane properties that allow a faithful transmission of the inputs in a more or less linear way. Phasic 2°VN, in contrast, show highly asymmetric postsynaptic response profiles upon sinusoidal pulse train stimulation. The large peak advance with respect to stimulus peak frequency indicates a high non-linearity in the transformation of sensory signals, which makes this subtype suitable for processing of transient, high-frequency components. Variation of particular stimulus parameters could, for instance, mimic changes in the amplitude and velocity of a head movement. An increasing stimulus peak frequency (see *Material and Methods*, Pfanzelt et al., 2008) simulates a larger and faster head rotation. The observed peak advance with high stimulus peak frequencies (rapid head movement) and the coherent discharge behavior could serve to quickly activate appropriate compensatory eye movements. Interestingly, the eye velocity profile (rapid, transient increase of eye velocity) during compensatory eye movements of frogs upon passive rotations on a turntable (Blanks and Precht, 1976) resembles the membrane potential course of phasic 2°VN following pulse train stimulation.

The pulse train stimulus paradigm provided a useful tool to investigate differences in response dynamics of tonic and phasic neurons under various conditions. However, the simulation of a head movement-related fiber discharge in this paradigm is an approximation with respect to the recruited fiber spectrum and the timing of fiber activation *in vivo*. Slow or rapid head movements stimulate hair cells with low or high dynamics, which, in turn, target thin or thick fibers,

respectively. A head rotation is composed of a fundamental and many higher, superimposed frequencies. As acceleration augments an increasing number of higher frequencies is involved. As long as the head accelerates, fibers with thicker and thicker diameters will be recruited. This leads to a subsequent activation of afferent fibers and thus to an asynchronous discharge in the vestibular nerve. Even though increasingly thicker fibers will be activated with higher acceleration, a low-dynamic head movement will nevertheless predominantly activate rather thin-diameter fibers compared to a high-dynamic movement where the slope of acceleration is much steeper. In contrast to the subsequent activation of afferent fibers, the pulse train stimulus recruits all fibers with the first pulse, given that the pulse stimulus intensity is above threshold for these fibers. The fiber spectrum that is activated by a current pulse depends on the current intensity. Thick fibers are recruited by low intensities; with higher intensities an increasing number of thinner fibers are activated. An electrical stimulation thus recruits the fiber spectrum in a different order compared to that activated during slow or rapid movements. In addition, it generates a synchronous discharge in the vestibular nerve. During natural activation, however, spike jitter in afferent nerve fibers has been reported as an important mechanism to enable high-fidelity responses in the VOR over a wide frequency range (Hospedales et al., 2008). Since tonic and phasic 2°VN receive inputs from a similar fiber spectrum (Straka and Dieringer, 2000) the use of *in vivo* discharge patterns as a template for electrical stimulation *in vitro* is nevertheless a well-suited step to consolidate the presence of neuronal subtypes with differential roles in sensory processing.

5.3 Co-adaptation of intrinsic membrane and emerging network properties

Response dynamics are not only due to the interplay between presynaptic, labyrinthine activity and postsynaptic, intrinsic properties, but also a result from the activity of local neuronal networks. But how do local networks shape the response dynamics of frog tonic and phasic vestibular neurons? A disynaptic feed-forward side loop and a cerebellar feed-back loop were known to project onto central vestibular neurons in the frog (Straka and Dieringer, 2004).

The oppositely directed change in impedance during depolarization in the two subtypes and the differential integration into inhibitory synaptic circuits suggests that intrinsic membrane properties and emerging properties are co-adapted in frog tonic and phasic neurons (Beraneck et al., 2007; Biesdorf et al., 2008). This organization principle is consistent with different roles of these two subtypes in sensory signal processing.

5.3.1 Co-adaptation of intrinsic properties and the disynaptic feed-forward loop

In frogs, a disynaptic inhibition that superimposes on the monosynaptic activation from afferent nerve fibers is present in about 90 % of recorded neurons (Straka and Dieringer, 1996). This complies well with the fact that only phasic 2°VN, which constitute ∼80–90 % of vestibular neurons, are the target of such an inhibitory side loop (Biesdorf et al., 2008). The before mentioned asymmetric profile with the large peak advance in phasic 2°VN upon pulse train stimulation is due to an efficient summation of the EPSPs with a subsequent shunting of the membrane potential. The shunting is indeed caused by synergistically acting membrane conductances and local circuits: the resonant conductances and the disynaptic inhibition act in concert to give rise to the non-linear response profile upon synaptic pulse train stimulation. Pharmacological blocking of GABAergic and glycinergic channels revealed the contribution of inhibitory side loops to the response dynamics (Pfanzelt et al., 2008); it is, however, not evident to which extent intrinsic properties versus network circuits contribute in shaping the response dynamics. Extension of the generated phasic cellular model with excitatory conductance-based synapses or excitatory and inhibitory conductance-based synapses provided more insight (Pfanzelt et al., 2008). The model that reproduced only the excitatory input from the labyrinthine fibers generated responses that were similar in quality compared to the real data. With increasing stimulus peak frequency an increasing peak advance was observed in the model neuron. The magnitude of the peak advance, though, was not high enough. The model that simulated in addition to the excitatory labyrinthine input also an inhibitory input onto the model neuron, yielded quantitatively similar results compared to our real data. Tonic neurons, in contrast, do not receive a disynaptic inhibition, but IPSPs with longer latencies are present in this subtype (Biesdorf et al., 2008). These longer-latency IPSPs make a contribution in sculpting the monosynaptic

excitation unlikely.

A co-adaptation of intrinsic membrane properties and emerging network properties is not a peculiarity of frogs. Similar local networks seem to be present also in the mammalian vestibular nuclei. A disynaptic feed-forward loop was described in monkey (Minor and Goldberg, 1991) and is likely also present in the rodent MVN. Camp et al. (2006) demonstrated a differential distribution of inhibitory inputs onto type A and B MVN neurons. While type A MVN neurons receive almost exclusively GABAergic inhibitory inputs, type B MVN neurons receive a significant additional glycinergic input. This organization might provide brief blocks of the discharge in type B MVN neurons. Thus, as frog phasic 2°VN, rodent type B MVN neurons would be the target of stronger inhibitory inputs compared to type A MVN neurons. In addition, glycinergic IPSPs are hypothesized to arise from ipsilateral local interneurons (Furuya et al., 1991), which is reminiscent of the feed-forward inhibition in frogs. A further important consequence that was deduced from the conductance-based model was that the GABAergic and glycinergic interneurons have to be of tonic type. With phasic type interneurons, the prominent drop in membrane potential following the large peak advance in phasic 2°VN upon pulse train stimulation could not be reproduced. This conclusion is in agreement with studies in mouse MVN neurons (Bagnall et al., 2007; Sekirnjak and du Lac, 2006), where a subset of GABAergic neurons, exhibiting type A characteristics were supposed to represent local interneurons. Since these GABAergic neurons are located in the parvocellular portion of the MVN, which is an intrinsically projecting region (Büttner-Ennever, 1992; Epema et al., 1988), these neurons are believed to participate in the feed-forward inhibition from the vestibular nerve to other MVN neurons (Bagnall et al., 2007). Thus, the concept of GABAergic (Camp et al., 2006; Sekirnjak and du Lac, 2006; Bagnall et al., 2007) and glycinergic (Camp et al., 2006) feed-forward loops that modulate the output behavior of central vestibular neurons appears to be a common principle in vertebrates.

5.3.2 Co-adaptation of intrinsic properties and the cerebellar feed-back loop

The cerebellum participates in motor behavior that ranges from the fine tuning of reflex movements to the acquiring of new motor programs. Neurons in the vestibular nucleus that receive a monosynaptic inhibition from the Purkinje cells seem to be a crucial site of plasticity in the

VOR pathway (Lisberger, 1998). Also in frog, monosynaptic projections from Purkinje cells onto central vestibular neurons are known to be present (Magherini et al., 1975). During *in vivo* recordings, a cerebellar lesion increased the gain of the discharge of abducens motoneurons during sinusoidal head rotation by about 50 % (Straka and Dieringer, 2004). This concurs with the observed changes in the response profile of phasic 2°VN upon pulse train stimulation during a reversible blockage of Purkinje cells (Pfanzelt et al., 2008). The response profile is characterized by enhanced amplitude and reduced peak advance.

However, only a subset of the recorded phasic neurons showed a change in response profile. This is consistent with the well-known connectivity observed in rodents. Purkinje cells have been described to target only a discrete subpopulation of type B MVN neurons (Babalian and Vidal, 2000; Sekirnjak et al., 2003), the so-called flocculus target neurons (FTN). These neurons are believed to transform the inhibitory synaptic drive from Purkinje cells into changes in postsynaptic signals that implement the plasticity and give rise to motor learning at the level of the vestibular nuclei. These assumptions are further corroborated by the finding that neurons in the deep cerebellar nuclei and FTN exhibit similar physiological response properties, such as a high spontaneous discharge rate and a prominent rebound firing (Sekirnjak et al., 2003).

The remarkable role of FTN in VOR plasticity and the non-linear membrane properties of mammalian type B MVN neurons render these neurons suitable to form the central substrate of a modifiable, non-linear pathway. Given the functional similarities between rodent type B MVN and frog phasic vestibular neurons as well as between FTN and the homologous frog phasic vestibular subgroup, the transformation of non-linear, modifiable and linear, non-modifiable vestibular signals in separate channels appears to be a common feature among vertebrates (Minor et al., 1999; Clendaniel et al., 2001; Ramachandran and Lisberger, 2006).

5.4 Parallel processing in the vestibulo-ocular reflex pathway

The inputs to the VOR pathway arise from vestibular afferent fibers of the peripheral endorgans, which discharge in relation to head acceleration and velocity. At the output level, extraocular motoneurons discharge with respect to eye velocity and position. This sensory motor transformation likely occurs in parallel pathways. The presence of at least two neuronal subtypes at

each synaptic level is in agreement with such an organizational scheme. Different signal components might be mediated, from the sensory periphery to the motor plant by different neuronal subtypes that contact postsynaptic elements with similar signal dynamics.

Sensory periphery

Since otolith organs sense translational acceleration as well as gravity they detect changes in head position as well as a static head deviation. Accordingly in frog, hair cell subtypes with rather phasic or tonic response dynamics encode differential signal components (Lewis and Li, 1975; Baird, 1994b,a; Baird and Lewis, 1986). This specificity for higher or lower-dynamic components is based on differential channel kinetics in the hair cell types (Baird, 1994b,a). A similar arrangement into different types of hair cells is likely to be present in the semicircular canals as well: cells with rather tonic and phasic characteristics are suited to detect slower and faster movements, respectively. Correlated with differential response dynamics of the hair cells are differences in their morphology and their epithelial locations. Hair cells associated with slower dynamics possess stereocilia that are almost equally long as the kinocilium and reside in the peripheral part of the canal cupula and the extrastriolar region of the otolith macula (Baird and Lewis, 1986). In contrast, hair cells that show higher dynamics have sterocilia, which are half as long as their kinocilium and occupy the central portions (center of cupula and striolar region) of the sensory epithelium (Baird, 1992). Although hair cell subtypes in frog differ in their morphology and response dynamics, they all belong to the cylindrically shaped type II hair cells. These hair cells are present in anamniotes and amniotes, whereas amniotes (e.g. mammals) are endowed with an additional hair cell type, the pear-shaped, type I hair cells. Type I hair cells in amniotes exhibit an enhanced sensitivity to high-frequency stimulation compared to type II cells. Despite the absence of type I cells, e.g. in frogs, the different type II subtypes demonstrate similar differences in sensitivity for low- or high-frequent dynamics as type II and I hair cells in amniotes.

The semicircular canals and otolith organs are connected to the brainstem by a large number of afferent nerve fibers. Unlike sensory cells, afferent fibers in vertebrates form rather a continuum with regard to several interrelated physiological and morphological properties than distinct subtypes. They are characterized by a broad spectrum of axon diameters. In anamniotes, thin to thick-diameter fibers comply with response dynamics that range from tonic over phasic-tonic

to phasic (Baird and Lewis, 1986). Regularly and irregularly discharging fibers in amniotes correspond to tonic and phasic-tonic fibers in anamniotes, in both, their response dynamics and their fiber diameter. Particular phasic afferents, in contrast, appear to be unique to fish and amphibians. This is consistent with the notion that information processing of vestibular signals in frogs is tuned to more phasic behaviors. Thin-diameter, low-dynamic fibers tend to target extrastriolar regions of the macular epithelium or the peripheral regions of the canal cupula, whereas thicker, higher-dynamic fibers contact the macular striola or the central region of the canal cupula. In amniotes, small-diameter fibers provide bouton endings to type II hair cells, while the thickest fibers provide calyx endings to type I hair cells. "Dimorphic" fibers with intermediate properties are endowed with bouton as well as calyx endings. In frog, the majority of hair cells are contacted by bouton endings. Despite the structural differences of the terminal structures, mammalian species and frogs, share a common innervation pattern: thin, lower dynamic and thick higher dynamic fibers target hair cells in the peripheral/extrastriolar or central/striolar region with matched dynamic properties (Goldberg, 2000). Thus, the various decomposed head motion components are largely kept and processed separately at the level of afferent nerve fibers.

Central vestibular neurons

The existence of multiple subtypes at the level of central vestibular neurons throughout vertebrates suggests that the segregation into distinct signal components is maintained at the brainstem level. In frog, vestibular neurons subdivide into tonic and phasic neurons that differ clearly in their filter properties. In addition, emerging network circuits seem to be adjusted to the intrinsic neuronal properties such that these properties are reinforced by the local circuits, in which tonic and phasic neurons are embedded. Further insight was gained by testing the synaptic processing in the two subtypes with a dynamic stimulus. The observed different response profiles indicate that labyrinthine inputs are in fact processed differentially in the two subtypes (Pfanzelt et al., 2008). Tonic and phasic frog 2°VN seem thus to be suited to form the cellular substrate for a signal processing in parallel channels. A sensory-motor transformation in parallel channels, however, not only requires the presence of distinct neuronal populations at each synaptic level, but also an interconnection between presynaptic and postsynaptic elements with adjusted processing properties. However, central vestibular neurons in vertebrates are known to

be targeted by a broad fiber spectrum that includes the thickest, high-dynamic as well as thinner, low-dynamic afferent fibers (Goldberg, 2000; Straka and Dieringer, 2004). A convergence from afferent fibers with different dynamics onto tonic and phasic 2°VN is thus present. Such a convergence of monosynaptic vestibular afferent EPSPs from a larger fiber spectrum (Goldberg, 2000; Straka and Dieringer, 2004) suggests a mixing of signals related to different dynamic aspects of head motion in most central vestibular neurons. However, a complete mixing of these signals would only occur if the inputs from the different afferent fiber types converge at the same postsynaptic sites. More likely, afferents with signals related to particular head motion dynamics contact different somato-dendritic sites of a given vestibular neuron (Sato and Sasaki, 1993). Consequently, the specific time constants of synaptic currents at different sites would then allow vestibular neurons to integrate or differentiate head motion-related signals. This organization would also explain the considerable spatially-specific monosynaptic convergence of semicircular canal and otolith signals (Straka and Dieringer, 2004). Thus, combining inputs from a spectrum of vestibular nerve afferents in vestibular neurons does not contradict an organization of VOR pathways into discrete frequency-tuned channels. It rather emphasizes the particular importance of the filtering properties in the different types of vestibular neurons. The distinct intrinsic membrane properties of tonic and phasic neurons might filter out particular frequency ranges and thus emphasize either the coding of head acceleration, velocity, position or a defined combination of these modalities. At the next synaptic level of the vestibulo-ocular reflex, the presence of several motoneuron subtypes corroborates the assumption that a separation of signals with respect to different dynamic components persists.

Motor plant

Central vestibular neurons project to extraocular motoneurons in the oculomotor, trochlear and abducens nucleus, which, in turn activate (and reciprocally inhibit) appropriate pairs of eye muscles to generate compensatory eye movements during head motion. In an *in vivo* experiment in frog, optokinetic and vestibular stimulation revealed three different types of abducens motoneurons that differ in their resting discharge rate, peak discharge and the decline of the firing rate at the end of the stimulus (Dieringer and Precht, 1986). The so-called small type C motoneurons show a rather low peak discharge and the evoked discharge rate at the end of the stimulus declines within a time constant of ∼90 seconds. Since this cell type outlasts the

stimulus for a prolonged time, it is likely that this motoneuron type encodes a position-related signal that keeps the frog's eyes at an eccentric position. This cell type is contrasted by the large type A extraocular motoneurons that exhibit an overshooting discharge rate at the beginning of the stimulus and which are immediately silenced when the stimulus ends. Since activity ceases with the end of an eye movement, this type of neuron supposedly mediates eye velocity-related signals.

During sinusoidal head rotation at 0.2 Hz, frogs demonstrate small-amplitude compensating eye movements (Dieringer, 1987). These movements consist of a rapid transient increase in eye velocity, which is followed by a rather stable eye position. The eye velocity profile thus exhibits a large non-linearity. This profile coincides with the non-linear discharge pattern of phasic 2°VN upon pulse train stimulation with a cycle length of 5 seconds, which corresponds to a head rotation of 0.2 Hz. The velocity component of the eye motion could hence be mediated by phasic 2°VN that project onto type A extraocular motoneurons (Fig 5.1). The position signal might be generated by type C motoneurons, which are likely contacted by tonic 2°VN.

The generation of a rapid eye movement followed by an eccentric eye position is possibly associated with behavioral strategies. During prey catching, frogs spend long periods of time motionless, waiting for its prey to move (Ewert, 1970). As long as the prey stays immobile it cannot be distinguished from the background. When it moves, the frog approaches the prey with rapid, reorienting body movements. As the frog keeps an eccentric eye position directed toward the prey, the frog is ready to catch the prey as soon as it moves again.

Recordings from abducens motoneurons in the *in vitro* frog brain suggest that extraocular motoneurons subdivide into three groups following pulse train stimulation of afferent nerve fibers (unpublished results): the first and second group exhibit response profiles, which are compatible with activation by phasic- or tonic-type 2°VN, respectively (Fig. 5.1). A third, group appears to receive a mixed input of tonic and phasic signals. Although signal convergence is not completely absent at the level of motoneurons, a separation of phasic and tonic signal components is still maintained to a considerable degree. It is tempting to speculate that these three groups, identified *in vitro*, correspond to type A, C and B motoneurons that have been identified *in vivo*. The latter type possesses intermediate response characteristics, which would be in agreement with a convergence of signal components from presynaptic tonic and phasic 2°VN.

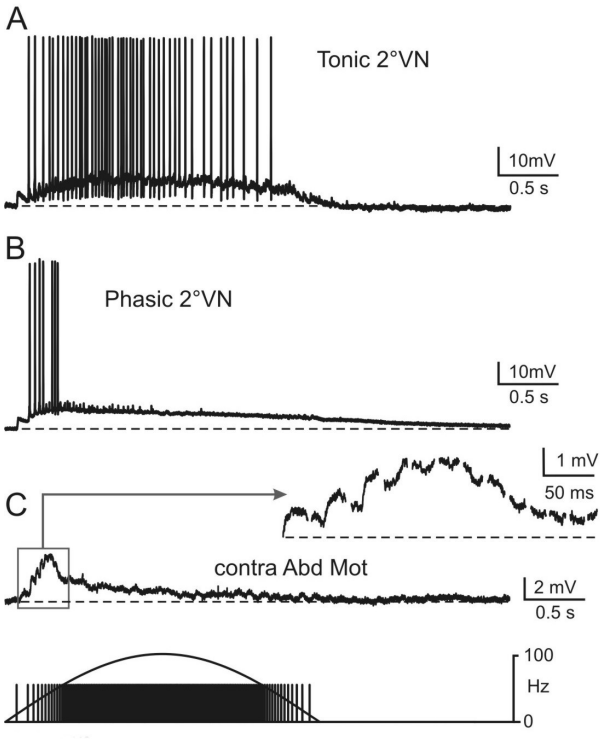

Figure 5.1: Typical responses of vestibular and motoneurons upon pulse train stimulation of the horizontal canal nerve. **C**, The synaptic compound response of the contralateral motoneuron is compatible with an activation by a phasic 2°VN (**B**) but not a tonic 2°VN (**A**). *Adapted from Straka et al. (2008).*

Precisely regulated extraocular motoneuronal activity is crucial for coordinate eye movements. The axons of oculomotor, trochlear and abducens motoneurons exit the brainstem to form the three extraocular nerves that innervate the six eye muscles. The accurate interplay of motoneurons with different response properties generates complex discharge patterns in the extraocular nerves. These population discharge patterns, in turn, drive the eye muscles to produce precise eye movements. Eye muscle fibers consist of a spectrum that ranges from slow-tonic fibers with very small diameters to rather thick twitch fibers (Büttner-Ennever, 2005; Spencer and Porter, 2005). Slow-tonic muscle fibers have tension-generating and fatigue-resistant properties. They are suited to maintain muscle tone and are thus likely innervated by type C motoneurons in frogs. Large twitch muscle fibers with faster and more transient response kinetics are presumably contacted by type A motoneurons. Also in mammals morpho-physiological evidences suggest a differential control of eye motion components by separate populations of extraocular motoneurons and muscle fibers, respectively (Evinger and Baker, 1991; Büttner-Ennever and Horn, 2002; Spencer and Porter, 2005).

In summary, a processing of different signal components occurs at the sensory periphery, in the brainstem and at the motor plant. At the central level in frog, tonic and phasic vestibular neurons form the cellular substrate for mediating different signal components. Differential intrinsic properties and synergistically acting intrinsic and network properties render these neuronal subtypes ideally suited for this task. In addition, the complex stimulus paradigm, the pulse train stimulation that was at the center of my current studies, tried to reproduce the activity in afferent fibers during a head movement *in vivo*. This dynamic stimulus succeeded in

bridging the gap between the response characteristics of tonic and phasic vestibular neurons and their respective functional roles in the sensory-motor transformation underlying the generation of vestibulo-motor responses.

Bibliography

Angelaki, D. E., Shaikh, A. G., Green, A. M., and Dickman, J. D. (2004). Neurons compute internal models of the physical laws of motion. *Nature*, 430(6999):560–564.

Ashcroft, D. W. and Hallpike, C. S. (1934). On the function of the saccule. *J. Laryngol.*, 49:450–458.

Av-Ron, E. and Vidal, P. P. (1999). Intrinsic membrane properties and dynamics of medial vestibular neurons: a simulation. *Biol Cybern*, 80(6):383–392.

Babalian, A., Vibert, N., Assie, G., Serafin, M., Mühlethaler, M., and Vidal, P. P. (1997). Central vestibular networks in the guinea-pig: functional characterization in the isolated whole brain in vitro. *Neuroscience*, 81(2):405–426.

Babalian, A. L. and Vidal, P. P. (2000). Floccular modulation of vestibuloocular pathways and cerebellum-related plasticity: An in vitro whole brain study. *J Neurophysiol*, 84(5):2514–2528.

Bagnall, M. W., Stevens, R. J., and du Lac, S. (2007). Transgenic mouse lines subdivide medial vestibular nucleus neurons into discrete, neurochemically distinct populations. *J Neurosci*, 27(9):2318–2330.

Baird, R. A. (1992). Morphological and electrophysiological properties of hair cells in the bullfrog utriculus. *Ann N Y Acad Sci*, 656:12–26.

Baird, R. A. (1994a). Comparative transduction mechanisms of hair cells in the bullfrog utriculus. II. sensitivity and response dynamics to hair bundle displacement. *J Neurophysiol*, 71(2):685–705.

Baird, R. A. (1994b). Comparative transduction mechanisms of hair cells in the bullfrog utriculus.I. responses to intracellular current. *J Neurophysiol*, 71(2):666–684.

Baird, R. A. and Lewis, E. R. (1986). Correspondences between afferent innervation patterns and response dynamics in the bullfrog utricle and lagena. *Brain Res*, 369(1-2):48–64.

Baird, R. A. and Schuff, N. R. (1994). Peripheral innervation patterns of vestibular nerve afferents in the bullfrog utriculus. *J Comp Neurol*, 342(2):279–298.

Beraneck, M., Hachemaoui, M., Idoux, E., Ris, L., Uno, A., Godaux, E., Vidal, P.-P., Moore, L. E., and Vibert, N. (2003). Long-term plasticity of ipsilesional medial vestibular nucleus neurons after unilateral labyrinthectomy. *J Neurophysiol*, 90(1):184–203.

Beraneck, M., Pfanzelt, S., Vassias, I., Rohregger, M., Vibert, N., Vidal, P.-P., Moore, L. E., and Straka, H. (2007). Differential intrinsic response dynamics determine synaptic signal processing in frog vestibular neurons. *J Neurosci*, 27(16):4283–4296.

Biesdorf, S., Malinvaud, D., Reichenberger, I., Pfanzelt, S., and Straka, H. (2008). Differential inhibitory control of semicircular canal nerve afferent-evoked inputs in second-order vestibular neurons by glycinergic and GABAergic circuits. *J Neurophysiol*, 99(4):1758–1769.

Blanks, R. H. and Precht, W. (1976). Functional characterization of primary vestibular afferents in the frog. *Exp Brain Res*, 25(4):369–390.

Büttner-Ennever, J. A. (1992). Patterns of connectivity in the vestibular nuclei. *Ann N Y Acad Sci*, 656:363–378.

Büttner-Ennever, J. A. (2005). The extraocular motor nuclei: organization and functional neuroanatomy. *Prog Brain Res*, 151:95–125.

Büttner-Ennever, J. A. and Horn, A. K. E. (2002). The neuroanatomical basis of oculomotor disorders: the dual motor control of extraocular muscles and its possible role in proprioception. *Curr Opin Neurol*, 15(1):35–43.

Camp, A. J., Callister, R. J., and Brichta, A. M. (2006). Inhibitory synaptic transmission differs in mouse type A and B medial vestibular nucleus neurons in vitro. *J Neurophysiol*, 95(5):3208–3218.

Caston, J., Precht, W., and Blanks, R. H. I. (1977). Response characteristics of frog's lagena afferents to natural stimulation. *J Comp Physiol*, 118:273–289.

Clendaniel, R. A., Lasker, D. M., and Minor, L. B. (2001). Horizontal vestibuloocular reflex evoked by high-acceleration rotations in the squirrel monkey. IV. responses after spectacle-induced adaptation. *J Neurophysiol*, 86(4):1594–1611.

Crill, W. E. (1996). Persistent sodium current in mammalian central neurons. *Annu Rev Physiol*, 58:349–362.

Dieringer, N. (1987). The role of compensatory eye and head movements for gaze stabilization in the unrestrained frog. *Brain Res*, 404(1-2):33–38.

Dieringer, N. and Precht, W. (1977). Modification of synaptic input following unilateral labyrinthectomy. *Nature*, 269(5627):431–433.

Dieringer, N. and Precht, W. (1986). Functional organization of eye velocity and eye position signals in abducens motoneurons of the frog. *J Comp Physiol*, 158:179 – 194.

Dutia, M. B., Lotto, R. B., and Johnston, A. R. (1995). Post-natal development of tonic activity and membrane excitability in mouse medial vestibular nucleus neurones. *Acta Otolaryngol Suppl*, 520 Pt 1:101–104.

Epema, A. H., Gerrits, N. M., and Voogd, J. (1988). Commissural and intrinsic connections of the vestibular nuclei in the rabbit: a retrograde labeling study. *Exp Brain Res*, 71(1):129–146.

Eugène, D., Deforges, S., Guimont, F., Idoux, E., Vidal, P.-P., Moore, L. E., and Vibert, N. (2007). Developmental regulation of the membrane properties of central vestibular neurons by sensory vestibular information in the mouse. *J Physiol*, 583(Pt 3):923–943.

Evinger, C. and Baker, R. (1991). *Are there subdivisions of extraocular motoneuronal pools that can be controlled separately.* Motor Control: Concepts and Issues. D. R.Humphrey & H.-J. Freund.

Ewert, J. P. (1970). Neural mechanisms of prey-catching and avoidance behavior in the toad (bufo bufo l.). *Brain Behav Evol*, 3(1):36–56.

Fitzpatrick, R. C. and Day, B. L. (2004). Probing the human vestibular system with galvanic stimulation. *J Appl Physiol*, 96(6):2301–2316.

Fuchs, A. F. and Kimm, J. (1975). Unit activity in vestibular nucleus of the alert monkey during horizontal angular acceleration and eye movement. *J Neurophysiol*, 38(5):1140–1161.

Furuya, N., Yabe, T., and Koizumi, T. (1991). Neurotransmitters regulating vestibular commissural inhibition in the cat. *Acta Otolaryngol Suppl*, 481:205–208.

Gallagher, J. P., Lewis, M. R., and Gallagher, P. S. (1985). An electrophysiological investigation of the rat medial vestibular nucleus in vitro. *Prog Clin Biol Res*, 176:293–304.

Gamkrelidze, G., Giaume, C., and Peusner, K. D. (1998). The differential expression of low-threshold sustained potassium current contributes to the distinct firing patterns in embryonic central vestibular neurons. *J Neurosci*, 18(4):1449–1464.

Gittis, A. H. and du Lac, S. (2006). Intrinsic and synaptic plasticity in the vestibular system. *Curr Opin Neurobiol*, 16(4):385–390.

Goldberg, J. M. (1979). Vestibular receptors in mammals: afferent discharge characteristics and efferent control. *Prog Brain Res*, 50:355–367.

Goldberg, J. M. (2000). Afferent diversity and the organization of central vestibular pathways. *Exp Brain Res*, 130(3):277–297.

Goldberg, J. M., Highstein, S. M., Moschovakis, A. K., and Fernandez, C. (1987). Inputs from regularly and irregularly discharging vestibular nerve afferents to secondary neurons in the vestibular nuclei of the squirrel monkey. I. An electrophysiological analysis. *J Neurophysiol*, 58(4):700–718.

Guth, P. S., Norris, C. H., and Barron, S. E. (1988). Three tests of the hypothesis that glutamate is the sensory hair cell transmitter in the frog semicircular canal. *Hear Res*, 33(3):223–228.

Highstein, S. M. and Holstein, G. R. (2005). The anatomy of the vestibular nuclei. *Prog Brain Res*, 151:157–203.

Him, A. and Dutia, M. B. (2001). Intrinsic excitability changes in vestibular nucleus neurons after unilateral deafferentation. *Brain Res*, 908(1):58–66.

Honrubia, V., Hoffman, L. F., Sitko, S., and Schwartz, I. R. (1989). Anatomic and physiological correlates in bullfrog vestibular nerve. *J Neurophysiol*, 61(4):688–701.

Hospedales, T. M., van Rossum, M. C. W., Graham, B. P., and Dutia, M. B. (2008). Implications of noise and neural heterogeneity for vestibulo-ocular reflex fidelity. *Neural Comput*, 20(3):756–778.

Hutcheon, B. and Yarom, Y. (2000). Resonance, oscillation and the intrinsic frequency preferences of neurons. *Trends Neurosci*, 23(5):216–222.

Ito, M. (1984). The modifiable neuronal network of the cerebellum. *Jpn J Physiol*, 34(5):781–792.

Johnston, A. R., MacLeod, N. K., and Dutia, M. B. (1994). Ionic conductances contributing to spike repolarization and after-potentials in rat medial vestibular nucleus neurones. *J Physiol*, 481 (Pt 1):61–77.

Larsell, O. (1967). *The Comparative Anatomy and Histology of the Cerebellum from Myxinoids through Birds.* University of Minnesota Press, Minneapolis.

Lewis, E. R. and Li, C. W. (1975). Hair cell types and distribution in the otolithic and auditory organs of the bullfrog. *Brain Res*, 83:35 – 50.

Lisberger, S. G. (1998). Physiologic basis for motor learning in the vestibulo-ocular reflex. *Otolaryngol Head Neck Surg*, 119(1):43–48.

Lowenstein, O. and Saunders, R. D. (1975). Otolith-controlled responses from the first-order neurons of the labyrinth of the bullfrog (rana catesbeiana) to changes in linear acceleration. *Proc R Soc Lond B Biol Sci*, 191(1105):475–505.

Magherini, P. C., Giretti, M. L., and Precht, W. (1975). Cerebellar control of vestibular neurons of the frog. *Pflugers Arch*, 356(2):99–109.

Markham, C. H. and Curthoys, I. S. (1972). Labyrinthine convergence on vestibular nuclear neurons using natural and electrical stimulation. *Prog Brain Res*, 37:121–137.

Matesz, C. (1979). Central projection of the VIIIth cranial nerve in the frog. *Neuroscience*, 4(12):2061–2071.

McCormick, D. A., Shu, Y., Hasenstaub, A., Sanchez-Vives, M., Badoual, M., and Bal, T. (2003). Persistent cortical activity: mechanisms of generation and effects on neuronal excitability. *Cereb Cortex*, 13(11):1219–1231.

Minor, L. B. and Goldberg, J. M. (1991). Vestibular-nerve inputs to the vestibulo-ocular reflex: a functional-ablation study in the squirrel monkey. *J Neurosci*, 11(6):1636–1648.

Minor, L. B., Lasker, D. M., Backous, D. D., and Hullar, T. E. (1999). Horizontal vestibuloocular reflex evoked by high-acceleration rotations in the squirrel monkey. I. normal responses. *J Neurophysiol*, 82(3):1254–1270.

Nakayama, H. and Oda, Y. (2004). Common sensory inputs and differential excitability of segmentally homologous reticulospinal neurons in the hindbrain. *J Neurosci*, 24(13):3199–3209.

Peusner, K. D. and Giaume, C. (1997). Ontogeny of electrophysiological properties and dendritic pattern in second-order chick vestibular neurons. *J Comp Neurol*, 384(4):621–633.

Pfanzelt, S., Rössert, C., Rohregger, M., Glasauer, S., Moore, L. E., and Straka, H. (2008). Differential dynamic processing of afferent signals in frog tonic and phasic second-order vestibular neurons. *J Neurosci*, 28(41):10349–10362.

Precht, W., Llinás, R., and Clarke, M. (1971). Physiological responses of frog vestibular fibers to horizontal angular rotation. *Exp Brain Res*, 13(4):378–407.

Quadroni, R. and Knöpfel, T. (1994). Compartmental models of type A and type B guinea pig medial vestibular neurons. *J Neurophysiol*, 72(4):1911–1924.

Ramachandran, R. and Lisberger, S. G. (2006). Transformation of vestibular signals into motor commands in the vestibuloocular reflex pathways of monkeys. *J Neurophysiol*, 96(3):1061–1074.

Raymond, J., Dememes, D., and Nieoullon, A. (1988). Neurotransmitters in vestibular pathways. *Prog Brain Res*, 76:29–43.

Ris, L., Hachemaoui, M., Vibert, N., Godaux, E., Vidal, P. P., and Moore, L. E. (2001). Resonance of spike discharge modulation in neurons of the guinea pig medial vestibular nucleus. *J Neurophysiol*, 86(2):703–716.

Sato, F. and Sasaki, H. (1993). Morphological correlations between spontaneously discharging primary vestibular afferents and vestibular nucleus neurons in the cat. *J Comp Neurol*, 333(4):554–566.

Schneider, D. (1954). Das Gesichtsfeld und der Fixiervorgang bei einheimischen Anuren. *Vergl. Physiol.*, 36:147 – 164.

Sekirnjak, C. and du Lac, S. (2006). Physiological and anatomical properties of mouse medial vestibular nucleus neurons projecting to the oculomotor nucleus. *J Neurophysiol*, 95(5):3012–3023.

Sekirnjak, C., Vissel, B., Bollinger, J., Faulstich, M., and du Lac, S. (2003). Purkinje cell synapses target physiologically unique brainstem neurons. *J Neurosci*, 23(15):6392–6398.

Serafin, M., de Waele, C., Khateb, A., Vidal, P. P., and Mühlethaler, M. (1991a). Medial vestibular nucleus in the guinea-pig. I. Intrinsic membrane properties in brainstem slices. *Exp Brain Res*, 84(2):417–425.

Serafin, M., de Waele, C., Khateb, A., Vidal, P. P., and Mühlethaler, M. (1991b). Medial vestibular nucleus in the guinea-pig. II. Ionic basis of the intrinsic membrane properties in brainstem slices. *Exp Brain Res*, 84(2):426–433.

Shimazu, H. and Precht, W. (1965). Tonic and kinetic responses of cat's vestibular neurons to horizontal angular acceleration. *J Neurophysiol*, 28(6):991–1013.

Spencer, R. F. and Porter, J. D. (2005). Biological organization of the extraocular muscles. *Prog Brain Res*, 151:43–80.

Straka, H., Baker, R., and Gilland, E. (2001). Rhombomeric organization of vestibular pathways in larval frogs. *J Comp Neurol*, 437(1):42–55.

Straka, H., Beraneck, M., Rohregger, M., Moore, L. E., Vidal, P.-P., and Vibert, N. (2004). Second-order vestibular neurons form separate populations with different membrane and discharge properties. *J Neurophysiol*, 92(2):845–861.

Straka, H. and Dieringer, N. (1996). Uncrossed disynaptic inhibition of second-order vestibular neurons and its interaction with monosynaptic excitation from vestibular nerve afferent fibers in the frog. *J Neurophysiol*, 76(5):3087–3101.

Straka, H. and Dieringer, N. (2000). Convergence pattern of uncrossed excitatory and inhibitory semicircular canal-specific inputs onto second-order vestibular neurons of frogs. Organization of vestibular side loops. *Exp Brain Res*, 135(4):462–473.

Straka, H. and Dieringer, N. (2004). Basic organization principles of the VOR: lessons from frogs. *Prog Neurobiol*, 73(4):259–309.

Straka, H., Holler, S., Goto, F., Kolb, F. P., and Gilland, E. (2003). Differential spatial organization of otolith signals in frog vestibular nuclei. *J Neurophysiol*, 90(5):3501–3512.

Straka, H., Lambert, F., Pfanzelt, S., and Beraneck, M. (2008). Vestibulo-ocular signal transformation in separate frequency-tuned channels. *Ann N Y Acad Sci*, (in press).

Straka, H., Vibert, N., Vidal, P. P., Moore, L. E., and Dutia, M. B. (2005). Intrinsic membrane properties of vertebrate vestibular neurons: function, development and plasticity. *Prog Neurobiol*, 76(6):349–392.

Usami, S. I., Takumi, Y., Matsubara, A., Fujita, S., and Ottersen, O. P. (2001). Neurotransmission in the vestibular endorgans–glutamatergic transmission in the afferent synapses of hair cells. *Biol Sci Space*, 15(4):367–370.

Vervaeke, K., Hu, H., Graham, L. J., and Storm, J. F. (2006). Contrasting effects of the persistent Na+ current on neuronal excitability and spike timing. *Neuron*, 49(2):257–270.

Wersäll, J. (1972). Morphology of the vestibular receptors in mammals. *Prog Brain Res*, 37:3–17.

Wersäll, J. and Bagger-Sjöback, D. (1974). *Morphology of the vestibular sense organ. In: Kornhuber, H. H. (Ed.), Handbook of Sensory Physiology. Vestibular System. Basic Mechanisms.* Springer, New York, pp. 123 –170.

Wu, N., Hsiao, C. F., and Chandler, S. H. (2001). Membrane resonance and subthreshold membrane oscillations in mesencephalic V neurons: participants in burst generation. *J Neurosci*, 21(11):3729–3739.

Danke et merci!

Nun ist es soweit, eine lange Episode neigt sich dem Ende zu. Viele Personen, Kollegen & Freunde, haben zur Entstehung dieser Arbeit auf unterschiedlichste Weise beigetragen.

Mein erster Dank geht an meinen Doktorvater Prof. Hans Straka, dessen Begeisterung für die Wissenschaft mich stets motiviert hat. Vielen Dank für die intensive Betreuung, die weiterhin bestand, auch nachdem ich das Labor in Paris verlassen hatte.

Ebenso möchte ich Dr. Stefan Glasauer danken, der meine Betreuung im Forschungshaus in München übernommen hat und der mir mit seinen fachlichen Kenntnissen eine große Hilfe war. Ein weiterer Dank gilt Prof. Dr. Benedikt Grothe für die Übernahme des Zweitgutachtens.

Ein großes Danke auch an meine deutschen, italienischen, griechischen, slovakischen und französischen Kollegen und Freunde, die mir entweder mit Ratschlägen, Diskussionen oder mit aufmunternden Worten zur Seite standen. Danke insbesondere an Olympia, Sigrid, Leni, Christian und Bernie.

Danke fürs Korrekturlesen, Mathias!

Ein großes Dankeschön an meine Mitbewohnerin, Sophie, für all die Unterstützung und Zuspruch bei der Doktorarbeit und drum herum.

Une longue période s'achève. Merci aussi au labo du LNRS: au directeur M. Vidal, à mes collègues, François, Mathieu, Erwin, Martine et Isabelle. Un salut au $3^{\text{ième}}$ étage!